博士論文

東京大学
THE UNIVERSITY OF TOKYO

Development of
Electrostatic Induction Feeding EDM with
Controlled Pulse Train Method
（パルス列制御による静電誘導給電放電加工の開発）

指導教員　国枝　正典　教授

東京大学大学院 工学系研究科 精密工学専攻

ノルリアナ　ビンティ　ムハマド　アッバス

Development of Electrostatic Induction Feeding EDM with Controlled Pulse Train Method

Norliana Binti Mohd Abbas

In the electrostatic induction feeding method (EIFM) a pulse voltage is coupled to the working gap of micro electrical discharge machining (EDM) through a capacitance. With EIFM, localized discharge and abnormal arc are less likely to happen because only one discharge can occur in every half cycle of the pulse power supply. Hence, stable machining can be achieved compared to the relaxation pulse generator or RC circuit which is widely used in industry. In micro EDM, tool is rotated to flush the debris in the gap. High speed tool electrode rotation helps in cooling the tool electrode surface. As a result, material removal rate (MRR) increases with increasing the speed of the tool electrode rotation. In RC circuit however, brush is used to connect the power supply to the tool electrode. Thus, it is not possible to rotate the tool at very high speed because it can cause vibration. With EIFM instead, non-contact electrical feeding can be realized and enables the tool to be rotated up to fifty thousand rpm without vibration. However, the material removal is extremely small because of the small capacitance, C_1 which is formed in the gap between the feeding electrode and the tool. This results in very small discharge energy per pulse and insufficient to conduct rough machining. To overcome the problem, controlled pulse train method (CPTM) is introduced. With this method, once discharge occurs, the high frequency discharge is allowed to continue within a controlled pulse train duration. Thus, with the same feeding capacitance C_1, larger diameter of craters can be obtained at higher frequency and longer pulse train duration compared to the conventional EIFM where individual pulse discharge was generated intermittently. The concentration of discharge location of multiple discharges within a pulse train duration was proved by observing the discharge location using a high speed video camera through a transparent electrode. Discharge energy is influenced by open circuit voltage, u_o and feeding capacitance, C_1. Thus, by utilizing resonance in the circuit, the amplitude of the working gap voltage can be amplified higher than the AC power supply. Discharge continuity within the pulse train duration was improved resulting in largest diameter of discharge craters and highest MRR. When machining is performed with non-contact electrical feeding, sufficiently large discharge energy cannot be obtained and discharge current is difficult to sustain within the pulse train duration due to the small C_1. Hence, the capacitance was increased by changing the configuration of the feeding electrode. Higher capacitance was able to form with the large diameter feeding electrode and the newly developed labyrinth feeding electrode. As a result, the influences of the tool

electrode rotation speed on the machining characteristics were investigated using a non-contact feeding capacitance of 111.8pF. The MRR was 5.7 times higher and machining accuracy was improved when the rotation speed of the tool was increased from 900rpm to 3300rpm.

Table of Contents

Chapter 1

Introduction

Machining is a material removal process to form a useful product having the required dimensions. In general, machining can be classified into two categories: traditional and non-traditional machining. In traditional machining, the workpiece is normally removed through contact between the tool and the workpiece. The removed materials are in the form of chips and the examples of the process are turning, drilling and grinding. For non-traditional machining, the materials are removed by electrical, chemical, thermal, hydrodynamic and optical powers or combination of any of these powers. With this, there is no contact between the tool and the workpiece during machining. The development and exploration in the non-traditional machining processes are important due to limitations in traditional machining such as machining-ability of hard materials, complex shapes of desired products, surface integrity, precision and miniaturization [1,2].

Electrical Discharge Machining (EDM) is one of the non-traditional machining processes. The basic EDM process consists of tool electrode, work piece, dielectric and pulse generator. The process is based on removing material from the workpiece surface by series of electrical discharges between tool and workpiece in the presence of dielectric fluid. By moving the tool electrode towards the workpiece, arc discharge can occur in a narrow gap of several µm to several tens µm between the two electrodes after high voltage is applied. Material is removed by melting and/or evaporating.

In general, EDM can be classified into two main categories: sinking EDM and wire EDM. The schematic diagrams of sinking and wire EDM are shown in Fig. 1.1 and 1.2 respectively. In sinking EDM, the tool electrode is shaped and made as a mirror image of the part that is to be produced. It should be made from conductive materials which can retain specified accuracy of the final shape. Most commonly used materials are copper,

copper-tungsten, graphite and brass [3-6]. Dielectric such as hydrocarbon-based oil, deionized water, gas or air [7-11] helps in cooling the machining area and to flush the debris after the discharge. Pulse generator is used to generate discharge pulse, and the gap width between the tool electrode and the workpiece is controlled by the servo feed controller.
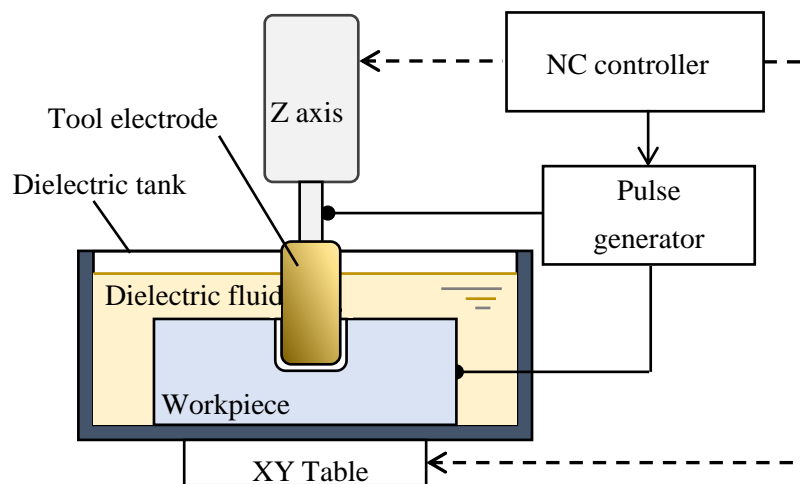
Fig. 1.1: Schematic diagram of sinking EDM
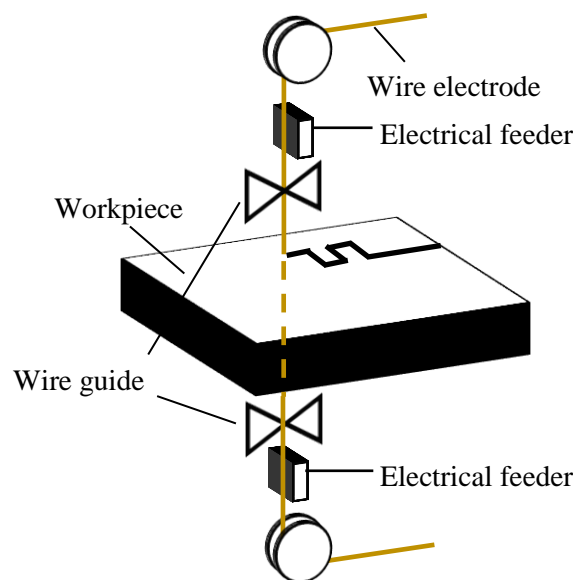
Fig. 1.2: Schematic diagram of wire EDM

In wire EDM, a thin wire tool electrode with diameter in range of 20-330μm [7,12] travels into the workpiece which is placed in x-y plane of the machine. New wire is continuously supplied during machining and problem related to tool wear can be ignored. Deionized water is usually used as the dielectric. By controlling the position of the upper wire guide relative to the lower guide, products with taper angle can be produced.

Since there is no direct contact between the electrode and the work piece with EDM, problems related to mechanical stresses, chatter and vibration during machining can be eliminated. Regardless of hardness, any conductive materials can be machined by EDM. The EDM process has been widely used in industry not only to produce dies and moulds but also to fabricate parts for example in the application of aerospace and automotive industry and also surgical components [13-15].

1.1 Principle of Electrical Discharge Machining (EDM)

When the tool electrode gets closer to the workpiece, the electric field increases. In a sufficiently narrow gap, where the electrical field is strongest, dielectric breakdown occurs at single spot between the two surfaces. The arc column is formed and discharge current flows through the gap. Due to the high heat flux from the arc column, the material is removed by melting and/or evaporation of the electrode materials in molten phase. A small crater is generated both on the tool electrode and workpiece surfaces. The removed materials are cooled and resolidified in the dielectric fluid and the flow of the dielectric will flush it away from the gap. The removal volume by the single discharge is very small. Thus, machining is accomplished by repeated discharges at a frequency of several thousand to several tens of thousands per second. The formation of discharge and material removal process is shown in Fig. 1.3.

a) Dielectric Breakdown and Generation of Arc Discharge

In a narrow gap of several tens of micrometer between parallel plane tool electrode (cathode) and workpiece (anode), electrons can exist even before a voltage of about 100V is applied. The free moving electrons are then accelerated by the generated electrical field. Collision between the accelerated electron and neutral particle happens causing the impact ionization; a neutral particle loses electron and change into a positive ion. As number of free electron increases, impact ionization occurs repeatedly until electron avalanche occurs. Due to ionization effect, positive ions are accelerated towards the cathode and impinge on the cathode surface.

The collision energy results in emission of secondary electrons coming out from the

3

cathode surface. In this way, dielectric breakdown takes place between the electrodes and current flows through the gap. The emission of electrons from heated cathode surface known as thermionic emission occurs when current density on the cathode surface increases. As the supply of electrons in the gap increases exponentially, arc discharge is formed at discharge voltage of about 20V. Due to high degree of ionization, discharge is less likely to occur at other location at the same time.

b) Generation of Bubble and Removal of Material

During the discharge between cathode and anode, the temperature of plasma channel is higher than 6000K with current density around 10^8 - 10^9A/m^2 [7,16,17]. Due to heat flux, cathode and anode surfaces are heated, melted and evaporated. The dielectric at the surrounding area will also evaporate by the heat from the arc plasma leading to generation of bubble. The gap is filled with a bubble because of boiling and dissociation of the dielectric liquid. The initial pressure of bubble can reach 10GPa [18] and can expand rapidly at a speed of 25m/s. The bubble expansion can continue even after the discharge ends because of the inertia of the dielectric. The radius of bubble can reach up to several millimeters around the arc column. Due to the high discharge energy, temperature of metal increases to the boiling point. Thus, removal action is believed to occur because of explosion of the molten metal [19,20]. From a molecular dynamic simulation, Yang et al. [21] found that the material removal occurs because of the extremely high pressure generated inside the melting area causing the atoms and clusters to accelerate out of the electrode surface. After that, the molten metal which is removed from the discharge point will be scattered and solidified in the form of spherical particles known as debris because of surface tension. The debris particles are removed from the area by flushing of dielectric.

c) End of Discharge, Recovery of Dielectric Breakdown Strength and Formation of Discharge Crater

At the end of discharge duration, there is no energy input into the plasma channel. Thus, temperature at the discharge point decreases and positive ions and electrons are recombined. Electrical conductivity of the plasma reduces and insulation between the electrodes in the gap is recovered. With several tens of microseconds of discharge duration, the recovery of dielectric strength can be achieved after about less than 3μs and the plasma temperature drops to under 5000K [22,23]. It is important to ensure the dielectric strength is fully recovered before the next pulse voltage is applied to avoid reoccurrence of discharge at the same location.
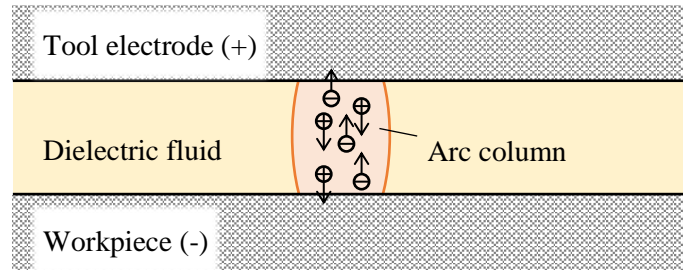
a) Dielectric breakdown and generation of arc discharge
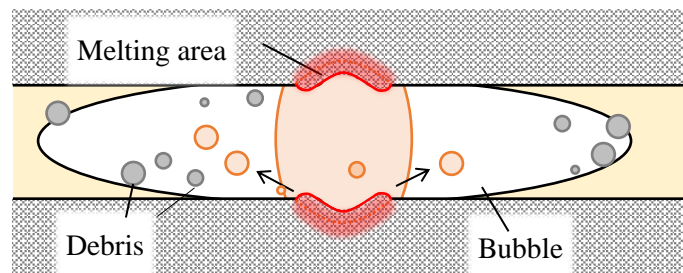
b) Generation of bubble and removal of material
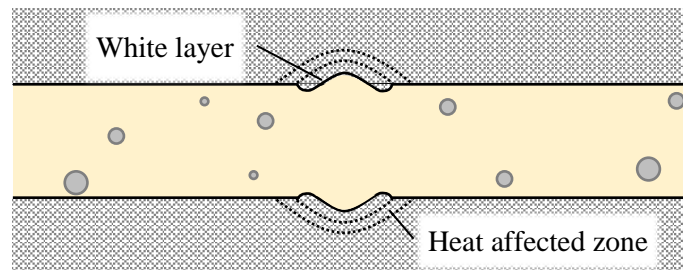
c) End of discharge, recovery of dielectric and formation of discharge crater

Fig. 1.3: Principle of Electrical Discharge Machining (EDM)

Fig. 1.4 shows the illustration on cross section of discharge crater after a single pulse discharge. During the discharge, molten metal cannot completely be removed. The remaining molten metal is left on the electrode surface, re-solidified and form a white layer. The upper part of the white layer is created in the form of crater and the size is determined by the discharge power and discharge duration. Under the white layer zone, there is an area known as heat affected zone (HAZ). During discharge, this area is exposed to high temperature and thermally modified although the exposed temperature is not high enough to melt the material.
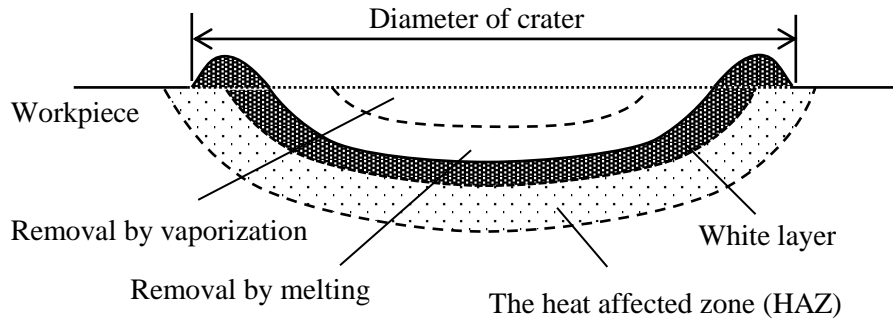
Fig. 1.4: Illustration on cross section of discharge crater after EDM process

1.2 Micro EDM

The increase in demand for micro parts and products has forced the manufacturer and researchers to explore methods to produce products which are small in size and high in accuracy. When EDM processes are applied to produce a product, holes, cavity or pin smaller than 500μm, it is categorized as micro EDM [12,24]. Example of the applications are drilling small and deep holes for turbine components or fuel injection nozzle [25-27]. Fig. 1.5 shows the example of a microcar mould made using EDM and the replicated plastic model [28]. In micro EDM process, the basic principle of material removal is the same as presented in Section 1.1. To realize machining in micro scale, two main requirements should be fulfilled: reduction of unit removal and improvement of equipment precision [12]. In addition, factors influencing the minimum limit of miniaturization includes HAZ, residual stress, size of discharge craters and tool wear [29-32].
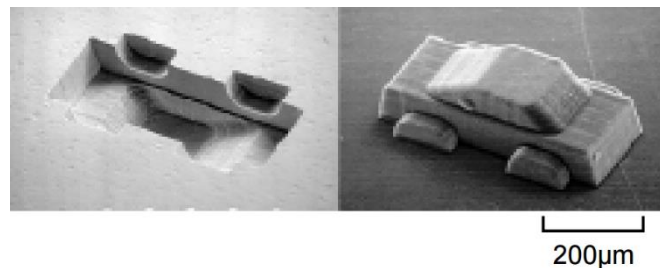
Fig. 1.5: Micro mould made by EDM and the replicated plastic model [28]

1.2.1   Comparison between Macro and Micro EDM

Basically, to produce products in micro scale, tool electrode in micro dimensions is used. The working gap width will be significantly small in several μm to several tens of μm compared to macro EDM which results in smaller arc plasma diameter [31,33,34]. Since the product is small, relatively small discharge crater should be generated. To

6

achieve small discharge crater in micro EDM, the discharge energy per pulse should be reduced so that unit removal per discharge can be decreased [12,31]. Fig. 1.6 shows the example on the difference in the size of discharge crater between macro and micro EDM after single discharge [35].
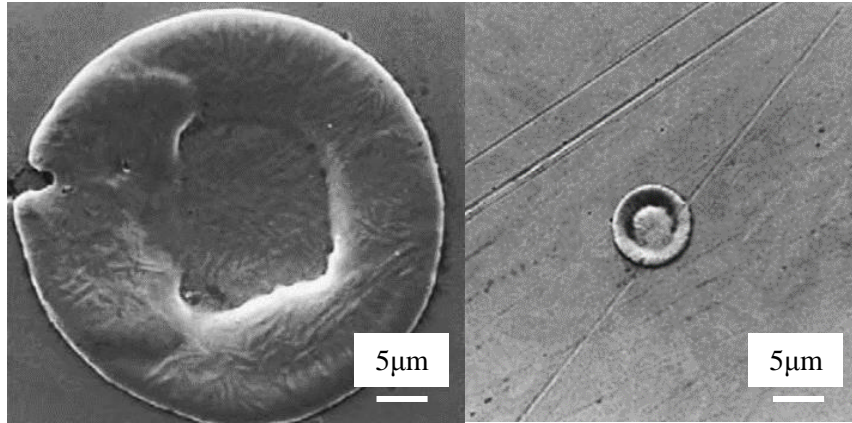
Fig. 1.6: Comparison on diameter of discharge crater between macro and micro EDM [35]

Fig. 1.7 shows the distribution of discharge energy during EDM process [36]. During discharging, energy can be distributed into tool electrode, workpiece and the gap between them as in Fig. 1.7a. Besides the consumption for material removal, the energy distributed into the workpiece is lost because of heat conduction, convection and radiation (Fig. 1.7b). Motoki and Hashiguchi [37], and Van Dijck [20] described that the energies distributed into anode and cathode can be changed with the discharge duration. However, Xia H. et al. [36,38] reported that the energy distributed to anode is always greater than that to cathode and rarely affected by the discharge duration: not only in single discharge but also in continuous pulse discharges [37].

Zahiruddin M. and Kunieda M. [39] found that energy distribution ratio into electrodes in micro EDM was comparatively lower than that in macro EDM. The comparison was made with the work reported by Xia H. et al. [36] and Hayakawa S. et al. [40] as shown in Fig. 1.8. This means that during the short discharge duration, large percentage of discharge energy is consumed for the plasma generation and increase of enthalpy in the plasma.

The difference in discharge duration between macro and micro EDM does influence the energy efficiency and removal efficiency. During the long discharge duration in macro EDM, plasma expands to the maximum diameter of about 5 times larger than the crater diameter [16]. The expansion finished within a couple microseconds after the dielectric

7

breakdown in air, thereafter the diameter was kept constant. In the case of micro EDM however, since the discharge duration is very short, the plasma diameter was assumed to increase with time until the end of discharge duration [16,41]. As a result, plasma diameter was only about 3 times larger than the crater diameter. Comparison on the diameter of plasma between macro and micro EDM is shown in Fig. 1.9. As a result, that the power density in micro EDM is higher about 30 times leading to higher energy efficiency and removal efficiency than those in macro EDM [42].
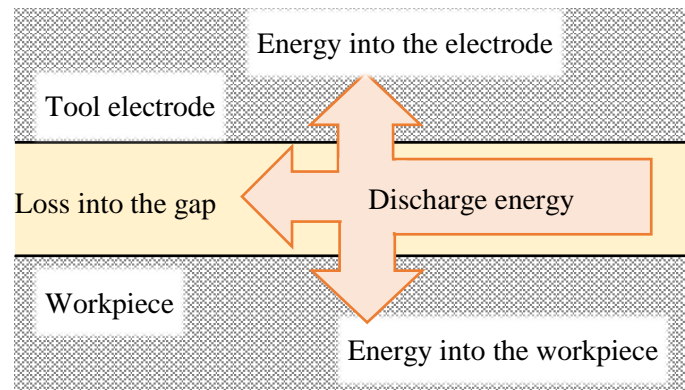
a) Distribution of discharge energy
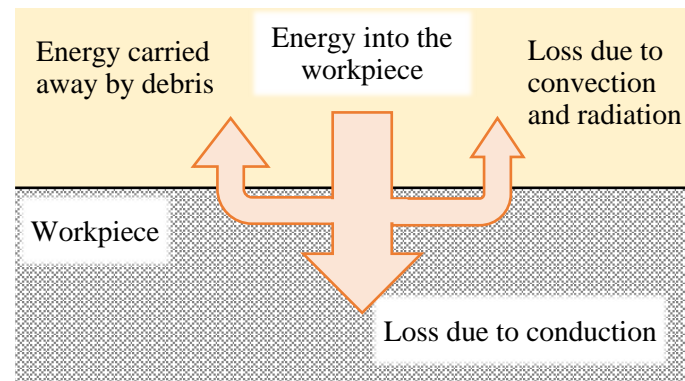
b) Energy distribution into workpiece

Fig. 1.7: Distribution of discharge energy during EDM process [36]
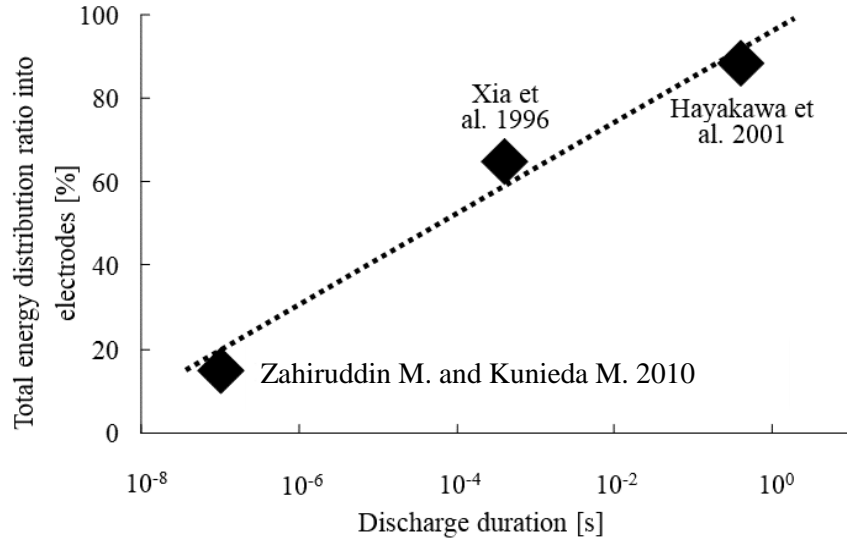
Fig. 1.8: Relationship between total energy distribution ratio into electrodes and discharge duration [39]
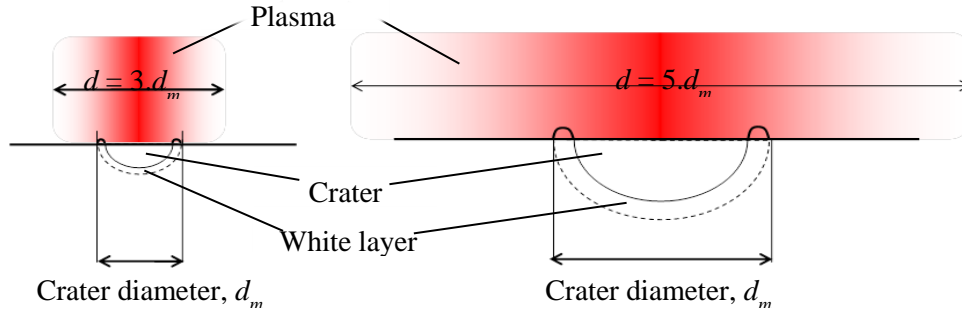
Fig 1.9: Comparison of plasma diameter between micro and macro EDM [41]

1.2.2   Pulse Generator in Micro EDM

There are two types of pulse generator which can be used for EDM process. First is the transistor type and the schematic diagram is shown in Fig. 1.10. The discharge voltage and discharge current waveform are presented in Fig. 1.11. In this figure, u_o is the open voltage, u_e is the discharge voltage, i_e is the discharge current, t_e is the discharge duration and t_o is the pulse interval.

The open voltage of about 100-200V is applied to the discharge gap after the transistor is switched on. This creates potential difference between the tool electrode and workpiece. Dielectric breakdown occurs between the two electrodes after a discharge delay time, t_d. This is because, time is needed to cause the electron avalanche; which occurrs due to the bombardment of cosmic, radioactive, ultraviolet and x-rays to generate the initial

9

electrons [43]. When the gap width is small, the dielectric breakdown strength decreases. The number density of the debris particles suspended in the gap increases the electric field locally. Therefore, t_d is influenced by the gap conditions, like gap width, electrode surface area and contamination in the gap [7,44,45]. B. Bommeli et al. [46] investigated the exponential distribution of discharge delay time using the Laue plot method. The discharge delay time was measured from the rise of the pulse voltage to the time when the dielectric breakdown starts. It was shown that the probability that discharge does not occur until time t can be expressed as,

$$exp\left(-\frac{t}{<t_d>}\right) \tag{1.1}$$

where $<t_d>$ is the average discharge delay time. It was also found that the contaminated liquid has influence on the discharge delay time. Morimoto et al. [44] found experimentally using the Laue plot method that average of t_d can be expressed as the following equation:

$$< t_d >= 8.2 \; x \; 10^{12} \left(\frac{gap^{8.8}r^{2.9}}{area^{1.2}conc^{1.6}}\right) \tag{1.2}$$

Here, *gap* is gap width, *r* is diameter of debris particles, *area* is machining area and *conc* is concentration of debris particles.

Then, the gap voltage drops to about 20V and discharge current flows between the two electrodes. The discharge current can be controlled by the number of transistors and/or the current-limiting resistor. Pulse control circuit is used to detect the occurrence of the discharge and the discharge in the gap is effectively cut off once the transistor turns off. By controlling the discharge duration, the material removal volume of single discharge can be the same in order to achieve better surface finish. Sufficient interval time can be achieved by turning off the transistor within a predetermined time, allowing the dielectric strength to recover, and the next discharge can occur at different location. Then, once the transistor is turned on again, voltage is applied between the electrodes and the process is reiterated.
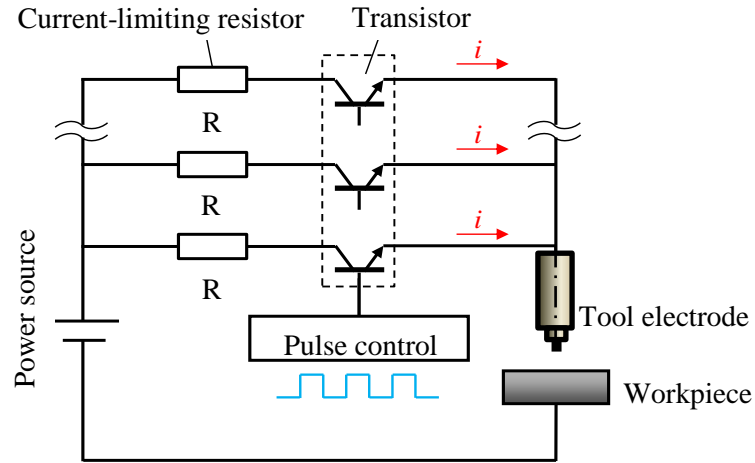
Fig. 1.10: Schematic diagram of transistor pulse generator
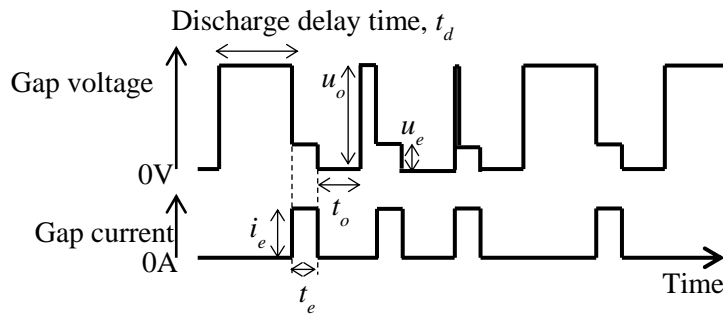
Fig. 1.11: Discharge voltage and discharge current waveform of transistor pulse generator

The second type is the relaxation pulse generator or RC circuit. The schematic diagram of RC circuit is shown in Fig. 1.12. When the voltage is applied, the capacitor C is charged through the resistor R, and the potential difference between the electrodes increases. The charging speed is determined by the time constant, τ which is the multiplication of R and C. Voltage in the gap between the tool electrode and the workpiece drops to the discharge voltage of around 20V, in the same way as the transistor pulse generator, when discharge is ignited. The accumulated charge in the capacitor is discharged between the electrodes.
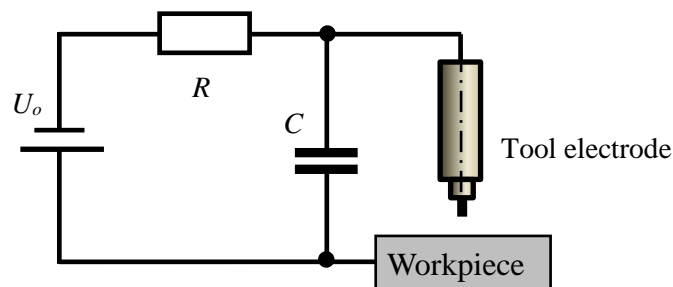
Fig. 1.12: Schematic diagram of relaxation pulse generator or RC circuit

11

It is known that the energy stored in the capacitor is $1/2Cu_o^2$. However, the energy per discharge can be expressed by,

$$W_{RC} = 2C\,u_e\,(u_o - u_e) \tag{1.3}$$

where C is the capacitance, u_e is the discharge voltage, and u_o is the value of the open voltage of the source [24,47]. When the discharge current becomes zero, the dielectric strength of the gap is recovered and the capacitor begins to be charged again. The potential difference between the electrodes increases gradually and the cycle is repeated.

Using the transistor pulse generator, it is difficult to achieve pulse duration shorter than 30ns because there is a delay in switching the transistors. Hence, to realize micro machining with micro EDM, the RC circuit is commonly used. With RC circuit, higher peak current and shorter pulse duration can be obtained resulting in higher power density and better removal efficiency. In macro EDM however, the transistor pulse generator is normally used because of the high controllability of the discharge duration, t_e and discharge interval, t_i to obtain higher discharge stability and machining accuracy.

1.2.3   Machine Tool for Micro EDM

To obtain small discharge energy, C should be decreased. Short pulse duration requires small inductance of the discharge circuit. Long electric feeders and large area size of machine structure result in large inductance and large stray capacitance, respectively [48]. Hence, micro EDM cannot be performed using normal EDM machines which are used for manufacturing dies and moulds of normal consumer products. Therefore, special machines dedicated to micro EDM should be designed so that the stray capacitance and inductance can be eliminated.

1.2.4   Servo Feed Control

In EDM, the tool electrode is fed to the workpiece and discharge can occur when the distance between the two electrodes is small enough; around several micrometers to several tens of micrometers. The tool electrode can be fed at a constant feed speed as far as short circuit between electrodes can be avoided. In most cases however, to achieve maximum machining efficiency, servo feed control is used to maintain a proper gap width during machining. The principle of servo feed control based on transistor pulse generator is shown in Fig. 1.13. The red line indicates the average gap voltage of the respective conditions.

When the feed speed is low, the gap between the tool electrode and the workpiece is large. The large gap between the electrodes causes difficulty for the dielectric breakdown to be achieved. Longer time is needed for discharge to occur; known as the discharge delay time, t_d. The long t_d results in low discharge frequency and the average value of the gap voltage is high. Other than the gap width, t_d also depends on the concentration of the debris particles in the gap. Conversely, if the feed speed is too fast, the gap width reduces. At the small gap, dielectric breakdown easily occurs and the t_d becomes shorter. By performing machining at this condition, the discharge frequency can be increased and the average gap voltage becomes low. However, machining will be unstable due to discharge localization in a small area where the temperature rises and debris particles concentration increases.

To overcome this problem, the feeding of the tool electrode can be controlled based on the difference between the measured gap voltage and the reference voltage so that proper discharge gap can be maintained during machining. The reference voltage can be obtained through experiment or empirical data. With the servo feed control, the tool will be fed to the workpiece if the measured average gap voltage is higher compared to the predetermined reference voltage. On the other hand, the tool will be retracted if the measured average gap voltage is lower compared to the predetermined reference voltage. With this, the gap width and discharge frequency can be controlled constant.
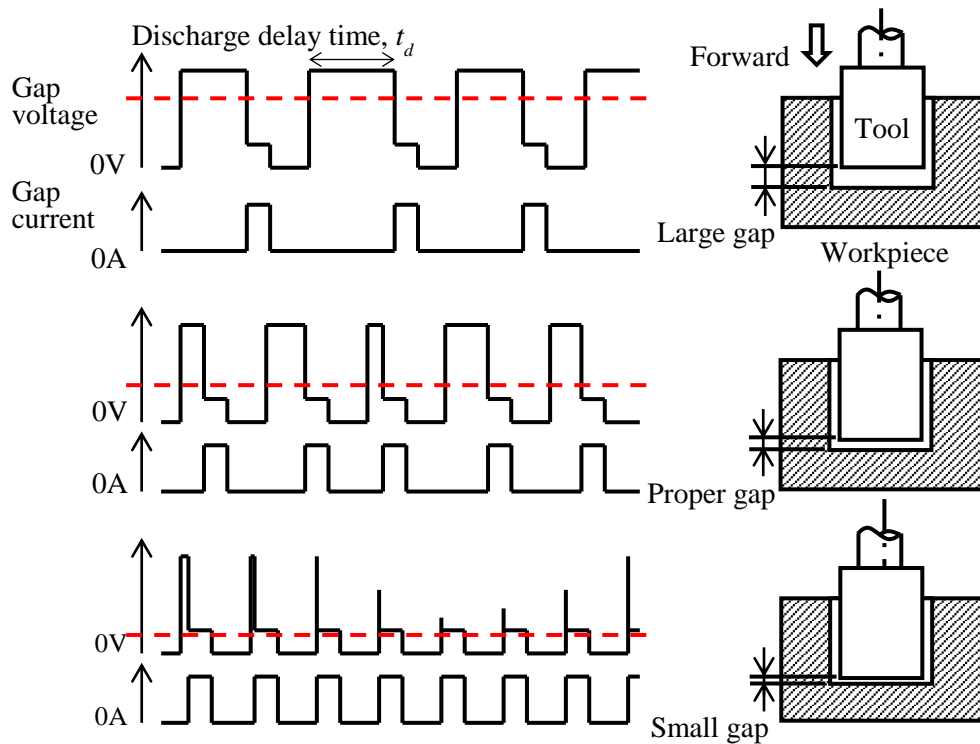
Fig. 1.13: Servo feed control

13

1.3 Micro EDM with Electrostatic Induction Feeding Method (EIFM)

To achieve minimum limit of miniaturization in micro EDM, discharge energy per pulse must be reduced as much as possible. By using RC circuit, the capacitor C should be decreased to the smallest possible to obtain minimum discharge energy. However, in the actual EDM machine as shown in Fig. 1.14, stray capacitance exists between electric feeders, between tool electrode holder and work table and between the tool electrode and workpiece [48]. Kawakami and Kunieda [31] investigated the minimum tool electrode diameter which can be achieved using an RC circuit. It was found that tool electrode with diameter smaller than 2.3μm is not possible to be machined. One of the reasons is because of the large stray capacitance. This means that the minimum discharge energy per pulse is determined by the stray capacitance; limiting the lowest energy per pulse and influencing the limit of miniaturization. Egashira and Mizutani [49] performed machining with a low open voltage of 20V without reducing the stray capacitance. A fine tool electrode of 1μm diameter was achieved. However, since the supply voltage is low, machining was unstable, thereby the machining speed was significantly reduced.

Another disadvantage of the RC circuit is that, on the outbreak of short circuit, electric current continues flowing through the gap [34]. The pulse discharge is interrupted during this time because the leak current does not allow the capacitance to be charged. At the short circuiting spot, Joule heat is generated. Even if the mechanical contact is released, the generation of high temperature plasma delays the recovery of dielectric strength, resulting in machining instability.
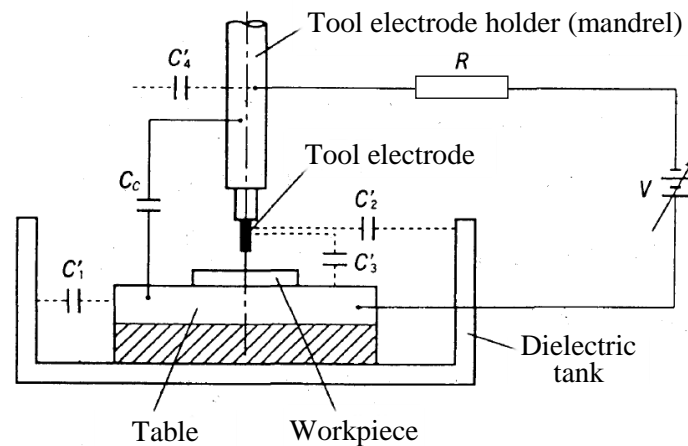
Fig. 1.14: Stray capacitance in EDM machine [48]

Therefore, Kunieda et al. [50] and Hanada et al. [51] developed a micro EDM pulse generator using electrostatic induction feeding. The schematic diagram of this method is

14

shown in Fig. 1.15. The pulse power supply induces pulse voltage with a constant period and it is coupled to the tool electrode by capacitance C_1. With this, discharge energy is determined by the value of the feeding capacitor C_1 and pulse voltage [52], and the influence of stray capacitance can be eliminated [53]. This pulse generator was established based on the idea from Niwa [54] who used an alternating discharge current for electrical discharge grinding using a capacity coupled circuit. In the work, high frequency AC voltage of 13.5MHz was supplied to a rotating disk electrode through a gap between a feeding electrode and the shaft of the rotating electrode, thereby use of brush was not necessary. However, since AC voltage of 1ms in constant duration was intermittently supplied, the duration of the AC discharge voltage was not controlled. In EIFM however, discharge occurs only once during the half cycle of the pulse voltage, allowing the dielectric strength to recover after every discharge.
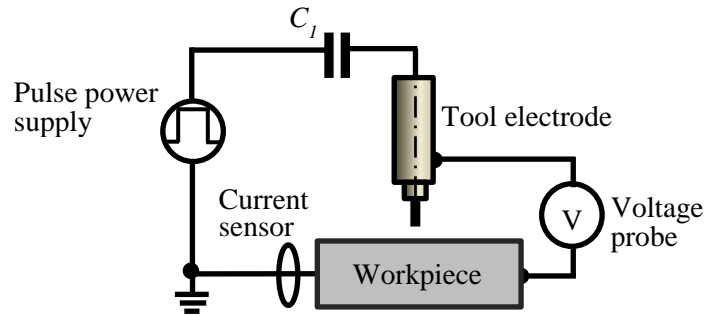
Fig. 1.15: Schematic diagram of electrostatic induction feeding method

1.3.1 Principle of EIFM

Fig. 1.16a shows the schematic diagram on discharge occurrence with EIFM and Fig. 1.16b shows the discharge voltage and current waveforms on the occurrence of discharge. Here, the gap voltage and current can be measured as shown in Fig. 1.15. The pulse power supply is coupled with the working gap by capacitance C_1. C_2 is the working gap capacitance between the tool electrode and the workpiece. In this example, C_1 is assumed to be 10 times larger than C_2 and the electric charges shown as $\oplus$ and $\ominus$ are 10 times as large as $+$ and $-$, respectively. When the voltage of the pulse power supply becomes E_0, the tool electrode and workpiece are charged positive and negative, respectively (i). Consequently, discharge occurs (ii). The discharge duration is very short, several ns to several tens of ns, depending on the capacitance of C_1. After every discharge, there is no current flowing through the circuit, thereby the gap voltage is kept equal to the discharge voltage. Hence, discharge does not occur until the next half cycle of the pulse power supply. After constant pulse duration, the voltage of the pulse power supply becomes 0.

$C_1 = 10C_2$

⊕ = 10 +
⊖ = 10 −

(i) Charge

C_1

E

Tool electrode

C_2
++ ++

Workpiece

(ii) Discharge

C_1

E

C_2
++

(iv) Discharge

C_1

C_2
++

(iii) Charge

C_1

C_2
++++
++++
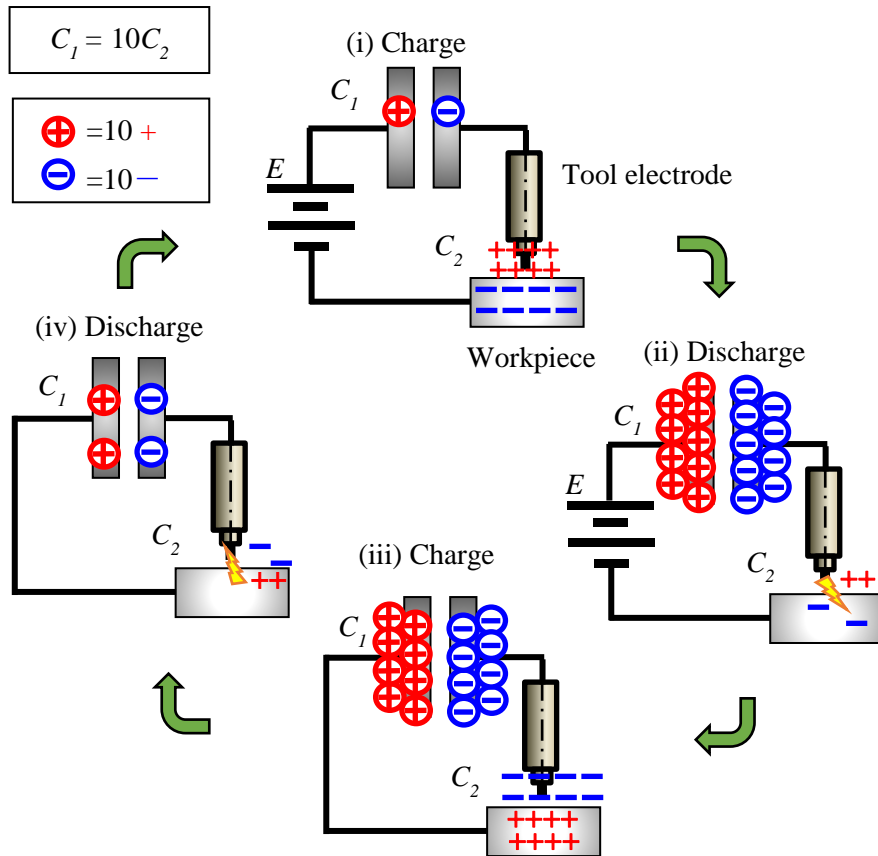
(a) Schematic diagram on the discharge occurrence

One cycle of pulse

Pulse power supply

E_0

0

Time

Gap voltage

(i)

(ii)

0

(iii)

(iv)

Time

Discharge current

0

ns - tens ns

Time
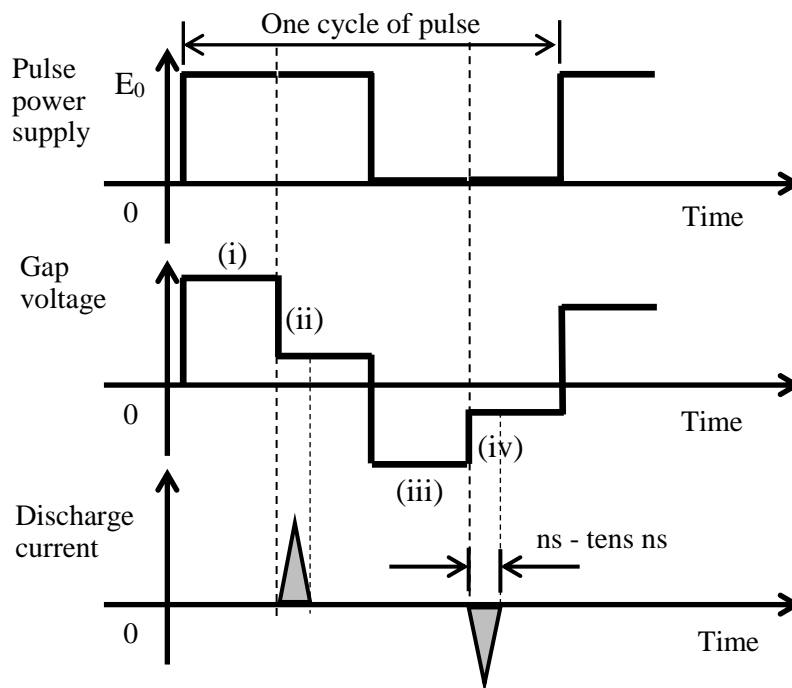
(b) Illustration of gap voltage and discharge current waveforms

Fig. 1.16: Principle of electrostatic induction feeding method (EIFM)

16

Since the tool electrode accepts electrons during the discharge, tool electrode is charged negative, and contrarily the workpiece is charged positive (iii).

Accordingly, discharge occurs with polarity opposite to the previous one, and electrons are conducted from tool electrode to workpiece (iv). Machining is carried out by repetition of this cycle. In principle, discharge is bipolar in this method. With this, only one discharge can occur within the half cycle of the pulse power supply. Dielectric strength can be recovered after every discharge and discharge craters can be scattered on the machined surface. Since the influence of stray capacitance is small, discharge energy is determined by the feeding capacitor. Thus, discharge energy can be reduced by using small feeding capacitance [55,56].

1.3.2 Equivalent Circuit

Fig. 1.17 shows the equivalent circuit of EIFM method during (a) charge and (b) discharge which was analyzed by Kunieda et al. [50], Hanada et al.[51] and Xiodong Yang [57]. E_0 is the amplitude of the rectangle pulse with constant pulse duration a, T is the rectangle pulse period, C_1 is the feeding capacitor, C_2 is the capacitance formed between the tool electrode and workpiece, $V(t)$ is the working gap voltage with respect to time and R_0 is the internal electric resistance. During discharge, voltage drop between the electrodes can be expressed by a resistance, R and discharge voltage, u_e. Current, $I_3(t)$ flows through the machining gap during the discharge. It should be noted that Fig. 1.17 (b) is showing the case that the tool electrode is positive as shown in Fig. 1.16(a)(ii). When discharge occurs with negative tool electrode as in Fig. 1.16(a)(iv), the sign of the direction of u_e is reversed. From these equivalent circuits, the Kirchoff's Current Law and Kirchoff's Voltage Law were applied. The resulting differential equations given in Eqs. 1.4-1.10 were used to calculate the gap voltage and discharge current.
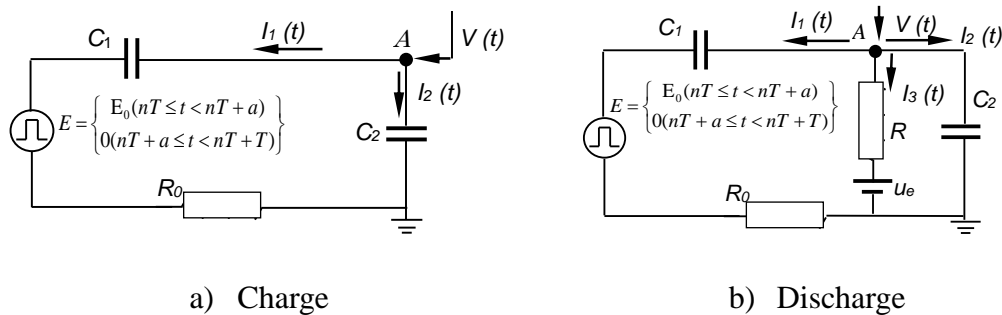

a) Charge   b) Discharge

Fig. 1.17: Equivalent circuit for EIFM

17

a) Charge

$$V(t) = \frac{1}{C_1} \int I_1(t)dt + \begin{Bmatrix} E_0(nT \le t < nT + a) \\ 0(nT + a \le t < nT + T) \end{Bmatrix} + R_0 I_1(t) \tag{1.4}$$

$$V(t) = \frac{1}{C_2} \int I_2(t)dt \tag{1.5}$$

$$I_1(t) + I_2(t) = 0 \tag{1.6}$$

b) Discharge

$$V(t) = \frac{1}{C_1} \int I_1(t)dt + \begin{Bmatrix} E_0(nT \le t < nT + a) \\ 0(nT + a \le t < nT + T) \end{Bmatrix} + R_0 I_1(t) \tag{1.7}$$

$$V(t) = \frac{1}{C_2} \int I_2(t)dt$$

$$\tag{1.8}$$

$$V(t) = RI_3(t) \pm u_e \quad (E_0 \ne 0: +, \ E_0 = 0: -)$$

$$\tag{1.9}$$

$$I_1(t) + I_2(t) + I_3(t) = 0 \tag{1.10}$$

Hanada et al. [51] compared the calculation results with experimental results during charging and discharging process. Fig. 1.18(a) shows the calculated gap voltage waveforms under conditions: amplitude of the pulse generator, $E_0 = 150V$, rectangle pulse period, $T = 110\mu s$. Other parameters used in the calculation were: $C_1 = 10pF$, $C_2 = 1pF$, $R = 100\Omega$, $R_0 = 1\Omega$, $u_e = 20V$. In the calculation, it was assumed that discharge does not occur during the first cycle but occurs at, $t = 5/4T$, $7/4T$, $9/4T$, $11/4T$. When the pulse voltage becomes E_0 at point (i), the potential difference between the electrodes is large. Then, discharge occurs at point (ii) and machining gap voltage drops instantly to 20V which is equal to discharge voltage, as described in Section 1.1. Then, the polarity of the pulse power supply is changed and the tool and the workpiece are charged in the opposite polarity. Then, discharge occurs in reversed polarity from the earlier discharge at point (iv). Fig. 1.18(b) shows the calculated discharge current through the working gap at the moment of discharge. Fig. 1.19 shows the points (i) to (iv) obtained from experiment, which correspond to the analysis results shown in Fig. 1.18.

From Eqs. 1.4-1.10, discharge current $I_3(t)$ can be obtained analytically as shown in Appendix 1. So, the discharge energy can be calculated as follows:

$$W_M = \int_0^{te} V(t) I_3(t)dt \tag{1.11}$$

W_M is the discharge energy per pulse and t_e is the discharge duration. However, since $I_3(t) = I_1(t) + I_2(t)$, W_M can be expressed as:

18
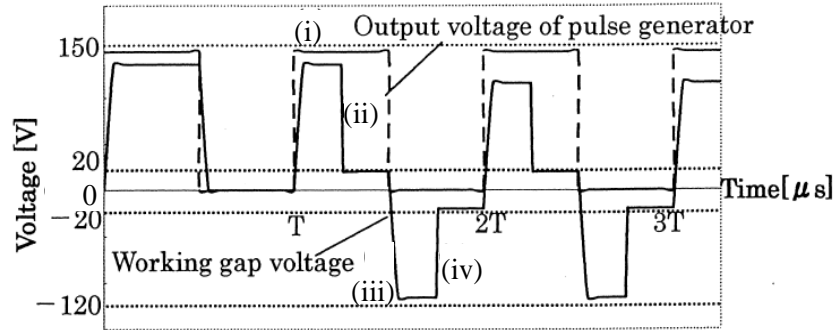
a) Calculated gap voltage
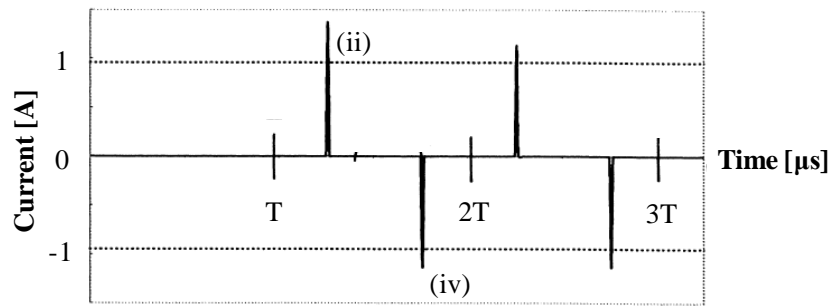
b) Calculated discharge current

Fig. 1.18: Analysis of gap voltage and discharge current [51]
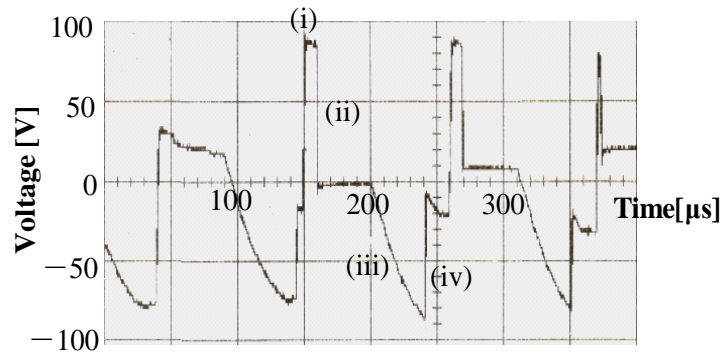
Fig. 1.19: Measured gap voltage [51]

$$W_M = W_1 + W_2 = \int_0^{te} V(t)\, I_1(t)\, dt + \int_0^{te} V(t)\, I_2(t)\, dt \qquad (1.12)$$

This can be simplified to:

$$W_M = u_e \int_0^{te} I_1(t)\, dt + u_e \int_0^{te} I_2(t)\, dt \qquad (1.13)$$

because discharge usually occurs at approximately 20V (known as discharge voltage, u_e). Here, W_1 can be obtained by integrating $I_1(t)$ by time, t using the equation shown in Appendix 1. On the other hand, it also can be obtained by

$$W_1 = 2C_1\, u_e\, (u_o - u_e) \qquad (1.14)$$

using the theory given by Masuzawa [47] with respect to the conventional RC circuit. Here, u_o is the open voltage. Conversely, W_2 can be expressed as

$$W_2 = C_2\, (u_o{}^2 - u_e{}^2)/2 \qquad (1.15)$$

Xiaodong Yang [58] found that $I_2(t)$ cannot be ignored compared to $I_1(t)$ when C_2 is large. From the above equations, it is found that the discharge energy can be increased with increasing C_1 and u_o.

In reality however, stray inductance exists in the circuit. Hence, precise analysis should be performed considering the inductance, L. Using the equivalent circuit shown in Fig. 1.20(a), Kimori et al. [52] performed the calculation and discussed the influence of inductance on the discharge current waveform under conditions: $R_0=1\Omega$, $C_1=15$pF, $L=1\mu$H, $E_o=120$V, and $u_e=20$V. In the figure, L is the inductance, I_1 and I_2 are the currents flowing through C_1 and C_2 respectively. Fig. 1.20(b) shows the calculated I_1 using the equivalent circuit and it agreed with the measured one. I_2 is difficult to measure in experiment due to impulse with infinite peak and duration. The study revealed that charging and discharging I_1 of C_1 exerts the dominant influence on the discharge energy, when C_1 is significantly larger than C_2.

Later, Koyano [59] used their theory and investigated the influence of C_1 and L on I_1 as shown in Fig. 1.21 and 1.22, respectively. The analysis was performed using $R_0=1\Omega$, $C_1=100$pF, $E_o=100$V, and $u_e=20$V. It is clear that I_1 increases with C_1. It was also found that peak decreases and duration increases with increasing L.

Influence of the stray capacitance was investigated by Yang et al. [60]. Using the same theory, they investigated the influence of measurement using oscilloscope because the voltage probe has its own capacitance and resistance [61]. It was found that the influence of the probe cannot be ignored when C_1 and C_2 are equivalent to the capacitance of the voltage probe of 8pF.
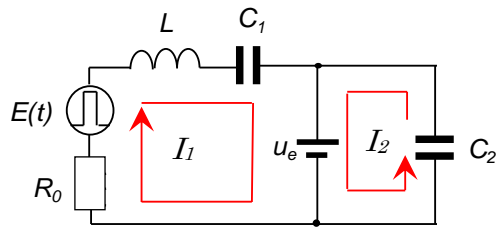
a) Equivalent circuit
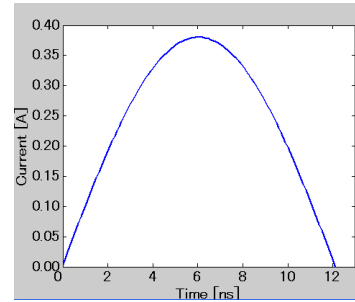
b) Calculated current, I_1

Fig. 1.20: Analysis of inductance, L on discharge current waveform [52]

Fig. 1.21: Influence of C_1 on discharge current [59]
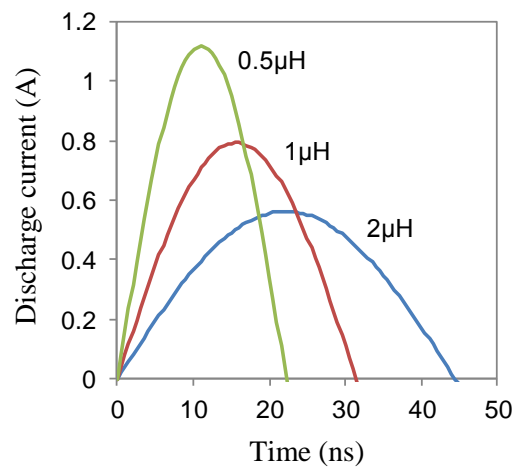
Fig. 1.22: Influence of L on discharge current [59]

1.3.3   Advantages of EIFM Compared to RC circuit

In RC circuit, capacitor is charged by the DC source voltage through a resistor. When the dielectric strength between tool electrode and workpiece breaks down, the charge in the capacitor flows through the gap. To achieve higher machining speed, the feed speed 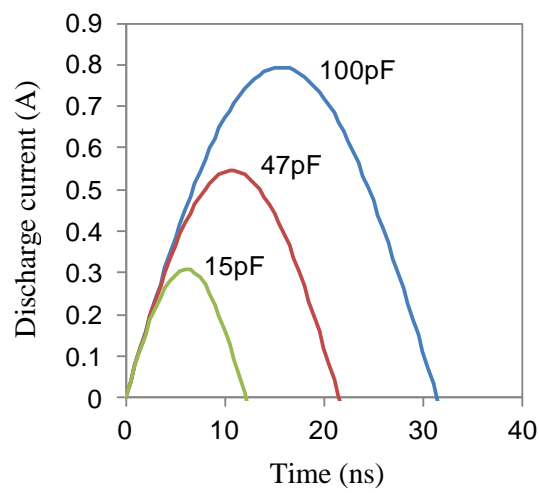of the tool electrode can be increased in order to increase discharge frequency. However, when the feed speed is increased, there is high possibility that the next discharge occur before the capacitance is fully charged [55]. It is important for the dielectric strength to recover after every discharge so that the temperature at the discharge point can be reduced and discharge spot can be shifted to different location. However, if the plasma generated by the previous discharge is not properly extinguished, the next discharge will occur at the same location [7,62]. This concentration of discharge causes the uneven distribution of discharge point and the surface temperature of the electrodes will increase leading to abnormal arc. The abnormal arc does not help in material removal leading to the decrease in the machining speed. On the other hand, in the case of EIFM, since only one discharge can occur for each half cycle of the periodic pulse voltage, the discharge gap can be cooled regularly during the discharge interval. Localized discharge and abnormal arc are less likely to occur resulting in stable machining [34,55].

Diameter of discharge crater has a substantial influence in producing parts in micro scale [32]. Thus, parts with size smaller than the crater size is difficult to be achieved. Investigation on the miniaturization of micro EDM shows that minimum discharge energy smaller than that of RC circuit can be achieved with EIFM [56]. As a result, probability to produce micro rods with diameter thinner than 2.0μm was two times higher than RC circuit. Fig. 1.23 shows the rod with 0.8μm diameter which was machined using EIFM.

Fig.1.23: Minimum rod diameter machined with EIFM [56]

In micro EDM, tool is rotated to flush debris from the machining gap. It is also effective to promote the reduction of the tempe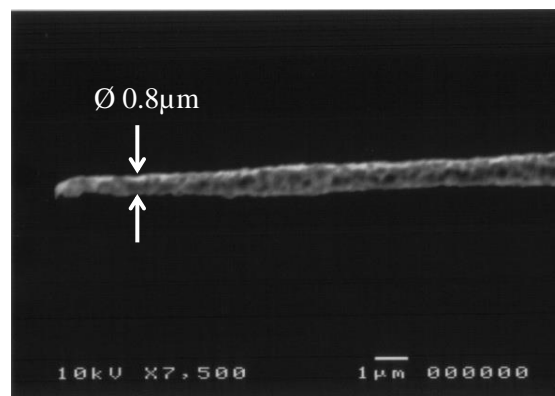rature on the tool electrode surface due to the flow of the working fluid. With this, machining stability can be achieved because localized discharge and abnormal arc can be avoided. Zhang et al. [63] drilled fine hole using RC circuit and investigated the influence of tool electrode rotation speed. It was found that machining speed was 6 times higher with the tool electrode rotated at 15000 rpm compared to 1000rpm. Koyano et al. [64] calculated the distribution of discharge location on the periphery of a cylindrical tool electrode. It was found that the interval between discharge locations increases with increasing the tool electrode rotation as shown in Fig. 1.24. With this, localized temperature can be reduced resulting in better machining stability. Hence, it is considered that MRR can be increased with increasing the tool electrode rotation.

Tool electrode surface   Discharge point

(a) 1000rpm   (b) 20000rpm   (c) 50000rpm
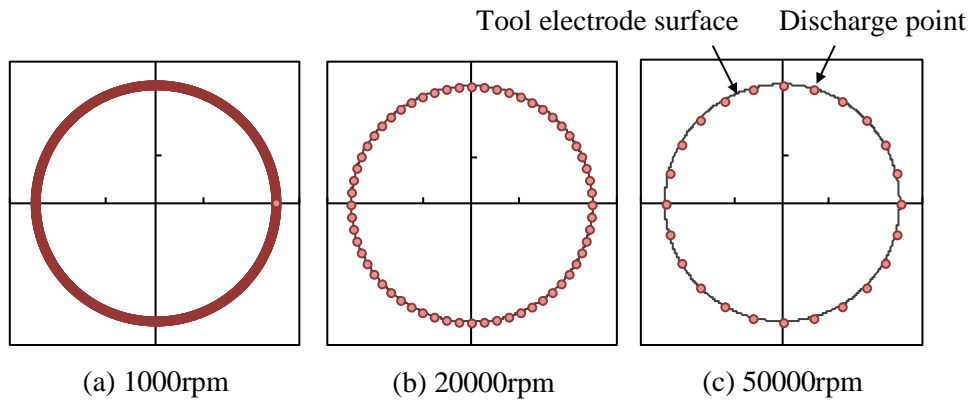
Fig. 1.24: Distribution of discharge locations [64]

With the RC circuit however, the power supply must be connected to the tool electrode using brush in order to rotate the spindle. This limits the rotation speed of the tool electrode because rotating the tool at very high speed can cause vibration and heating influencing the machining accuracy. In the case of EIFM, a pulse power supply is connected to the tool electrode by C_1. Thus, by fixing a cylindrical feeding electrode coaxially to the tool electrode holder (mandrel), capacitance can be formed in the gap between the two electrodes. With this, electrical feeding to the tool can be done without contact [50]. Fig. 1.25 shows the schematic diagram of non-contact electrical feeding. The tool electrode can be rotated at very high speed up to 50,000rpm using a motorized spindle without any problems related to vibration and heating, and MRR increases with increasing the rotation speed as shown in Fig 1.26 [65]. At high speed tool electrode rotation, debris can be removed efficiently from the discharge gap and the surface of the tool electrode can be cooled. As a result, better machining accuracy [66], better straightness, hole with high aspect ratio and lower tool wear ratio can be achieved [67].

These characteristics are important in producing products with deep micro holes such as fuel injection nozzle and turbine blade as shown in Fig. 1.27 and Fig.1.28 the respectively.

Fig. 1.25: Schematic diagram of non-contact electrical feeding

Fig. 1.26: Relationship between material removal rate and tool electrode rotation [64]
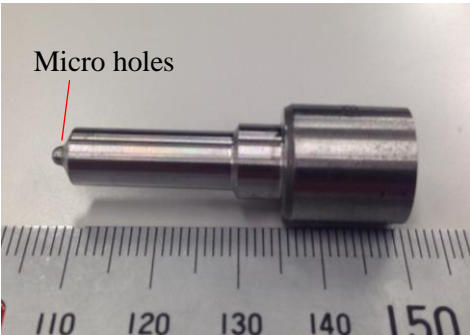
Fig. 1.27: Fuel injection nozzle
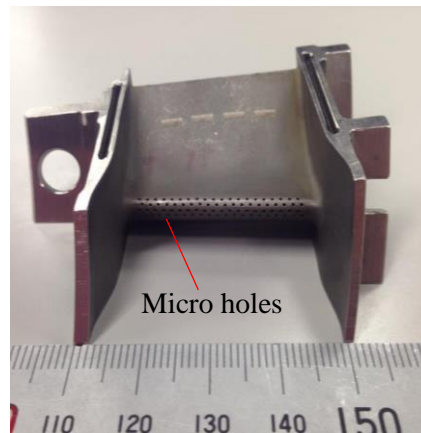
Fig. 1.28: Turbine blade

1.4 Purpose of the study

With EIFM, discharge concentration and abnormal arc can be eliminated because only one discharge can occur during the half cycle of the pulse power supply. Hence, stable machining can be achieved leading to higher machining speed compared to RC circuit. In EIFM, since the electrical feed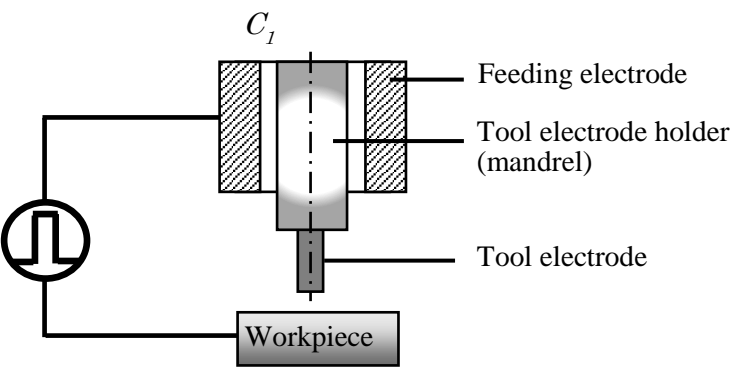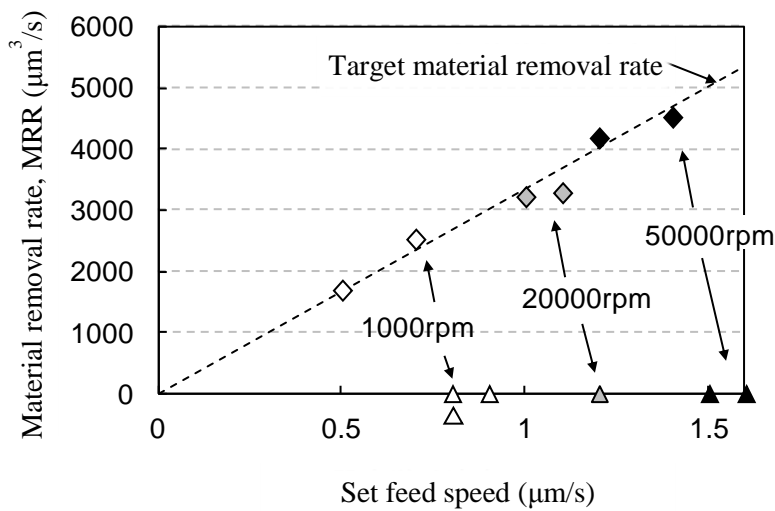ing can be performed without contact, tool can be rotated at a higher speed and material removal rate increases with increasing the rotation speed. This method can be employed in drilling deep micro holes where tool with high aspect ratio is used; for example in the application to the drilling of turbine blades or fuel injection nozzles.

This work is a continuity from the previous research aiming to achieve a complete machining process: from roughing to finishing, using the same pulse generator with non-contact electrical feeding. With conventional EIFM however, the material removal is extremely small when the machining is performed with non-contact electrical feeding. This is because, the capacitance formed in the gap of the non-contact feeding was only 16.3pF leading to small discharge energy which is suitable only for finishing process in micro machining. The small discharge energy results in low machining speed. Fig. 1.29 shows the experimental setup. The length of the feeding electrode was only 5mm and the gap between the feeding electrode and the tool electrode holder was 50μm. By increasing the discharge frequency, higher machining speed can be obtained. However, the discharge frequency cannot be increased without a limit with this method, because of the reason presented in Chapter 2. In addition, capacitance cannot be increased significantly by increasing the length of the feeding electrode, because long feeding electrode may also cause run-out error of the tool electrode rotation. The gap width between the feeding electrode and the tool electrode holder (mandrel) cannot be decreased smaller than 50μm because of the risk of electric discharge in the feeding gap.
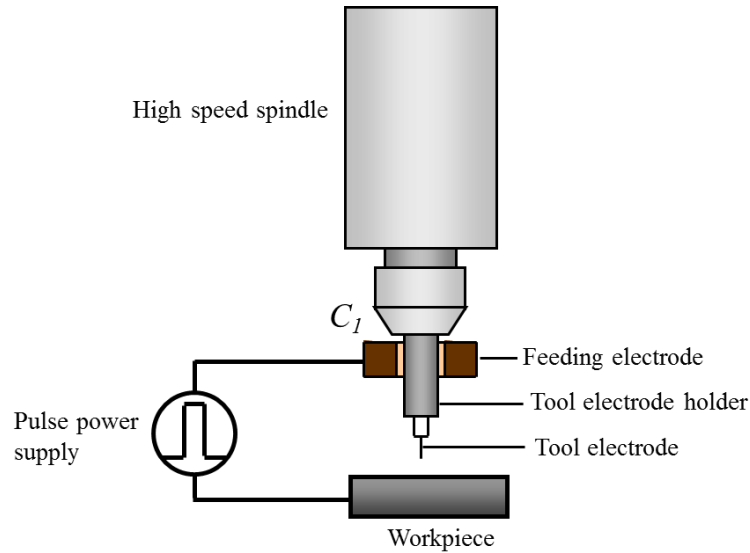
Fig. 1.29: Non-contact micro EDM with high speed tool electrode rotation

Therefore, this study aims to increase discharge energy and enlarge the unit removal per discharge for non-contact electrical feeding of EIFM. Since the feeding capacitance is fixed by the configuration and size of the feeding electrode, the discharge energy cannot be changed arbitrarily in EIFM. Hence, this study also aims to develop a method to control discharge energy arbitrarily using the same feeding capacitance. To achieve this, three methods were proposed. The first method is called controlled pulse train method (CPTM). The idea of the pulse train method (PTM) was first introduced by Niwa [54] where a high frequency AC voltage of 13.5MHz was supplied through a capacitance to a rotating tool electrode. However, the occurrence of continuous AC discharges was not supported by any machining results or current waveforms for verification. Moreover, the duration of the AC voltage was fixed. Hence, actual AC discharge duration was not kept constant, resulting in varied discharge crater diameter. This is because, discharge delay time is always varied significantly. Then, Yahagi et al. [68] found that larger craters can be obtained from the PTM. However, machining was difficult because the tool electrode was fed manually and was not rotated. Moreover, the duration of the AC discharge was not controlled to be constant in their study either.

With CPTM on the other hand, high frequency voltage is intermittently supplied to the gap. Once discharge ignition is detected, it is allowed to continue during a predetermined time defined as pulse train duration permitting plural discharges to occur consecutively at the same location. Thus, even if a small feeding capacitance is used, larger discharge crater and higher material removal can be achieved. Furthermore, the discharge energy can be controlled arbitrarily using the same feeding electrode by changing the pulse train duration. To realize the idea, an additional circuit was developed

and used together with the circuit of EIFM.

To obtain better discharge continuity within the predetermined pulse train duration, discharge energy per individual pulse must be increased. In Section 1.3.2, it was discussed that discharge energy can be increased with increasing open voltage, u_o and capacitance, C_1; according to Eq. 1.14. Since capacitance, C and inductance, L exist in the circuit, the resonance in the circuit can be utilized in increasing the discharge energy. This is because impedance can be minimized at this condition. It is known that C stores energy in electric field and L stores energy in magnetic field. When the pulse power supply is applied to the circuit, oscillation of AC voltage can be observed in the discharge gap due to the exchange of energy between C and L. The amplitude of oscillation depends on the size of C and L. Thus, the increase in u_o can be used to increase the discharge energy and the machining speed.

In the non-contact electrical feeding method, a feeding electrode is fixed coaxially to the mandrel. Small capacitance C_1 can be formed in the gap between the two. However, the C_1 is very small causing discharge discontinuity within the pulse train duration. Even if u_o is increased, the discharge continuity within the pulse train duration does not show significant improvement. Since discharge energy can be increased by increasing C_1, a new configuration of feeding electrode is proposed. Larger C_1 can be obtained by increasing the area where capacitance can be formed. The findings of this study can also be applied not only in sinking EDM but also wire EDM where a preliminary investigation on wire EDM with EIFM was performed by Koyano [69].

1.5 Organization of the Thesis

Chapter 1 introduces the characteristics of EDM processes, and the differences between macro and micro EDM are highlighted. Different types of pulse generator for micro EDM were presented. Advantages of EIFM as the pulse generator over the RC circuit were highlighted. In the end, the purpose of the study was clarified.

The principle of CPTM and preliminary investigation on the workability of the idea is discussed in Chapter 2. Using a transparent electrode, the concentration of discharges at the same discharge location is observed to verify the idea of CPTM. The observation also leads to the investigation of deionization time of discharge plasma in micro EDM, compared to that in macro EDM.

In Chapter 3, the influence of pulse train duration on the diameter of discharge craters and material removal was examined. Pulse train duration is the pre-determined time during which the discharge is allowed to continue in CPTM. In addition, comparison on machining characteristics between CPTM and EIFM and also between CPTM and RC

circuit are given.

Method to increase the discharge energy through resonance in circuit is discussed in Chapter 4. Discharge waveforms at different frequencies were observed. Influences of capacitance and inductance on the resonant frequency are presented. Machining characteristics at different frequencies including the resonant frequency are compared.

Methods to increase the feeding capacitance in the non-contact electrical feeding of method are given in Chapter 5. The configuration of the new feeding electrode and the development of the device are explained. With the newly fabricated feeding electrode, the influence of tool electrode rotation speed on the material removal rate is investigated.

Chapter 6 concludes the findings of the studies. Recommendations for future works are also given. At the end of the thesis, the acknowledgements and list of papers published through this work are given.

1.6 References

1. K.P. Rajurkar, Edited by Richard C. Dorf and Andrew Kusiak, 1994, Chapter13: Nontraditional Manufacturing Processes, Handbook of Design, Manufacturing and Automation. USA: John Wiley and Sons.
2. Geoffrey Boothroyd and Winston A. Knight, 1989, Fundamental of Machining and Machine Tools, 2nd Edition. New York: Marcel Dekker Inc.
3. Shankar Singh, S. Maheshwari, P.C. Pandey, 2004, Some investigations into the electric discharge machining of hardened tool steel using different electrode materials, Journal of Materials Processing Technology, vol. 149, pp. 272 - 277.
4. J.A. McGeough, 1998, Advanced Methods of Machining. London: Chapman and Hall.
5. Eric Oberg, Franklin D. Jones, Halbrook L. Horton and Henty H. Ryffel, 2004, Machinery's Handbook 27th Edition. New York: Industrial Press Inc.
6. Li Li, Y.S. Wong, J.Y.H. Fuh, Li Lu, 2001, Effect of TiC in copper-tungsten electrodes on EDM performance, Journal of Material Processing Technology, vol. 113 pp. 563-567.
7. Kunieda M., Lauwers B., Rajurkar K.P. and Schumacher B.M., 2005 Advancing EDM Through Fundamental Insight into the Process, Annals of the CIRP, vol. 54, no. 2, pp. 64-87.
8. S. Tariq Jilani and P.C. Pandey, 1984, Experimental investigations into the performance of water as dielectric in EDM, International Journal of Machine Tool Design and Research, vol. 24, pp 31-43.
9. Konig W. and Siebers F. J., 1993, Influence of the working medium on the removal process in EDM sinking, American Society of Mechanical Engineers, Production

Engineering Division (Publication) PED 64, pp. 649-658.

10. M. Kuineda, M. Yoshida, 1997, Electrical discharge machining in gas, CIRP Annals-Manufacturing Technology, vol.46, 143-146.

11. Y. Shen, Y. Liu, W. Sun, 2016, High-efficient dry hybrid machining of EDM and arc machining, 18th CIRP Conference on Electro Physical and Chemical Machining (ISEM XVIII), Procedia CIRP 42, 149-154.

12. Masuzawa T., 2000, State-of-the-art in micro machining, Annals of the CIRP, vol. 49, no. 2, pp. 473-488.

13. K.H. Ho and S.T. Newman, 2003, State of the art electrical discharge machining (EDM), International Journal of Machine Tools & Manufacture, vol. 43, pp. 1287-1300.

14. Katsushi Furutani, Akinori Saneto, Hideki Takezawa, Naotake Mohri and Hidetaka Miyake, 2001, Accretion of titanium carbide by electrical discharge machining with powder suspended in working fluid, Journal of the International Societies for Precision Engineering and Nanotechnology, vol. 25, pp. 138-144.

15. J. Simao, H.G. Lee, D.K. Aspinwall, R.C. Dewes and E.M. Aspinwall, 2003, Workpiece surface modification using electrical discharge machining, International Journal of Machine Tools and Manufacture, vol. 43, pp. 121-128.

16. A. Kojima, W. Natsu and M. Kunieda, 2008, Spectroscopic measurement of arc plasma diameter in EDM, Annals of the CIRP, vol. 57, pp. 203-207.

17. Hidehumi Yoshida and Masanori Kunieda, 1996, Determination of arc plasma temperature in EDM process by spectroscopic analysis, Journal of Precision Engineering, vol 62, no. 10, pp. 1464-1468, (in Japanese).

18. P. K. Eckman and E. M. Williams, 1960, Plasma Dynamics in an arc formed by low-voltage spark over of a liquid dielectric, Applied Science Research, Sec. B, vol. 8, pp. 299-320.

19. Philip T. Eubank, Mukund R. Patel, Maria A. Barrufet and Bedri Bozkurt, 1993, Theoretical models of the electrical discharge machining process. III. The variable mass, cylindrical plasma model, Journal of Applied Physics, vol. 73, no. 11, pp. 7900-7909.

20. F. S. Van Dijck, 1973, Physico-mathematical analysis of the electro discharge machining process, Dissertation of Katholieke Universiteit Leuven.

21. X. Yang, J. Guo, X. Chen, M. Kunieda, 2011, Molecular dynamics simulation of the material removal mechanism in micro-EDM, Precision Engineering, vol. 35, no. 1, pp. 51-57.

22. Shinya Hayakawa, Hiroyuki Kojima, Masanori Kunieda, Nobuhiko Nishiwaki, 1996, Influence of plasma extinction on machining stability in EDM process, Journal of the Japan Society for Precision Engineering, vol. 62, no. 5, pp. 686-690 (in Japanese).

23. Shinya Hayakawa, Heng Xia, Masanori Kunieda, Nobuhiko Nishiwaki, 1996, Analysis of time required to deionize an EDM gap during pulse interval, Symposium on Molecular and Micro Scale Heat Transfer in Materials Processing and Other Applications, pp. 368-377.

24. T. Masuzawa, 2001, Micro EDM, The 13th Proceedings of The International Symposium on Electromachining (ISEM XIII), vol. 1, pp. 3-19.

25. E. Uhlmann, and D. C. Domingos, 2013, Investigations on vibration-assisted EDM-machining of seal slots in high-temperature resistant materials for turbine components The 17th CIRP Conference on Electro Physical and Chemical Machining (ISEM XVII), Procedia CIRP 6, pp. 71-76.

26. C. Diver, J. Atkinson, H.J Helml, L.Li, 2004, Micro-EDM drilling of tapered holes for industrial applications, Journal of Materials Processing Technology, vol. 149, pp. 296-303.

27. Tong Hao, Li Yong, Zhang Long and Li Baoquan, 2013, Mechanism design and process control of micro EDM for drilling spray holes of diesel injector nozzles, Precision Engineering, vol. 37, pp. 213-221.

28. Z.Y. Yu, T. Masuzawa, M. Fujino, 1998, Micro-EDM for three-dimensional cavities-development of uniform wear method, Annals of the CIRP, vol. 47, no.1, pp. 169-172.

29. Maradia U., Boccadoro M., Stirnimann J., Beltrami I., Kuster F., Wegener K., 2012, Die-sink EDM in meso-micro machining, Fifth CIRP Conference on High Performance Cutting 2012, Procedia CIRP, no. 1, pp. 166-171.

30. Muttamara A., Fukuzawa Y., Mohri N., Tani T., 2003, Probability of precision micro-machining of insulating Si3N4 ceramics by EDM, Journal of Materials Processing Technology, vol. 140, no. 1-3, pp. 243-247.

31. Kawakami T., Kunieda M., 2005, Study on factors determining limits of minimum machinable size in micro EDM, Annals of the CIRP, vol. 54, no. 1, pp. 167-170.

32. Fuzhu Han, Yuji Yamada, Taichi Kawakami and Masanori Kunieda, 2013, Investigations on feasibility of sub-micrometer order manufacturing using micro EDM, The Proceedings of American Society of Precision Engineering (ASPE) Annual Meeting, vol. 30, pp. 551-554.

33. Klocke F., Lung D., Noethe T., 2001, Micro contouring by EDM with fine wires, The 13th Proceedings of The International Symposium on Electromachining (ISEM XIII), vol. 13, pp. 767-779.

34. Masanori Kunieda, 2008, Challenges to miniaturization in micro EDM, Proceeding of the 23rd Annual Meeting of the ASPE and 12th ICPE, October 19-24, Portland.

35. Uhlmann E., Piltz S., Doll U., 2005, Machining of micro/miniature dies and moulds by electrical discharge machining - Recent development, Journal of Materials Processing Technology, vol. 167, no. 2-3, pp. 488-493.

36. Xia H., Kunieda M., and Nishiwaki N., 1996, Removal amount difference between anode and cathode in EDM process, International Journal of Electrical Machining, no. 1, pp. 45-52.

37. Motoki M., Higashiguchi K., 1967, Energy distribution at the gap in electric discharge machining, CIRP Annals – Manufacturing Technology, vol.14, pp. 485-489.

38. Heng Xia, Hiroaki Hashimoto, Masanori Kunieda, Nobuhiko Nishiwaki, 1996, Measurement of energy distribution in continuous EDM process, Journal of Japan Society of Precision Engineering, vol. 62, no. 8, pp. 1141-1145 (in Japanese).

39. Mohd Zahiruddin and Masanori Kunieda, 2010, Energy distribution ratio into micro EDM electrodes, Journal of Advanced Mechanical Design, Systems, and Manufacturing, vol.4, no.6, pp. 1095-1106.

40. Hayakawa S., Yuzawa M., Kunieda M., Nishiwaki N., 2001, Time variation and mechanism of determining power distribution in electrodes during EDM process, International Journal of Electrical Machining, no. 6, 19-26.

41. Mohd Zahiruddin, 2015 Doctoral Thesis, Fundamental research with respect to thermal phenomena of micro EDM, The University of Tokyo.

42. Mohd Zahiruddin and Masanori Kunieda, 2012, Comparison of energy and removal efficiencies between micro and macro EDM, CIRP Annals – Manufacturing Technology, vol. 61, no. 1, pp. 187-190.

43. Meek J. M., Craggs J. D., 1978, Electric breakdown of gases, John Wiley & Sons.

44. Kenji Morimoto and Masanori Kunieda, 2009, Sinking EDM simulation by determining discharge locations based on discharge delay time, CIRP Annals – Manufacturing Technology, vol. 58, pp. 221-224.

45. B.M. Schumacher, 1990, About the role of debris in the gap during electrical discharge machining, Annals of the CIRP, vol. 39, no. 1, pp. 197-199.

46. B. Bommeli, C. Frei, A. Ratajski, 1979, On the influence of mechanical perturbation on the breakdown of a liquid dielectric, Journal of Electrostatics, vol. 7, pp. 123-144.

47. T. Masuzawa, 2001, An overview of Micro EDM, Journal of Electrical Processing, vol. 35, no. 80 pp. 5-20 (in Japanese).

48. Koichi Kawata, Takeo Sato, Takeshi Masaki and Takahisa Masuzawa, 1994, Study on micro EDM (1st Report) – Feasibility study, Journal of Japan Society of Electrical Machining Engineers, vol. 28, no. 57, (in Japanese).

49. K. Egashira, K. Mizutani, 2005, EDM at low open-circuit voltage, International Journal of Electrical Machining, no. 10, pp 21-25.

50. M. Kunieda, A. Hayasaka, X. D. Yang, I. Araie, 2007, Study on nano edm using capacity coupled pulse generator, Annals of the CIRP, vol. 56, no. 1, pp. 213-216.

51. Michihiro Hanada, Masanori Kunieda and Ichiro Araie, 2006, Development of micro EDM using electrostatic induction feeding, Precision Engineering Journal, vol. 72, no.5, pp. 636-640 (in Japanese).

52. M. Kimori, M. Kunieda, S. Sano, 2007, Mechanism of determining discharge energy in electrostatic induction feeding EDM, Proceeding of Asian Electrical Machining Symposium '07, pp. 242-245.

53. Xiaodong Yang, Masanori Kunieda and Sadao Sano, 2007, Study on influence of stray capacitance on micro EDM using electrostatic induction feeding, Proceeding of Asian Electrical Machining Symposium AEMS'07, Nagoya, Japan, pp. 236-241.

54. Yoshie Niwa, 1977, Grinding machining using high frequency arc discharge, Japan Society of Electrical Machining Engineers (JSEME) Research Meeting, no. 86, pp. 9-11 (in Japanese).

55. Tomohiro Koyano, Masanori Kunieda, 2010, Achieving high accuracy and high removal rate in micro-EDM by electrostatic induction feeding method, Annals of the CIRP, vol. 59, issue 1, pp. 219-222.

56. M. Kimori and M. Kunieda, 2006, Miniaturization of micro EDM using electrostatic induction feeding method, Precision Engineering Journal, vol. 76, no.10, pp. 1151-1155 (in Japanese).

57. Xiaodong Yang, 2007, Analysis on properties of micro electric discharge machining circuit using electrostatic induction feeding, Kunieda laboratory internal meeting report on 20 July 2007 (in Japanese).

58. Xiaodong Yang, 2006, Theoretical analysis of the electrostatic induction power supply, Kunieda laboratory internal meeting report no. 1 on 6 January 2006 (in Japanese).

59. Tomohiro Koyano, 2013, Research on micro electromachining using electrostatic induction feeding method, Doctoral Thesis, The University of Tokyo (in Japanese).

60. Xiaodong Yang, Masanori Kunieda and Sadao Sano, 2008, Study on influence of stray capacitance on micro EDM using electrostatic induction feeding, International Journal of Electrical Machining, no. 13, pp. 35-40.

61. Xiaodong Yang, 2006, Impact oscilloscope and probe of the electrostatic induction power supply electro-discharge machining, Kunieda laboratory internal meeting report no. 3 on 1 May 2006 (in Japanese).

62. M. Kunieda, H. Kojima, 1990, On-line detection of EDM spark locations by multiple connections of branched electric wires, Annals of CIRP, vol. 39, no. 1, pp. 171-174.

63. Y. Zhang, H. Zhao, G. Zhang, Z. Wang, W. Zhao, 2008, Research on a micro-EDM system and its techniques, Journal of China Mechanical Engineering, vol. 5, no. 19, pp. 526-530, (in Chinese).

64. Tomohiro Koyano, Yuna Yahagi, Masanori Kunieda, Xiaodong Yang, 2010, High spindle speed micro EDM using electrostatic induction feeding method, Proceedings of the 16th International Symposium on Electromachining, pp. 599-602.

65. Yuna Yahagi, Tomohiro Koyano, Masanori Kunieda, and Xiaodong Yang, 2010, High speed spindle wire electrical discharge grinding using electrostatic induction feeding method, Key Engineering Materials, vol 447-448, pp. 268-271.

66. Yuna Yahagi, Tomohiro Koyano, Masanori Kunieda, and Xiaodong Yang, 2011, High spindle speed micro EDM using electrostatic induction feeding method, Journal of Precision Engineering, vol.77, no. 4, pp. 394-399 (in Japanese).

67. Yuna Yahagi, Tomohiro Koyano, Masanori Kunieda and Xiaodong Yang, 2012, Micro drilling EDM with high rotation speed of tool electrode rotation using electrostatic induction feeding method, 5th CIRP Conference on High Performance Cutting 2012, Procedia CIRP 1, pp. 168-171.

68. Yuna Yahagi, Wataru Natsu, Masanori Kunieda, 2012, Control of discharge energy in electrostatic induction feeding EDM using high frequency discharge, Proceeding Spring Meeting of The Japan Society for Precision Engineering (JSPE), pp. 125-126 (in Japanese).

69. Tomohiro Koyano, 2008, Research on wire EDM using electrostatic induction feeding method, Bachelor Degree Thesis, Tokyo University of Agricultural and Technology (in Japanese).

(This page is intentionally left blank)

# Chapter 2

Controlled Pulse Train Method (CPTM)

In micro EDM using electrostatic induction feeding method (EIFM) as the pulse generator, the use of low pulse frequency between 0.2-1MHz [1-4] during machining allows sufficient time for dielectric strength to recover and to promote machining stability. Material removal rate (MRR) can be increased by increasing the frequency. However, by increasing the frequency, there is a limit of maximum material removal. Thus, the idea and principle of EIFM with controlled pulse train method (CPTM) is introduced. This method allows discharges to occur consecutively at the same location within a pre-determined time defined as pulse train duration. Initial investigations are done to examine the workability of the idea by identifying the relationship between the diameter of craters and the pulse train duration. To prove that the discharges are concentrated at the same location when CPTM is utilized, observation through a transparent electrode using a high speed video camera is performed. From now on, the EIFM method is also called as the conventional electrostatic induction feeding method or conventional EIFM.

## 2.1 Principle of Controlled Pulse Train Method (CPTM)

In the conventional EIFM, the feeding capacitance, C_1 determines the discharge energy [5,6]. When machining is done at low pulse frequency, the bipolar discharge can occur at every half cycle causing the craters to be scattered at different locations for every discharge. This is because, there is enough time for dielectric strength to recover between intermittent discharges. The illustration of this condition is shown in Fig. 2.1(a). Increasing the frequency of the pulse power supply, the discharge frequency is elevated which results in the increment in material removal rate (MRR). However, if the frequency is increased higher than a certain limit, discharge cannot occur in every half cycle of the pulse as shown in Fig. 2.1(b).

35
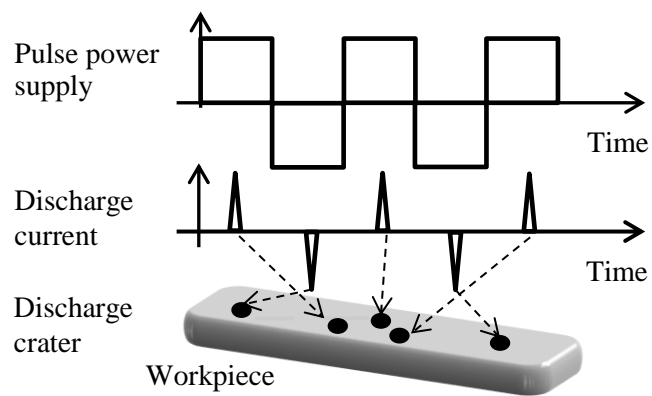
a) Conventional method
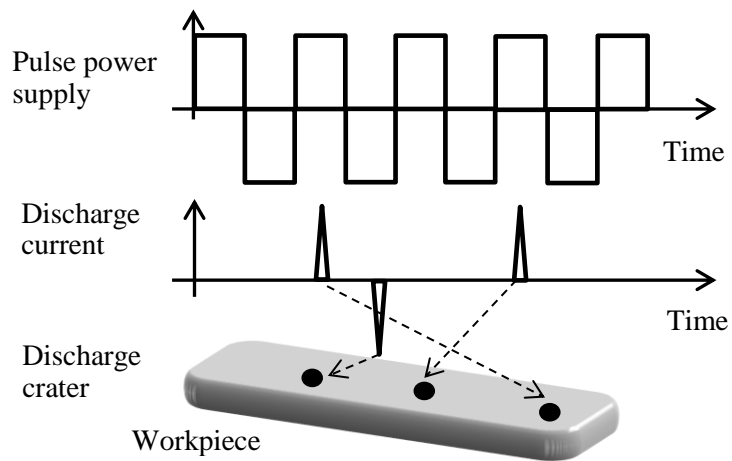
b) At higher frequency
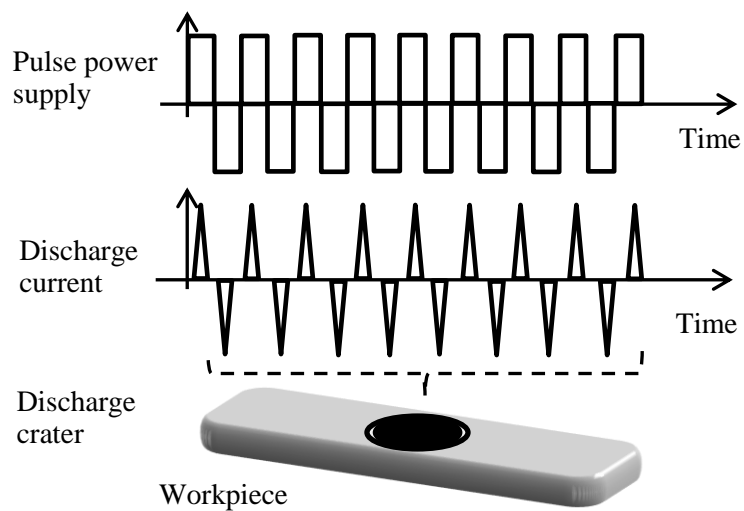
c) At very high frequency without interval time

Fig. 2.1: Discharge current using conventional electrostatic induction feeding method

This is because discharge delay time is necessary for discharge to ignite. The average discharge delay time depends on the gap width and contamination in the gap which statistically obeys the exponential distribution [7] as described in Section 1.2.2. Thus, at the high frequency discharge cannot occur at every half cycle of the pulse because the pulse duration becomes shorter than the discharge delay time causing reduction in MRR. Moreover, if the pulse frequency is increased further, there will be no interval time sufficient for the dielectric breakdown strength to recover. Arcing pulses can occur due to contamination in the gap during continuation of high frequency discharge, and also due to incomplete deionization. The arcing pulses do not help in removing the workpiece. In addition, once discharge is ignited, very large crater will be generated at only one location, which will damage the machined surface as presented in Fig. 2.1(c). An experiment on limitation of MRR by increasing the frequency was performed and is presented in Section 2.2.

To solve the problem, CPTM was introduced in order to increase the discharge energy or to increase the removal volume per discharge. Even though the same small capacitance C_1 used in conventional EIFM is being applied in CPTM, higher discharge energy can be obtained in CPTM because high frequency alternating current (AC) pulse discharge is maintained without interruption within a fixed pulse train duration. The idea of the pulse train method was first introduced by Niwa [8]. A high frequency AC current of 13.5MHz was supplied to a rotating disk electrode through a capacitance during an electrical discharge grinding. However, the pulse train was not kept at a constant duration and the discharge current was not controlled. Furthermore, the occurrence of continuous AC discharges was not supported by any machining results or current waveforms for verification.

Later, Yahagi et al. [9] investigated a method to increase discharge energy in EIFM by using the high frequency pulses. It was found that discharge energy can be accumulated at the same location. In addition, larger diameter of craters and higher material removal can be achieved when machining is performed at higher frequency although the same C_1 was used. Fig. 2.2 shows the machined hole and cross sectional shape at different frequencies using this method. However, they found that even if high frequency voltage pulses were supplied intermittently with a constant duration, discharge ignition is usually delayed because a time is needed for discharge to be ignited. Therefore, the duration of the train of pulse discharges was not constant.
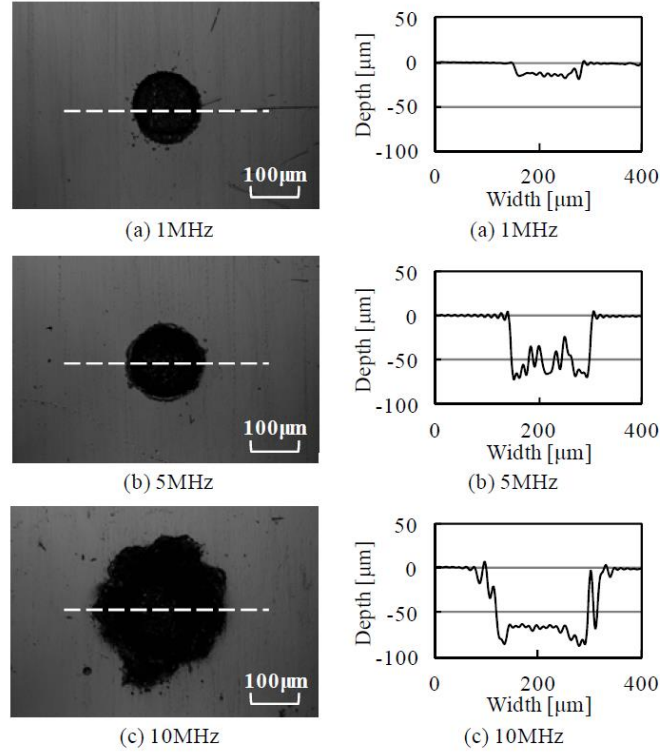
Fig. 2.2: Machined hole and cross sectional shape at different frequencies using tool electrode 125μm in diameter [9]

Li et al. [10] developed a multi-mode pulse power supply in order to obtain different ranges of energy. Five pulses with a high frequency were supplied intermittently with a regular cycle. The objective was to achieve high discharge current and short discharge duration in order to improve surface roughness and machining efficiency of arrayed micro holes. Hence, the purpose of this method is different from the present work where AC pulse discharge continues to occur at the same spot.

Based on the preliminary study on PTM by Niwa [8] and Yahagi et al. [9], it was found that controlling the duration of high frequency discharges is important, and a method to control the discharge duration must be introduced. This is because, the uncontrolled discharges will result in different crater size and influence the surface roughness. In addition, if the discharges occur at the same location for a long duration, it will damage the machined surface. Therefore, this study introduced a method to allow multiple discharges to occur within a constant discharge duration so that similar crater size can be achieved. In addition, since a pulse interval is given in between the discharge durations, discharge location can be shifted after a certain duration. This is important for stable machining and preventing the machined surface from being damaged. Fig. 2.3 shows the illustrated idea of CPTM which was proposed to extend the limit of MRR in

38

conventional EIFM. The idea was realized by adding one-shot multivibrator and switching circuit to the machining system as shown in Fig. 2.4.

In this method, high frequency voltage is intermittently supplied to the gap. Once discharge ignites, it is detected by the current sensor. The current sensor then sends a signal to one-shot multivibrator circuit to allow discharges to continue within a controlled pulse train duration. The one-shot multivibrator circuit was used because it can generate an output pulse corresponding to the pre-determined time and the circuit will automatically switch back to the original stable state and will remain there until another pulse is applied. The pulse train is a group of discharges which is allowed to occur within the pre-determined time. With this, a number of discharges can occur at the same location. After the end of the pre-determined time, a signal is sent to the switching circuit to stop the pulse power supply within another pre-determined time which is called pulse train interval. During this time, dielectric strength can be recovered. After that, the pulse power supply is switched on again. Then, the cycle is reiterated. The next discharge can occur at a different location. Hence, higher discharge energy and larger crater size than those generated by individual pulse discharge using the conventional method can be obtained even with the same small feeding capacitance, C_1.
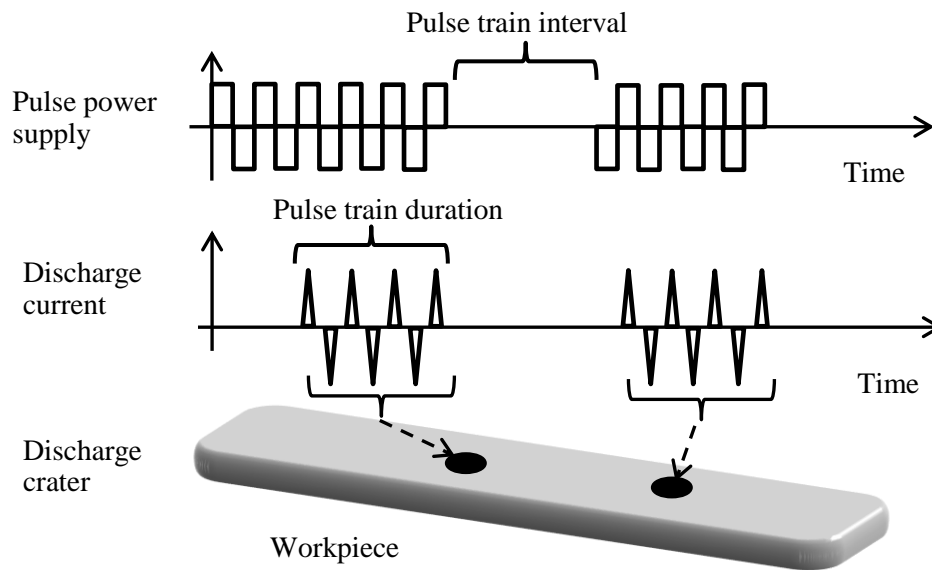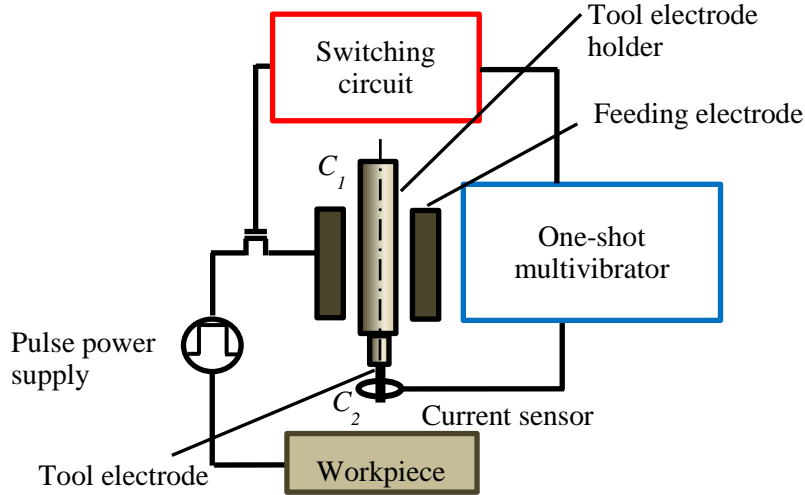

Fig. 2.3: Controlled pulse train method

39

Fig. 2.4: Machining system for CPTM

Although Niwa [8] and Yahagi et al. [9] proposed the PTM with the pulse interval between the discharges, the pulse train duration was not controlled. By supplying constant high frequency pulses within a constant duration, number of discharges during the durations may not be the same due to the ignition delay time. On the other hand, since the pulse train duration and pulse interval are controlled to be constant with this method, uniform crater size and better material removal can be achieved. The preliminary investigation on the workability of the idea is presented in Section 2.3.

2.1.1 Machining Equipment

In this study, Panasonic (MG-ED72) micro EDM machine as shown in Fig. 2.5 was used. The tool electrode with diameter between 100-300μm was held by the mandrel. As in Fig. 2.6, the mandrel is placed on the V-guide on the z-axis of the machine. The V-guide served as the holder to the mandrel and at the same time permits the mandrel to rotate freely. A rubber belt was used to secure the pulley of the mandrel for positioning and to allow the tool to be rotated during machining. The machine is equipped with wire electrical discharge grinding (WEDG) which was developed by Masuzawa et al. [11]. Principle of WEDG is shown in Fig. 2.7. WEDG is used to machine a micro rod using a wire electrode travelling along the groove of a wire guide. As in the wire EDM process, renewable wire is used as the tool electrode eliminating the problem related to tool electrode wear. Compared to wire EDM, higher machining accuracy can be achieved with WEDG because the wire is supported by the wire guide which eliminates the problem related to wire vibration. After the tool shape is formed, the polarity of the tool is changed to negative. Then, it can be used to produce micro features on a workpiece.
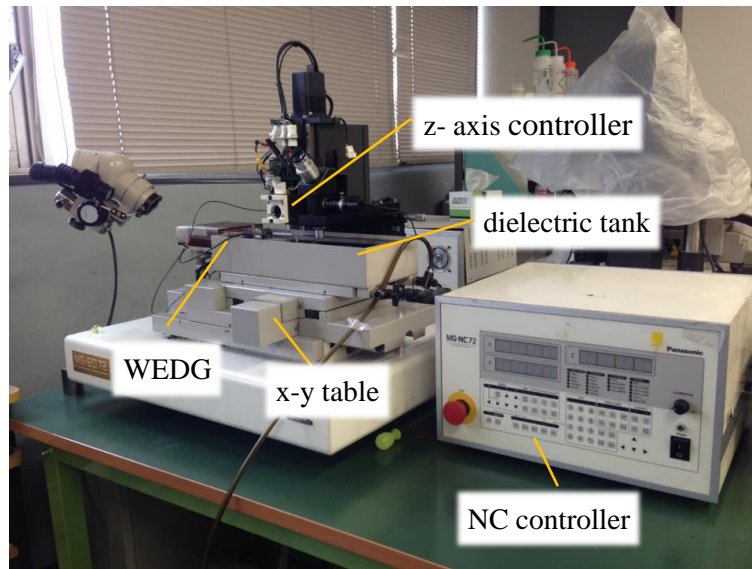
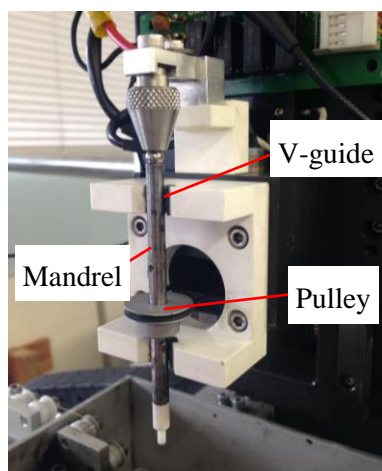Fig. 2.5: Panasonic (MG-ED72) micro EDM machine

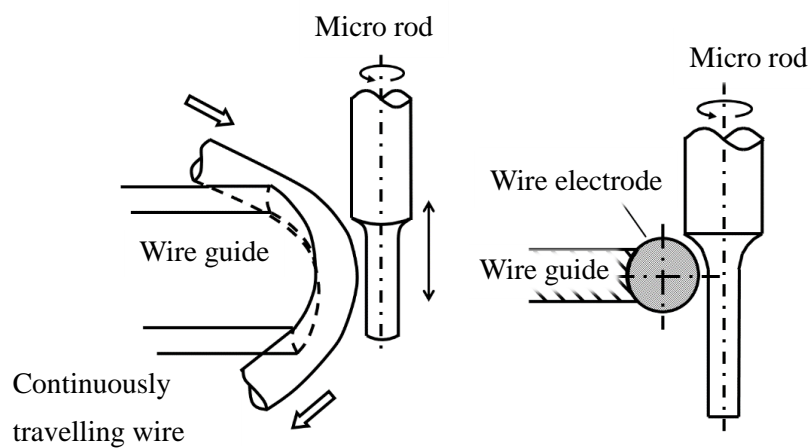Fig. 2.6: Mandrel and mechanism of the tool electrode rotation

Fig. 2.7: Principle of WEDG

2.2 Limitation in Increasing Material Removal Rate (MRR) with Electrostatic Induction Feeding Method (EIFM)

When conventional EIFM is used as the pulse generator for micro EDM, discharge occurs only once for every half cycle of the pulse voltage. With this, localized discharge and abnormal arc can be eliminated because the discharge gap can be cooled during the discharge interval [12-14]. Larger capacitance can be used to increase MRR in conventional EIFM. However, in the application of EIFM with non-contact electrical feeding, capacitance is formed between the feeding electrode and the tool. No capacitor is inserted into the system. Thus, other method should be considered to increase the MRR. Alternatively, MRR can be increased by increasing the frequency of the pulse power supply. However, if frequency of the pulse power supply is increased to increase the MRR, the interval time becomes shorter and time to cool the gap will decrease, leading to machining instability. To prove this, an investigation was performed to examine the maximum MRR in EIFM by increasing the frequency.

The experiment was conducted using the machining setup as shown in Fig. 2.8. To simplify the machining process, the experiment was performed using a capacitance of 470pF which was inserted into the circuit replacing the non-contact feeding electrode. A brush was used to supply the voltage from the pulse power supply to the tool. The tool was rotated at 3000rpm with the machining conditions shown in Table 2.1. In the experiment, a frequency was selected and machining was done by increasing the feed speed at that particular frequency until the maximum MRR was reached. When the feed speed is low, since the gap width is large, the discharge delay time is long. Hence, discharge does not occur at every half cycle of the pulse voltage. Therefore, MRR can be increased with the increase of the feed speed until the discharge frequency becomes equal to the pulse frequency. However, when the feed speed exceeds the maximum MRR, the tool will collide with the workpiece surface, and machining is not possible to continue. Then, another frequency was selected, and the process was reiterated. With this, graphs on relationship between MRR and feed speed at every frequency can be drawn. Finally, the maximum MRR at every frequency was plotted in a graph, and the maximum MRR at different frequency was compared.
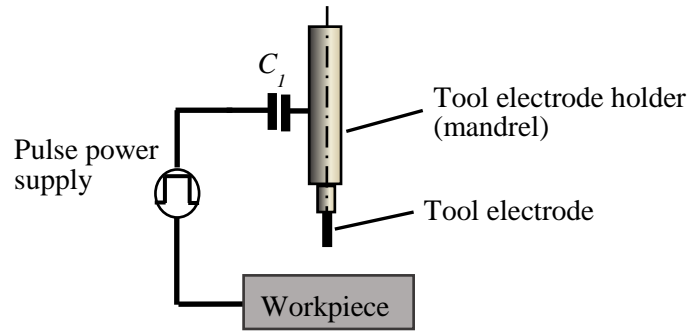
Fig. 2.8: Experimental setup

Table 2.1: Experimental conditions for investigation on maximum limit of MRR using conventional electrostatic induction feeding method

Amplitude of pulse voltage (V)	100
Feeding capacitance, C_1 (pF)	470
Frequency (MHz)	0.5, 1, 2, 3
Electrode (Rod)	Tungsten carbide (Ø = 250μm)
Workpiece	Stainless steel (SUS 304)
Dielectric	EDM oil
Machining time (s)	120

Fig. 2.9(a) shows the relationship between MRR and feed speed when machining was performed at frequency of 0.5MHz. MRR was calculated by dividing the removal volume by machining time. The removal volume was determined by measuring the diameter and depth of machined hole using Olympus confocal laser microscope, OLS3000.

The MRR increased as the feed speed increased, and the highest MRR for the frequency was at $20.541 \times 10^3 \mu m^3/s$ with the feed speed of 0.9μm/s. The MRR decreased after the feed speed of 0.9μm/s. Under a low speed, discharge does not occur at every half cycle of the pulse voltage, while the probability of discharge occurrence increases with increasing the feed speed, resulting in higher discharge frequency. However, the tool will collide with the workpiece when the feed speed exceeds the maximum MRR which can be achieved when discharge occurs at every half cycle of the pulse voltage. For machining with 1MHz, 2MHz and 3MHz, the results are given in Fig. 2.9 (b), 2.9(c) and 2.9(d) respectively. The maximum points from these graphs represent the maximum MRRs of the frequencies. From these maximum points, a graph showing the relationship between the maximum MRR and frequency is tabulated as shown in Fig. 2.10.

In Fig. 2.10, the results show that the maximum MRR as for each frequency peaks at frequency of 2MHz. However, even if the frequency was increased after the maximum

MRR is peaked, the maximum MRR decreased instead. This experiment proved that MRR cannot be increased infinitely with this method. Therefore, the CPTM was proposed, and the preliminary investigation on realizing the idea is explained in the next section.
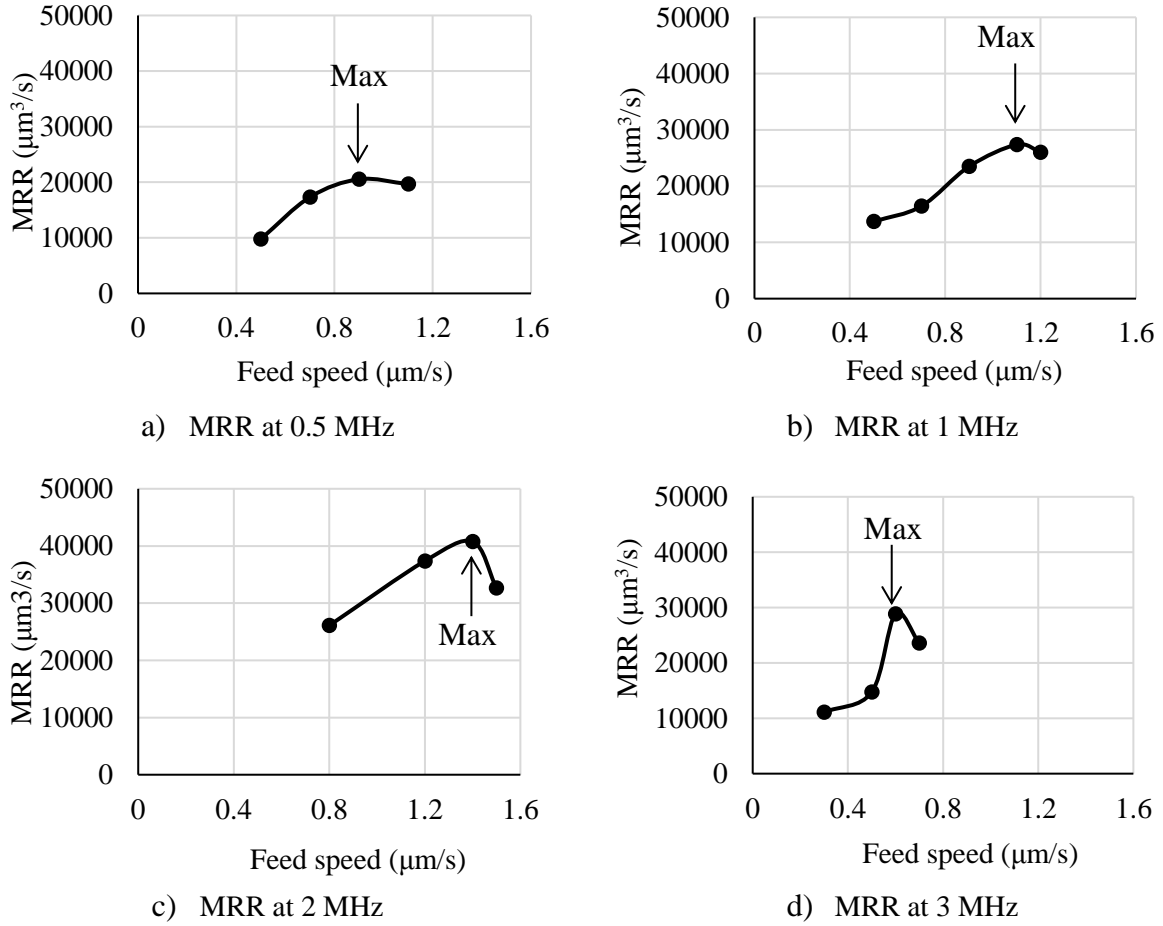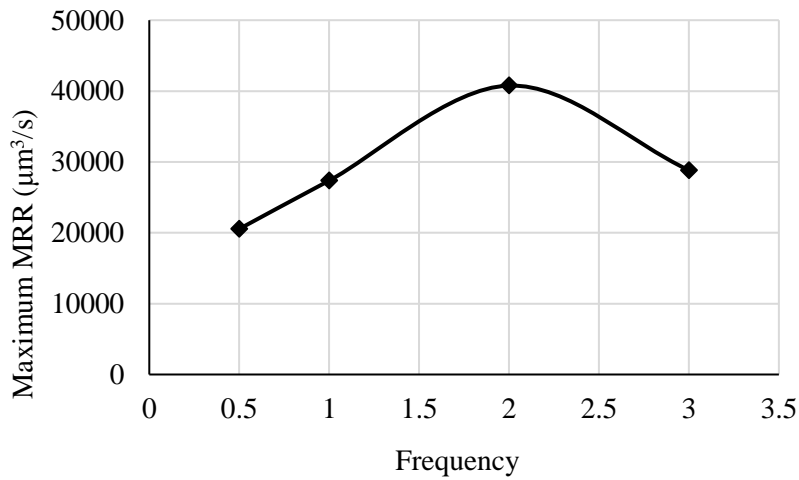

a) MRR at 0.5 MHz

b) MRR at 1 MHz

c) MRR at 2 MHz

d) MRR at 3 MHz

Fig. 2.9: MRR at respective frequencies

Fig. 2.10: Relationship between maximum MRR and frequency with conventional EIFM

2.3 Preliminary Investigation on Machinability with CPTM

In the conventional EIFM, size of discharge crater is influenced by discharge energy per pulse. However, in CPTM, the size of discharge crater is determined by discharge energy per pulse train. To examine the feasibility of CPTM, a preliminary investigation on the influence of pulse train duration towards the diameter of discharge craters has been performed. For simplicity, the machining setup shown in Fig. 2.11 was used. With this setup, a capacitor of C_1=470pF was added to the circuit, and the voltage was supplied to the tool using a brush. Tektronix Tek CT-1 current probe was used to detect the discharge current. The voltage and current signals during the experiment were monitored using Textronix DP 4104 Digital Phosphor Oscilloscope. Scanning electron microscope (SEM) was used to observe the image of machined surface. The machining was performed using the machining conditions shown in Table 2.2.
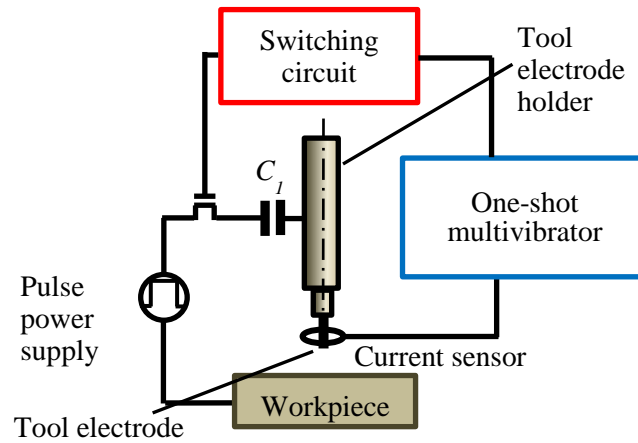

Fig. 2.11: Experimental setup

Table 2.2: Experimental conditions in investigating size of discharge crater

Amplitude of pulse voltage (V)	100
Frequency (MHz)	5
Feeding capacitance, C_1 (pF)	470
Electrode (Rod)	Tungsten carbide ($\varnothing$ = 300µm)
Workpiece	Stainless steel (SUS 304)
Dielectric	EDM oil
Pulse train duration (ns)	50, 300, 900, 1400
Pulse train interval (ns)	4600

Fig. 2.12 shows the example of discharge waveforms with 470pF, 5MHz and 300ns pulse train duration. In the figure, (a) refers to discharge delay time. Then, the gap voltage drops at point (b) to about 40V. Then, discharge starts to occur with discharge duration per single pulse of about 80ns; labeled as (c). After that, the half cycle of the pulse power supply ends and the polarity is changed at point (d). The duration labeled as (e) is the rise time of the pulse power supply and happens to be equal to the discharge delay time within the pulse train duration. In the same way as the first discharge, the gap voltage drops to about -40V at (f) and the second discharge occurs within the duration marked as (g). After the end of the half cycle of the pulse power supply, the polarity of the pulse is changed and the cycle is reiterated. In the early discharges, the discharge voltage is about 40V; slightly higher than the one usually observed in macro EDM which is around 20V. This is probably due to the small diameter of the discharge column which is being developed rapidly in the transient state immediately after the discharge breakdown.

By looking at the duration of (e) and (h) until (k), it can be seen that the discharge delay time within the pulse train duration becomes shorter as the time progress. This is because the temperature at the discharge spot increases, thereby it becomes difficult for the plasma to be extinguished causing the discharges to occur at the same location. In this figure, the total discharge duration is slightly longer than the set pulse train duration of 300ns. This is because, there are delays of about 400ns in total to activate the one-shot multivibrator and to stop the pulse power supply.
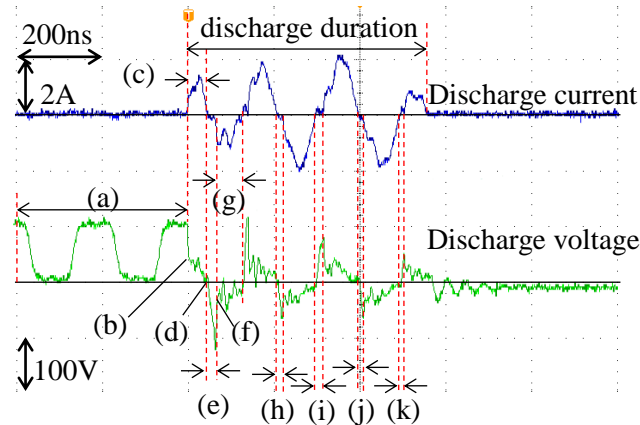

Fig. 2.12: Discharge waveform of CPTM

Fig. 2.13 shows the images of machined surface with different pulse train durations. It can be seen that there is difference in the size of discharge craters for different pulse train durations. Fig. 2.14 shows the results of measured diameter of discharge craters with respect to the pulse train duration. As the pulse train duration increases, the diameter of craters can be enlarged. This is because number of discharges per pulse train increases

with increasing the pulse train duration, and the discharges occur continuously at a single spot during the period of the pulse train.

a) 50ns   b) 300ns

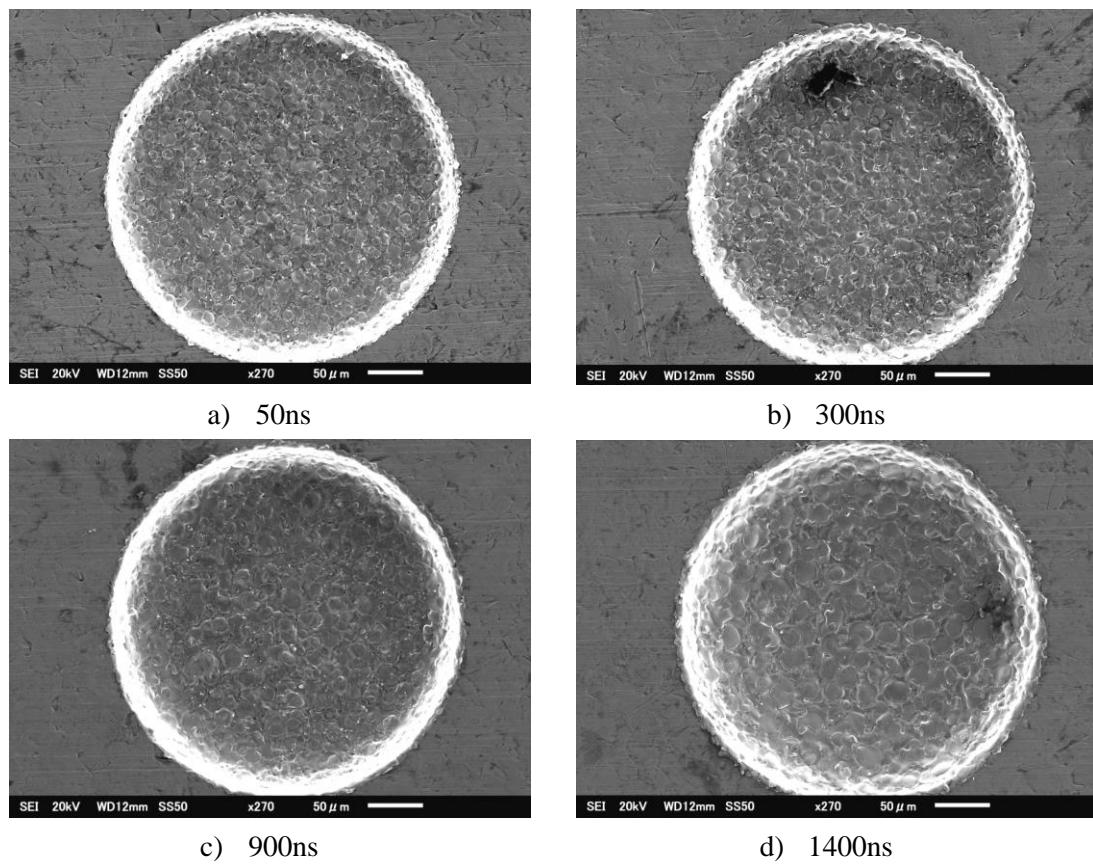c) 900ns   d) 1400ns
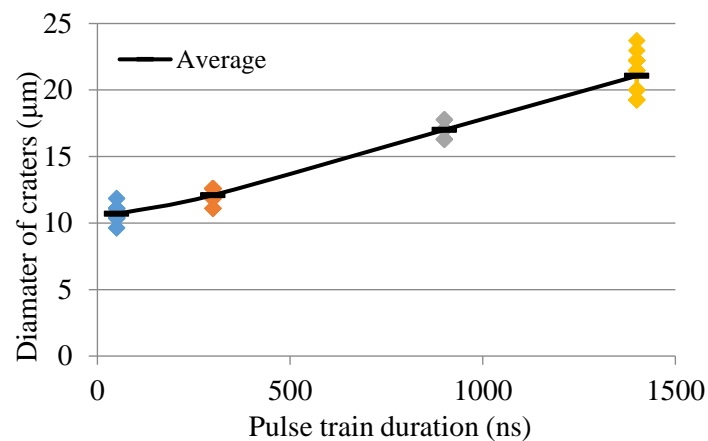
Fig. 2.13: Machined surface at 5MHz

Fig. 2.14: Relationship between diameter of craters and pulse train duration

The initial investigation on the feasibility of CPTM shows that discharges can be concentrated at the same spot. This can be seen from the difference in the diameter of discharge craters when different pulse train durations are used. To confirm that discharge

is localized with CPTM, observation on the concentration of discharges was performed using a high-speed video camera.

2.4 Observation on Concentration of Discharge Location

In CPTM, the high frequency pulses are applied during the pulse train duration by allowing several discharges to continuously occur within the controlled duration. It is believed that the discharges are concentrated at a single location because there is no sufficient time for the dielectric strength to recover during high frequency discharge within the pulse train duration. Furthermore, the average diameter of craters increases with the increase in pulse train duration.

With the availability of transparent conductive materials, observation of EDM gap can be performed using a high-speed video camera from the direction normal to the discharge surface. Investigation on discharge location and clarification of discharge phenomena in EDM have been successfully performed by several researchers [15-17]. Since multiple discharges can occur within a pulse train duration in CPTM, this observation method can help to confirm whether the generated discharges within a pulse train duration are localized or dispersed.

2.4.1 Experimental setup

In this experiment, a transparent ITO (indium tin oxide) film coated on a glass plate was utilized as the workpiece. ITO is an oxygen saturated composition with 74% In, 18% O_2 and 8% Sn by weight. ITO is suitable to be used in this observation due to its electrical conductivity and optical transparency. The specifications of the ITO coated glass are shown in Table 2.3. Since the depth of the discharge crater is in the same order as the ITO film thickness, the use of ITO will not affect the gap phenomena observed in micro EDM. However, ITO may not be used to observe the gap phenomena in normal EDM processes because the discharge energy is larger.

With the experimental setup shown in Fig. 2.15, the locations of discharges were observed through the glass plate coated with ITO using Shimadzu HPV-1 high speed video camera. In the setup, the tool electrode was held by a mandrel which was supported by V-guide and secured using a rubber belt on the Z-axis of Panasonic (MG-ED72) micro EDM machine. ITO was placed initially at a distance of 10μm from the side surface of the tool electrode. The gap between ITO and the tool electrode was filled with EDM oil using a pipette. The observational area was set between the top edge of ITO coated glass and bottom end of the tool electrode with the observed length of the tool electrode of about 1mm.

Table 2.4 shows the machining conditions used for the observation. During the experiment, the tool was fed towards ITO at a speed of 0.1μm/s. The current sensor detected the ignition of discharge, and the rise of discharge current triggered the oscilloscope. The trigger signal was sent by the oscilloscope to the high-speed video camera to freeze the memory. The imaging conditions of the high-speed video camera are given in Table 2.5. The frame rate of 500fps and the exposure time of 1ms were determined based on the fact that no more than one discharge spot can be observed in a frame when the pulse frequency was 0.5kHz in EIFM.

Table 2.3: Specifications of ITO coated glass

Thickness of glass substrate (mm)	1.1
Resistivity (Ω/sq)	5
ITO film thickness (μm)	0.33
Transmittance	$\geq 70\%$

Table 2.4: Experimental conditions for the observation of discharge location using transparent electrode

Parameters	Conventional EIFM	CPTM
Amplitude of pulse power supply (V)	100	100
Pulse frequency (kHz)	0.5, 5	3000
Capacitance, C_1 (pF)	470	
Workpiece	ITO coated glass	
Tool electrode (Rod)	Tungsten carbide(Ø = 300μm)	
Pulse train duration (μs)	-	1.4
Pulse train interval (μs)	-	1800

Table 2.5: Settings of high-speed video camera

Resolution (pixel)	312 x 260
Frame rate (fps)	500
Exposure time (ms)	1
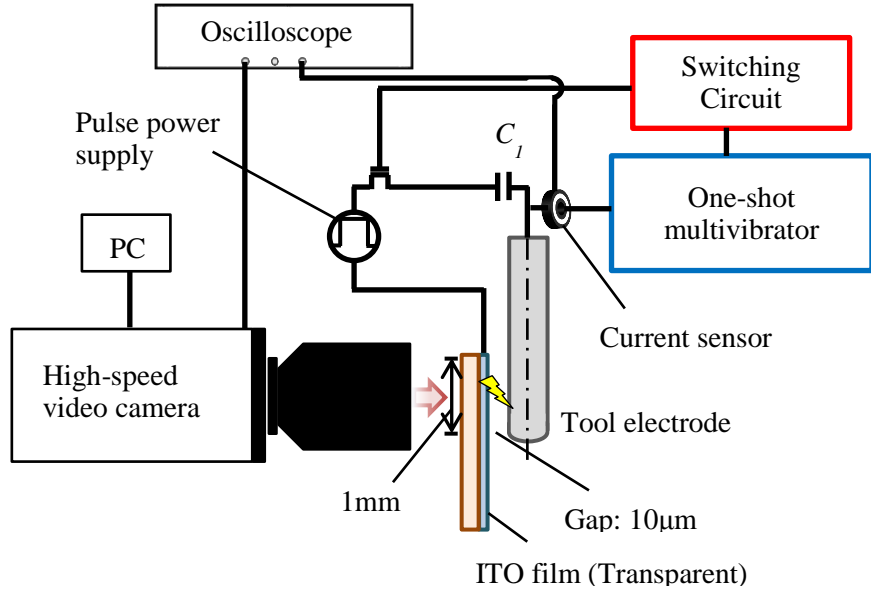
Fig. 2.15: Experimental setup

2.4.2 Observation of Discharge Location with Conventional EIFM

Observation of single pulse discharge using conventional EIFM was performed at very low pulse frequency of 0.5kHz. Since one discharge can occur at every 1ms, no more than one pulse can be recorded within the frame at the frame rate of 500fps and exposure time of 1ms. Fig. 2.16a shows the image of light emission from the discharge spot during observation. For the presented discharge spot, the discharge waveform is shown in Fig. 2.16b. In the figure, timing signal refers to the time where the camera shutter opens and trigger signal means the signal sent from the oscilloscope to the camera. With capacitance C_1 of 470pF, the discharge current recorded was about 800mA, and discharge duration was about 100ns.

a) Image of discharge spot

b) Discharge waveforms
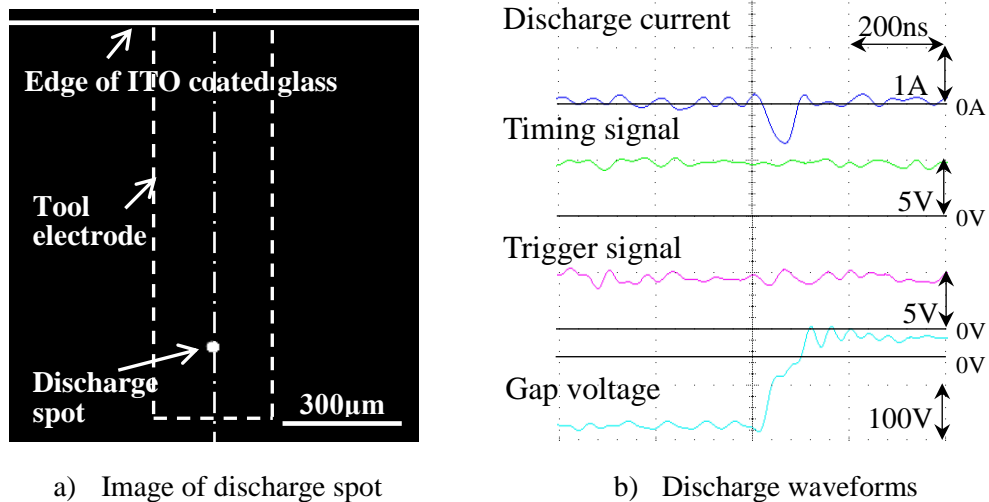
Fig. 2.16: Single pulse discharge using conventional EIFM

Then, the frequency was increased to 5kHz. At this frequency, 10 discharges can occur within the same exposure time of 1ms. Fig 2.17a shows the image of the discharges captured in a frame during the observation. The discharge waveforms in Fig 2.17b shows the occurrence of discharges within the exposure time: in between the red dotted lines. Since there is enough time for the dielectric breakdown strength to recover after every discharge, the discharges are separated at different locations. Since 10 discharge pulses were generated, it is expected that 10 small discharge spots having nearly similar size to the one shown in Fig. 2.16a can be seen in Fig. 2.17a. However, since there are several small and big discharge spots in the same frame, it is considered that the big discharge spots are due to several discharges which were located very near to each other.

a) Image of discharge spots   b) Discharge waveforms
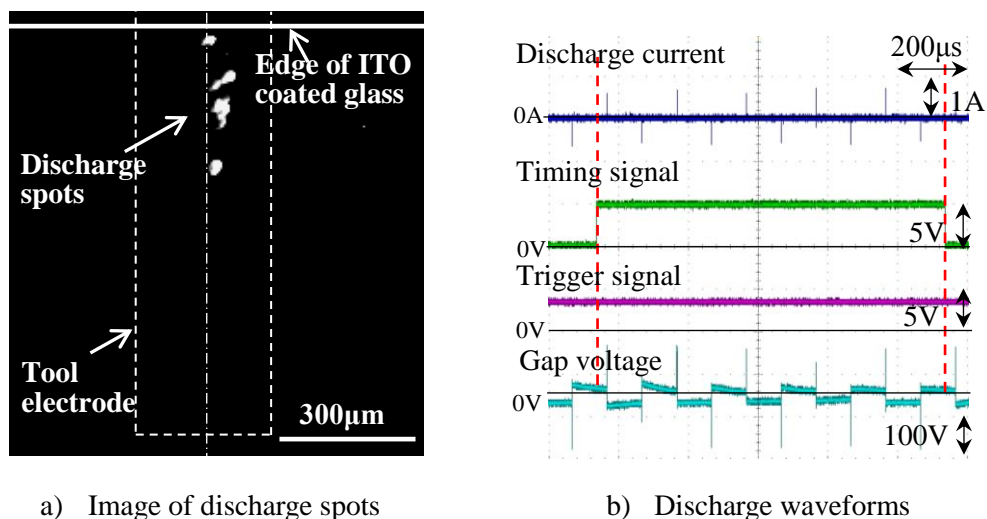
Fig. 2.17: Multiple discharges using conventional EIFM

From the observation with the conventional EIFM, it was found that if discharges are dispersed, more than one discharge spots can be seen in one frame. In addition, if more than one discharge occurred at the same location, the diameter of the discharge spot probably should be larger than the single discharge spot shown in Fig. 2.16a.

In Fig. 2.17(b), it can be seen that the gap voltage is slightly different from the gap voltage waveforms normally observed in the EIFM method. Kimori [18] investigated the influence of inductance on discharge waveforms. Fig. 2.18(a) shows the typical condition of discharge current and gap voltage according to the principle. In this figure, E_0 is the amplitude of the rectangle pulse, T/2 is the pulse width of the applied voltage, V_{C2} is voltage in the machining gap between the tool and workpiece, u_0 is the open voltage, u_e is the discharge voltage (approximately 20V) and I is discharge current. When the pulse power supply becomes E_0, dielectric breakdown occurs after discharge delay time and

gap voltage drops to u_e. Discharge current flows within a certain discharge duration. After the end of discharge current, there is no current flowing and the gap voltage maintains at u_e until the next half cycle of the pulse power supply.

In reality however, the first discharge current is sometimes followed by the secondary discharge as shown in Fig. 2.18(b). The secondary discharge current with reversed polarity caused the change in the gap voltage to $-u_e$. Then, after the secondary discharge ends, the gap voltage remains at $-u_e$ and retained the condition until the end of T/2. This condition occurred because the dielectric strength in the gap was not recovered after the first discharge.
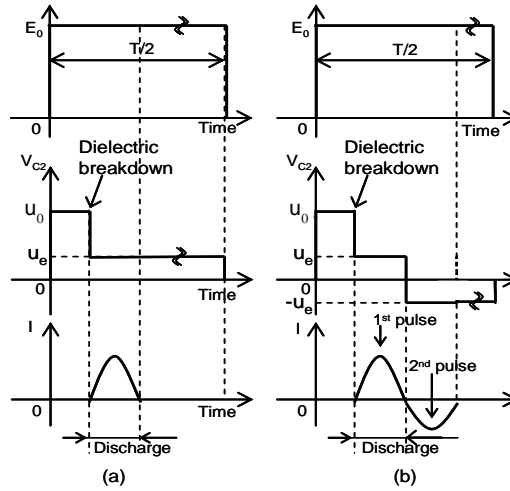
Fig. 2.18: Schematic timing chart of gap voltage and discharge current: (a) according to principle, (b) with influence of inductance [16]

2.4.3 Observation of Discharge Location with CPTM

With CPTM, the duration of pulse train was set to be 1.4µs, and the pulse train interval was 1800µs. With this, only one group of discharges can occur within one frame because the shutter was open for 1ms only. Fig. 2.19a shows the image of light emission generated from the discharge spot. Here, only one discharge spot can be seen, and the light emission was found to be larger than the one shown in Fig. 2.16a. Fig. 2.19b shows the discharge waveforms for the generated discharges. Ten discharges were generated within the pulse train duration. Therefore, it is confirmed that all the discharges were localized at the same discharge location because there is only one discharge spot from the captured image.

Since the same capacitance of 470pF was used, the duration of one pulse discharge is about 100ns; which is the same with the single pulse discharge generated using conventional EIFM. At pulse frequency of 3MHz, the duration of half cycle of the pulse is 166.7ns, and there is an interval of about 66.7ns between the discharges. This shows

that multiple discharges can occur at the same location even if there is an interval between the discharges within the pulse train duration.
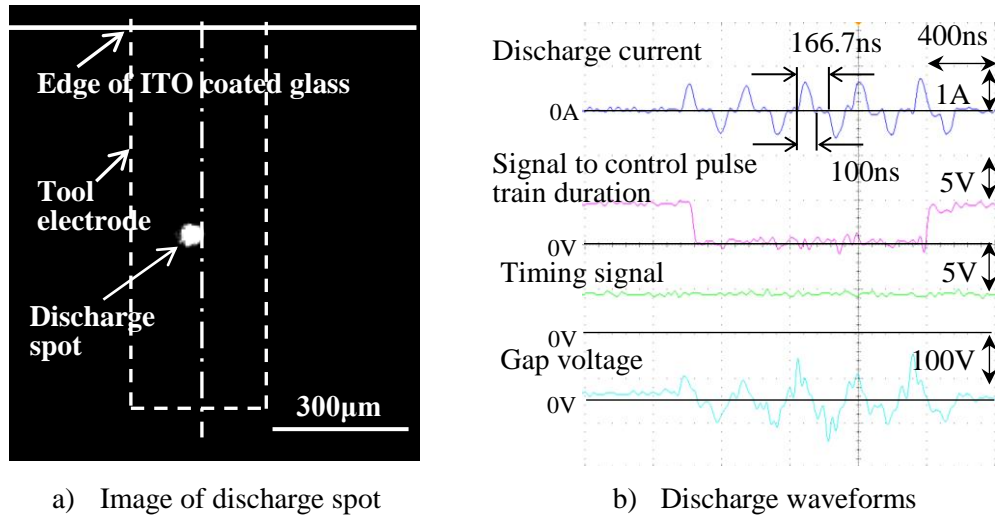

a) Image of discharge spot   b) Discharge waveforms

Fig. 2.19: Discharges during a pulse train duration using CPTM

2.5 Characteristics of Discharges in CPTM

The observation on concentration of discharges verified that discharges can be concentrated at the same location with CPTM. During observation, machining was performed with CPTM at frequency of 3MHz. Even if almost all discharges concentrated at a single spot, it was found that some discharges were dispersed as in Fig. 2.20 This dispersion of discharges within the pulse train duration does not always occur. Discharge can be reignited after a slight interval within the same pulse train duration, or may not occur again within the pulse train duration. These phenomena are illustrated in Fig. 2.21. With 470pF, the width of discharge pulse is about 100ns, and the pulse width is 166.7ns at 3MHz.

Usually, after the pulse train interval, discharge can occur after a certain duration known as discharge delay time. Once the first discharge (pulse discharge 1) is ignited, there is an interval between the end of the pulse discharge and the end of the pulse width of the pulse power supply since the discharge duration is shorter than the half cycle of the pulse power supply. This is marked as (a). Then, pulse discharge 2 can occur several ns after the pulse polarity is changed. This is marked as (b) which is named as discharge delay time within the pulse train duration which is statistically variable like the discharge delay time before the pulse train duration. Here, there is an interval between the first and the second pulse discharge. After that, suppose pulse discharge 3 occurs immediately after pulse discharge 2 and discharge 4 occurs after discharge delay time within the pulse train duration, the interval here can be longer than 66.7ns. After pulse discharge 4, there is a

53

possibility that there is no discharges between pulse discharges 4 and 5 within the pulse train duration even if the pulse frequency is continuously applied. No discharges within the pulse train duration is also another reason why discharge spots are separated. Based on this discussion, investigation on the threshold of deionization in micro EDM was performed in order to identify the interval time which causes the discharge to be dispersed.
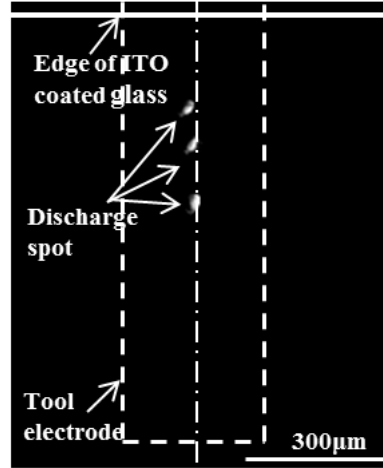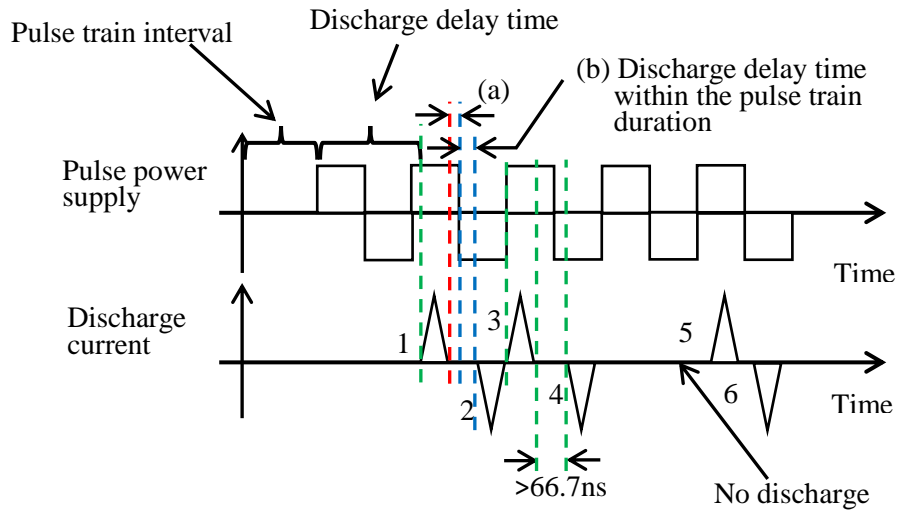

Fig. 2.20: CPTM with three separated discharges

Fig. 2.21: Phenomena of separated discharges in CPTM

2.6 Investigation on Deionization of Discharges in CPTM

When machining is performed with CPTM at lower frequency, the long interval time between the discharges within pulse train duration caused discharges to be dispersed due to deionization of plasma. However, the threshold of deionization in micro EDM is not known and has not been investigated. In macro EDM, the threshold of deionization was

found to be about 2μs when the discharge current is 25A with discharge duration of 500μs [19]. It is expected that the time necessary to deionize the discharge plasma will be much shorter in micro EDM because the discharge current and discharge duration are much smaller compared to macro EDM.

2.6.1   Experimental Method

Investigation on the threshold of deionization in micro EDM was performed by direct observation using a high speed video camera through a transparent electrode. The same experimental setup as discussed in Section 2.4.1 was employed. In this experiment, the frame rate was determined so that only two discharges can be allowed to occur within one frame. The pulse train duration was set to be 0.2μs based on a preliminary observation. With this, the localized or dispersed discharges can be seen in the captured image. Then, the image was compared with the discharge waveforms recorded by the oscilloscope. Thus, the time necessary to extinguish the discharge plasma can be identified by measuring the interval time between the two discharges. The experimental conditions are shown in Table 2.6. Three different feeding capacitances were tested, and 300 samples were observed for each capacitance. The frequency of the pulse power supply was changed from 1.1 to 2MHz so that the interval time can be varied. The collected data were classified with the following rules:

a) two discharges occur within the pulse train duration and only one discharge spot is seen as in Fig. 2.22a.

b) two discharges occur within the pulse train duration, and two discharge spots are seen as in Fig. 2.22b.

Due to delay in the switching circuit to stop the pulse power supply, the following cases were also accepted:

c) more than two discharges continuously occur, and only one discharge spot is observed as in Fig. 2.22c.

d) more than two discharges intermittently occur, and multiple discharge spots are observed as shown in Fig. 2.22d.

In the event where there is only one pulse discharge within the pulse train duration, the data were ignored.

Table 2.6: Experimental conditions to investigate the threshold of deionization

Amplitude of pulse voltage (V)	100
Frequency (MHz)	1.1-2
Feeding capacitance, C_1 (pF)	220, 470, 680
Electrode (Rod)	Tungsten carbide (Ø = 300μm)
Workpiece	ITO coated glass
Dielectric	EDM oil
Pulse train duration (μs)	0.2
Pulse train interval (μs)	1800
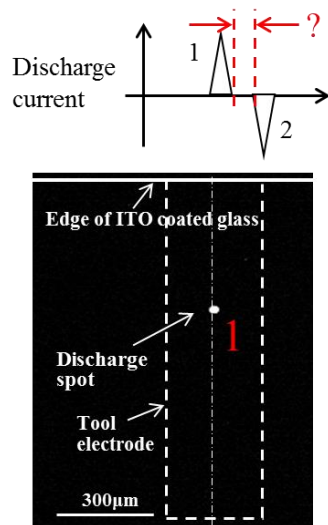
a) Two discharges at the same location
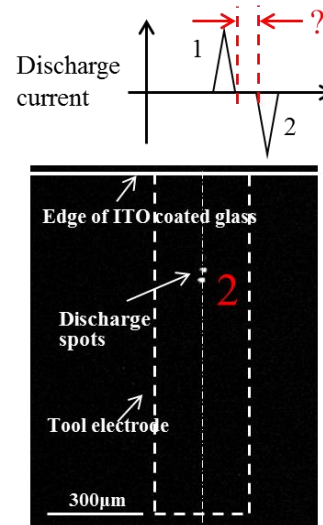
b) Two discharges in separate locations
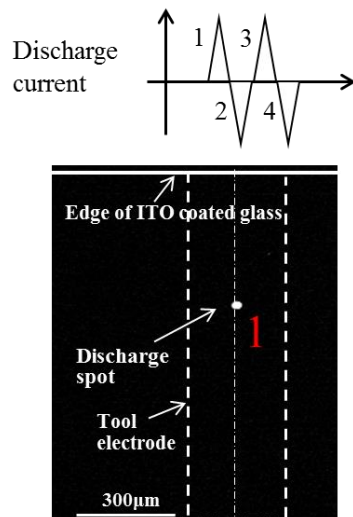
c) Multiple discharges at the same location
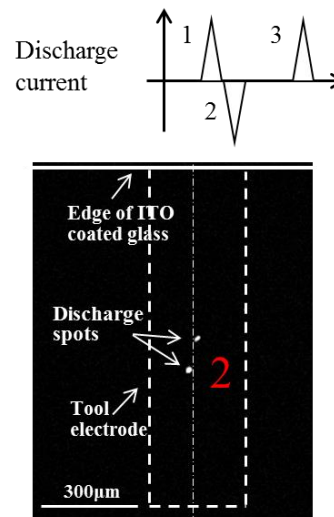
d) First two discharges are continuous

Fig. 2.22: Method of analysis to investigate the threshold of deionization

2.6.2   Examples of Observation Results

Fig. 2.23 shows the example of the images of discharge spots and discharge waveforms captured during the observation using 470pF. Fig. 2.23a shows the case that discharge occurred at the same location when there was no interval between the discharges. Fig. 2.23b shows the case that discharge occurred at the same location even if there was an interval between the discharges. Fig. 2.23c shows the separated discharges due to long discharge interval. With the developed circuit, there are lags of about 0.4μs in total to activate the one-shot multivibrator circuit and to stop the pulse power supply. During these times, discharge can continue to occur. This is the reason why discharge can be observed even if the duration is much longer than the set pulse train duration of 0.2μs.

a) Continuous discharge and 1 discharge spot

b) Separated discharges and 1 discharge spot

c) Separated discharges and 2 discharge spots
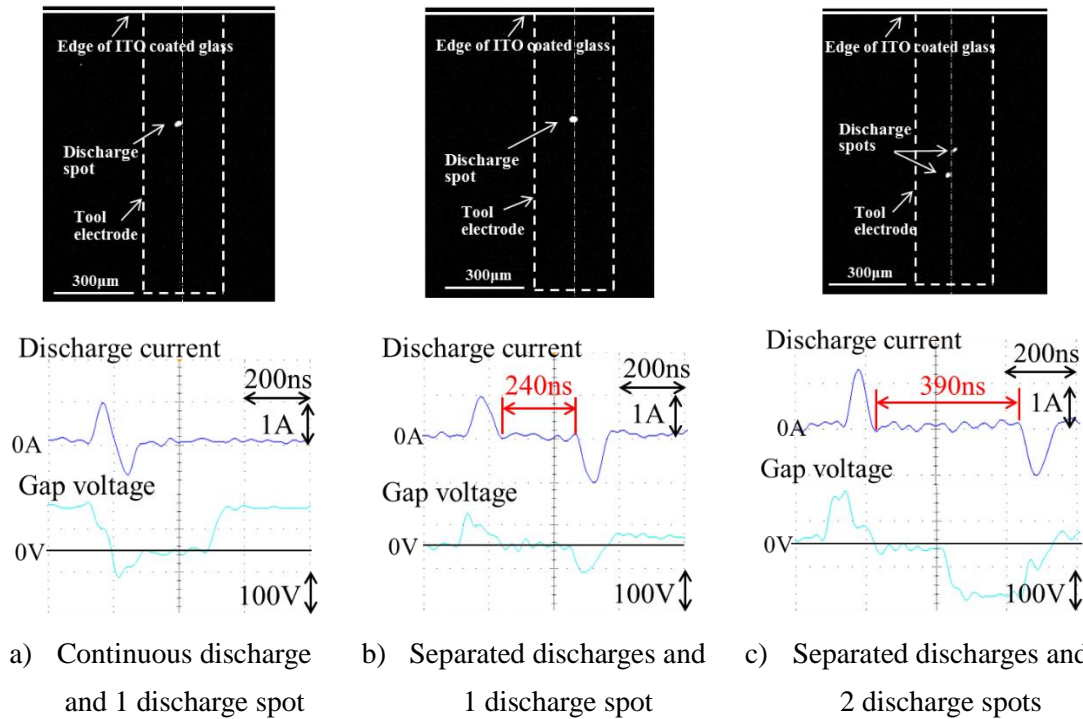
Fig. 2.23: Examples of observational results in determining the threshold for deionization in micro EDM using 470pF

2.6.3   Results of Observation using 220pF

Fig. 2.24 shows the example of single pulse discharge waveforms at 220pF. The amplitude of discharge current was about 0.8A, and the discharge duration was about 60ns. All the results obtained from the observation are shown in Fig. 2.25. In this graph, x-axis refers to the range of the interval time between the pulse discharges, and y-axis refers to the repeatability of the interval time during the observation. The blue column in the graph represents the localized discharges (Fig. 2.22a and c), and the red column represents the dispersed discharges (Fig. 2.22b and d).

57

In order to decide when the dispersion is likely to occur, the percentage of dispersed discharges was calculated. The calculation was performed by dividing the number of dispersed discharges with a total number of discharges for every range of interval time. The percentage of dispersed discharges will not be considered in the case where the population of discharges within the interval time is less than 10 because of the lack of reliability. The calculated results are shown in Table 2.7. The highest percentage of dispersed discharges is 51%. Thus, the interval time which caused the discharges to be dispersed with the percentage over 50% was 281-320ns or longer.
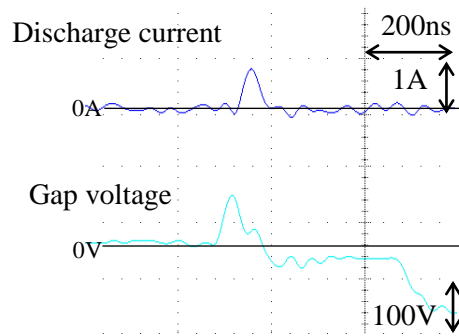
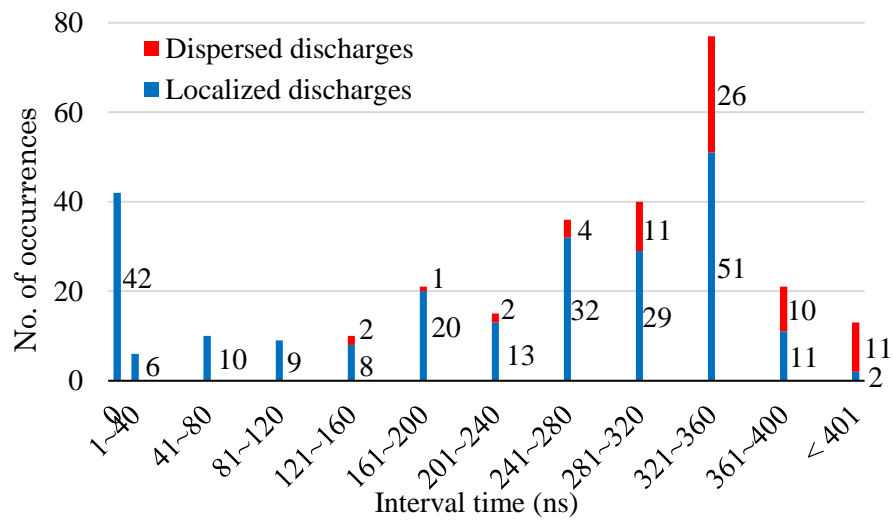Fig. 2.24: Discharge current waveform at 220pF
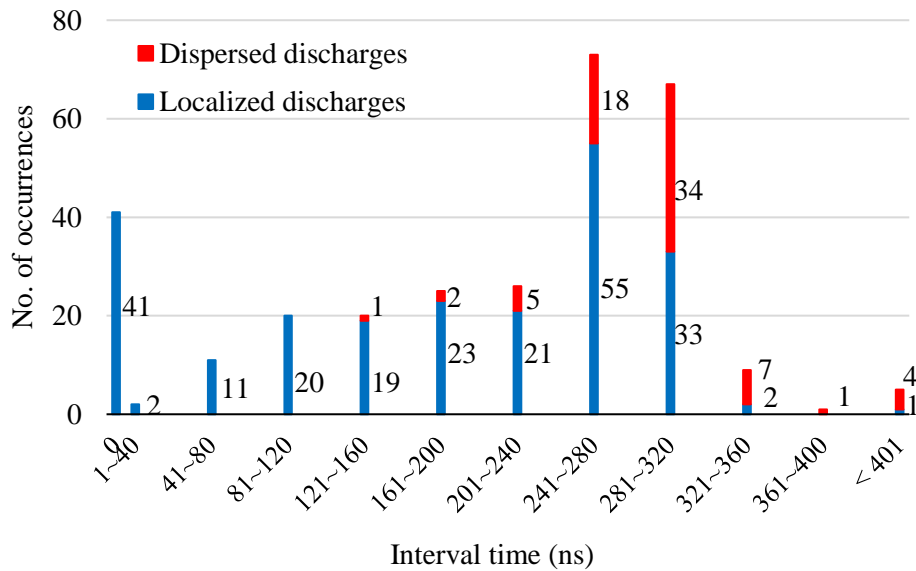
Fig. 2.25: Experimental results using 220pF

Table 2.7: Percentage of dispersed discharges using 220pF

Interval time (ns)	% of dispersed discharges
121-160	5
161-200	8
201-240	19
241-280	25
281-320	51

2.6.4 Results of Observation using 470pF

Fig. 2.26 shows the discharge waveforms using capacitance of 470pF. The amplitude of discharge current was about 1A, and the discharge duration was about 100ns. Fig. 2.27 shows all the results obtained during observation. Table 2.8 shows the percentage of dispersed discharges. The interval time with which the percentage of dispersed discharges exceeds 50% was between 281-320ns.
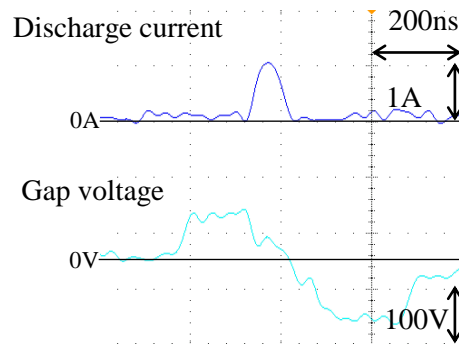
Fig. 2.26: Discharge waveform at 470pF
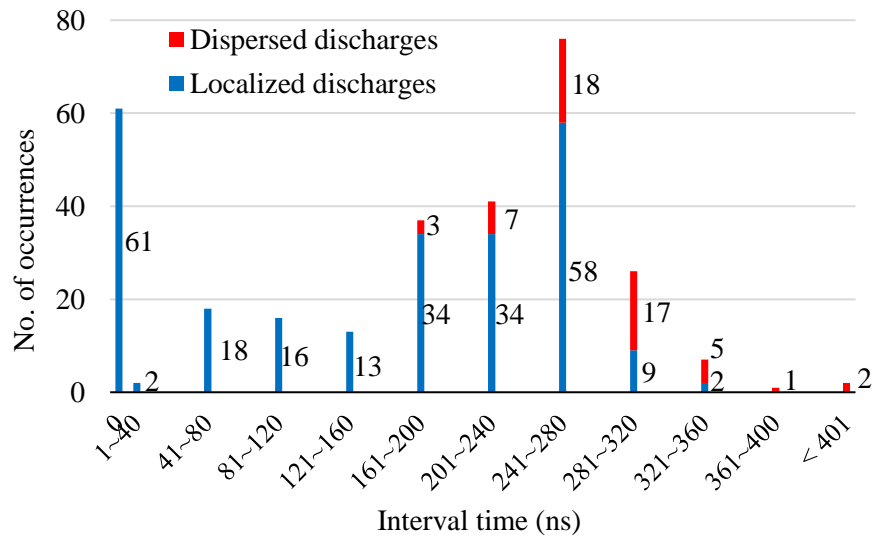
Fig. 2.27: Experimental results at 470pF

59

Table 2.8: Percentage of dispersed discharges using 470pF

Interval time (ns)	% of dispersed discharges
161-200	8
201-240	17
241-280	24
281-320	65

2.6.5   Results of Observation using 680pF

When the 680pF capacitance was used, the amplitude of discharge current was about 2A, and the discharge duration was about 125ns as shown in Fig. 2.28. Fig. 2.29 shows the observed results. Table 2.9 shows the results of the calculated percentage of dispersed discharges. In this case, the percentage of dispersed discharges reached around 50% at the interval time between 361-400ns.
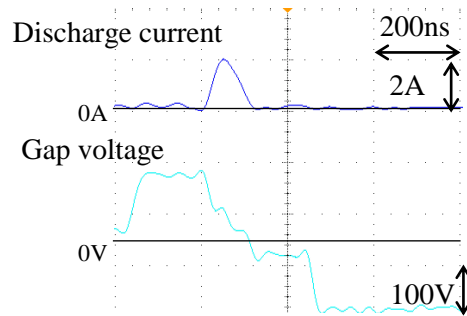
Fig. 2.28: Discharge waveform at 680pF

Fig. 2.29: Experimental results at 680pF

Table 2.9: Percentage of dispersed discharges using 680pF

Interval time (ns)	% of dispersed discharges	Interval time (ns)	% of dispersed discharges
121-160	2	281-320	28
161-200	5	321-360	34
201-240	13	361-400	48
241-280	11		

Fig. 2.30 shows the relationship between the interval time with which the percentage of dispersed discharges reaches 50% and the capacitance. As capacitance increases, discharge energy is increased and longer time is needed to deionize the plasma. This is the reason why the interval time necessary to extinguish the plasma is longest at 361-400ns with 680pF. However, the results show that the interval time was the same at 281-320ns for 220pF and 470pF.

Compared with macro EDM, where the time necessary for the plasma to be extinguished is about 2μs, the interval time necessary to deionize the plasma in micro EDM is about 5 times shorter. This is because the discharge energy in micro EDM is significantly small.
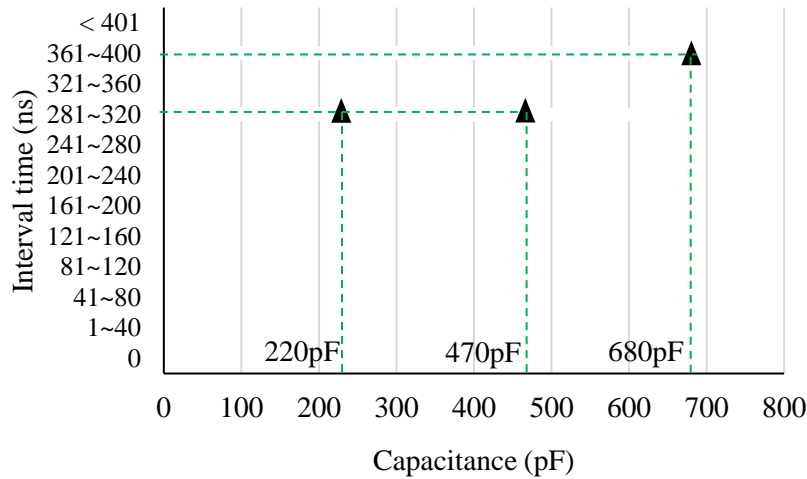
Fig. 2.30: Relationship between interval time and capacitance

2.7 Concluding Remarks

This chapter discussed about the fundamental of the controlled pulse train method, CPTM. The method is proposed since there is a limitation in increasing the discharge energy in conventional EIFM. This was proved through an experiment which shows that

MRR cannot be increased infinitely by increasing the pulse frequency. EIFM has another problem that the discharge energy per pulse cannot be changed arbitrarily, because the feeding capacitance is fixed by the configuration and the size of the feeding electrode. Hence, a preliminary study was performed to investigate the feasibility of the idea of CPTM. The results show that discharges generated within a pre-determined time called pulse train duration can be accumulated at the same location. In addition, the diameter of discharge craters increases with increasing the pulse train duration. An observation using a high speed video camera through a transparent electrode confirmed that a number of discharges generated with alternating polarity during the pulse train duration are localized at the same spot. Thus, it was verified that the discharge energy can be controlled by the pulse train duration in CPTM. Furthermore, an investigation on the interval time that leads to plasma extinction was performed. It was found that the threshold of deionization in micro EDM is about 5 times shorter than in macro EDM.

2.8 References

1. Tomohiro Koyano, Masanori Kunieda, 2010, Achieving high accuracy and high removal rate in micro-EDM by electrostatic induction feeding method, CIRP Annals-Manufacturing Technology, vol. 59, pp.219-222.
2. Tomohiro Koyano, Yuna Yahagi, Masanori Kunieda and Xiaodong Yang, 2010, High spindle speed micro EDM using electrostatic induction feeding method, Proceedings of the 16th International Symposium on Electromachining, pp.599-602.
3. Tomohiro Koyano, Masanori Kunieda, 2006, Electrolysis free micro EDM in water using electrostatic induction feeding method, Journal of Advances Mechanical Design, Systems and Manufacturing, vol 6-6, pp. 800-807.
4. Xiaodong Yang, Chunwei Xu and Masanori Kunieda, 2010, Miniaturization of WEDM using electrostatic induction feeding method, Precision Engineering, vol. 34, pp. 279-285.
5. Michihiro Hanada, Masanori Kunieda and Ichiro Araie, 2006, Development of micro EDM using electrostatic induction feeding, Journal of The Japan Society for Precision Engineering vol. 72, no. 5, pp. 636-640, (in Japanese).
6. M. Kimori, M. Kunieda, S. Sano, 2007, Mechanism of determining discharge energy in electrostatic induction feeding EDM, Proceeding of Asian Electrical Machining Symposium (AEMS07) Nagoya, Japan, pp. 242-245.
7. B. Bommeli, C. Frei, A. Ratajski, 1979 On the influence of mechanical perturbation on the breakdown of a liquid dielectric, Journal of Electrostatics, vol. 7, pp. 123-144.
8. Yoshie Niwa, 1977, Grinding machining using high frequency arc discharge, Japan Society of Electrical Machining Engineers (JSEME) Research Meeting, no. 86, pp.

9-11 (in Japanese).

9. Yuna Yahagi, Wataru Natsu, Masanori Kunieda, 2012, Control of discharge energy in electrostatic induction feeding EDM using high frequency discharge, Proceeding of The Japan Society for Precision Engineering (JSPE) Spring Meeting, pp. 125-126 (in Japanese).

10. Q. Li, J. Bai, C. Li and S. Li, 2013, Research on multi-mode pulse power supply for array micro holes machining in micro-EDM, The Seventeenth CIRP Conference on Electro Physical and Chemical Machining (ISEM), Procedia CIRP 6, pp. 169-174.

11. Masuzawa, T., Fujino, M., Kobayashi, K., 1985, Wire electro-discharge grinding for micro-machining, Annals of the CIRP, vol. 34, no. 1, pp. 431-434.

12. M. Kunieda, A. Hayasaka, X. D. Yang, S. Sano and I. Araie, 2007, Study on nano EDM capacity coupled pulse pulse generator, Annals of CIRP, vol. 56, no. 1, 213-216.

13. Tomohiro Koyano, Masanori Kunieda, 2010, Achieving high accuracy and high removal rate in micro-EDM by electrostatic induction feeding method, Annals of the CIRP, vol. 59, issue 1, pp. 219-222.

14. Michihiro Hanada, Masanori Kunieda and Ichiro Araie, 2006, Development of micro EDM using electrostatic induction feeding, Precision Engineering Journal, vol. 72, no.5, pp. 636-640 (in Japanese).

15. Tomoo Kitamura, Masanori Kunieda, Kohzoh Abe, 2015, Observation of relationship between bubbles and discharge locations in EDM using transparent electrodes, Precision Engineering, vol. 40, pp.26-32.

16. Tomoo Kitamura and Masanori Kunieda, 2014, Clarification of EDM gap phenomena using transparent electrodes, CIRP Annals – Manufacturing Technology, vol. 63, pp. 213-216.

17. Azumi Mori, Tomoo Kitamura, Masanori Kunieda, Kohzoh Abe, 2015, Direct observation on multiple discharge phenomena in EDM using transparent electrodes, International Journal of Electrical Machining, no. 20, pp. 53-57.

18. Masahito Kimori, 2008, Study on the electrical discharge machining using an electrostatic induction power supply, Kunieda laboratory internal meeting report no. 18 on 29 April 2008 (in Japanese).

19. Shinya Hayakawa, Heng Xia, Masanori Kunieda, Nobuhiko Nishiwaki, 1996, Analysis of time required to deionize an EDM gap during pulse interval, Symposium on Molecular and Micro Scale Heat Transfer in Materials Processing and Other Applications, pp. 368-377.

(This page is intentionally left blank)

Chapter 3

Machining Characteristics using Controlled Pulse Train

Method (CPTM)

From the preliminary investigation presented in the previous chapter, it was found that the discharges can be accumulated at the same location when the controlled pulse train method (CPTM) is used. As a result, control of discharge energy became possible under the same feeding capacitance of the non-contact feeding method. Thus, further experiments were performed to investigate the characteristics of this method. This chapter begins by investigating the influence of pulse train duration on the diameter of discharge craters and material removal rate (MRR). Then, the influence of frequency on discharge continuity was examined. To verify the effectiveness of the method, comparisons between CPTM and conventional electrostatic induction feeding method (EIFM), and also between CPTM and relaxation pulse generator or RC circuit were performed.

3.1 Investigation on the Influence of Pulse Train Duration

In the preliminary investigation presented in the previous chapter, it was found that the diameter of discharge craters can be increased with the increase in the pulse train duration. Here, the influence of pulse train duration is explored further by identifying the effect of different frequency on the diameter of discharge craters. In addition, influence of pulse train duration on MRR was also investigated.

3.1.1 Effect of Pulse Train Duration on Diameter of Discharge Craters

The machining was performed using the experimental setup as shown in Fig. 3.1. In the setup, a silver mica capacitor of 470pF was inserted in the system. The pulse power supply was connected to the tool electrode using a brush, and the tool was rotated at 3000rpm during machining. Table 3.1 shows the machining parameters used in the experiment. The experiment was performed by increasing the duration of the pulse train under three different frequencies. Then, the machined surface was observed using a scanning electron microscope (SEM) and the diameter of discharge craters were measured.
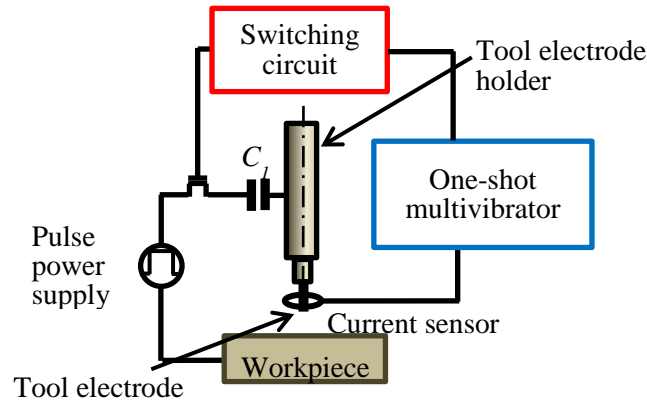
Fig. 3.1: Experimental setup

Table 3.1: Experimental conditions in investigating size of discharge crater

Amplitude of pulse voltage (V)	100
Frequency (MHz)	3, 5, 10
Feeding capacitance, C_1 (pF)	470
Electrode (Rod)	Tungsten carbide (Ø = 300µm)
Workpiece	Stainless steel (SUS 304)
Dielectric	EDM oil
Pulse train duration (ns)	50, 300, 900, 1400
Pulse train interval (ns)	4600

In the system, there was a time lag of about 400ns in total to activate the one-shot multivibrator circuit and to stop the pulse power supply. Due to the delay in response, discharge can continue to occur for a duration longer than the pre-determined pulse train duration. Fig. 3.2 shows the relationship between the diameter of discharge craters and pulse train duration. Under the same pulse train duration, diameter of craters at higher frequency was larger than 3MHz because the number of discharges generated within the same pulse train duration was larger while the discharge energy per pulse is constant. Fig.

3.3 shows the comparison of machined surfaces at the pulse train duration of 300ns and 1400ns under the pulse frequency of 3 and 5MHz. In addition, examples of discharge current waveforms for all the frequencies with the pulse train duration of 1400ns are shown in Fig. 3.4.
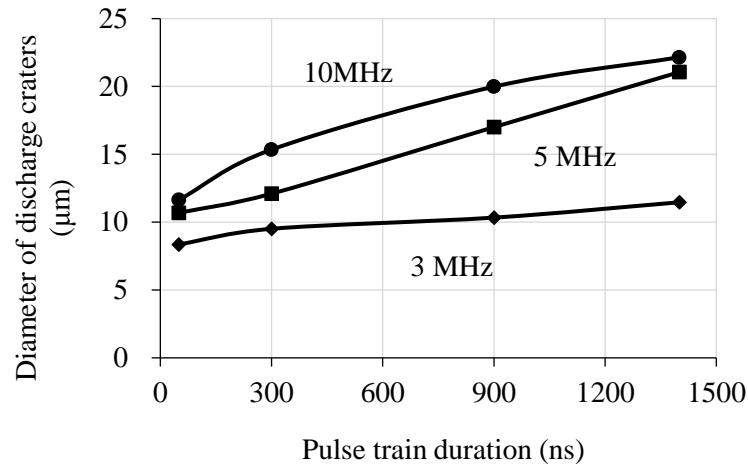
Fig. 3.2: Relationship between diameter of craters and pulse train duration at three different frequencies

a) 5MHz, 300ns

b) 5MHz, 1400ns

c) 3MHz, 300ns

d) 3MHz, 1400ns
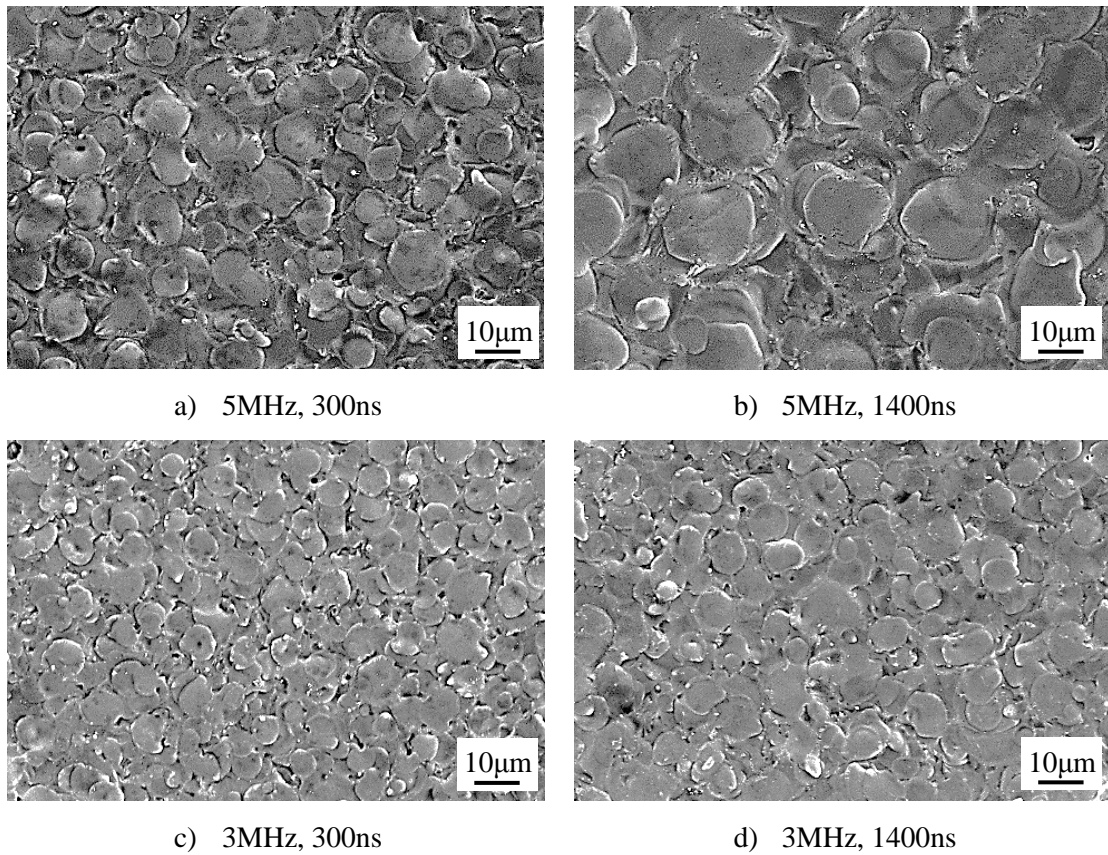
Fig. 3.3: Machined surfaces at two different frequencies and pulse train durations
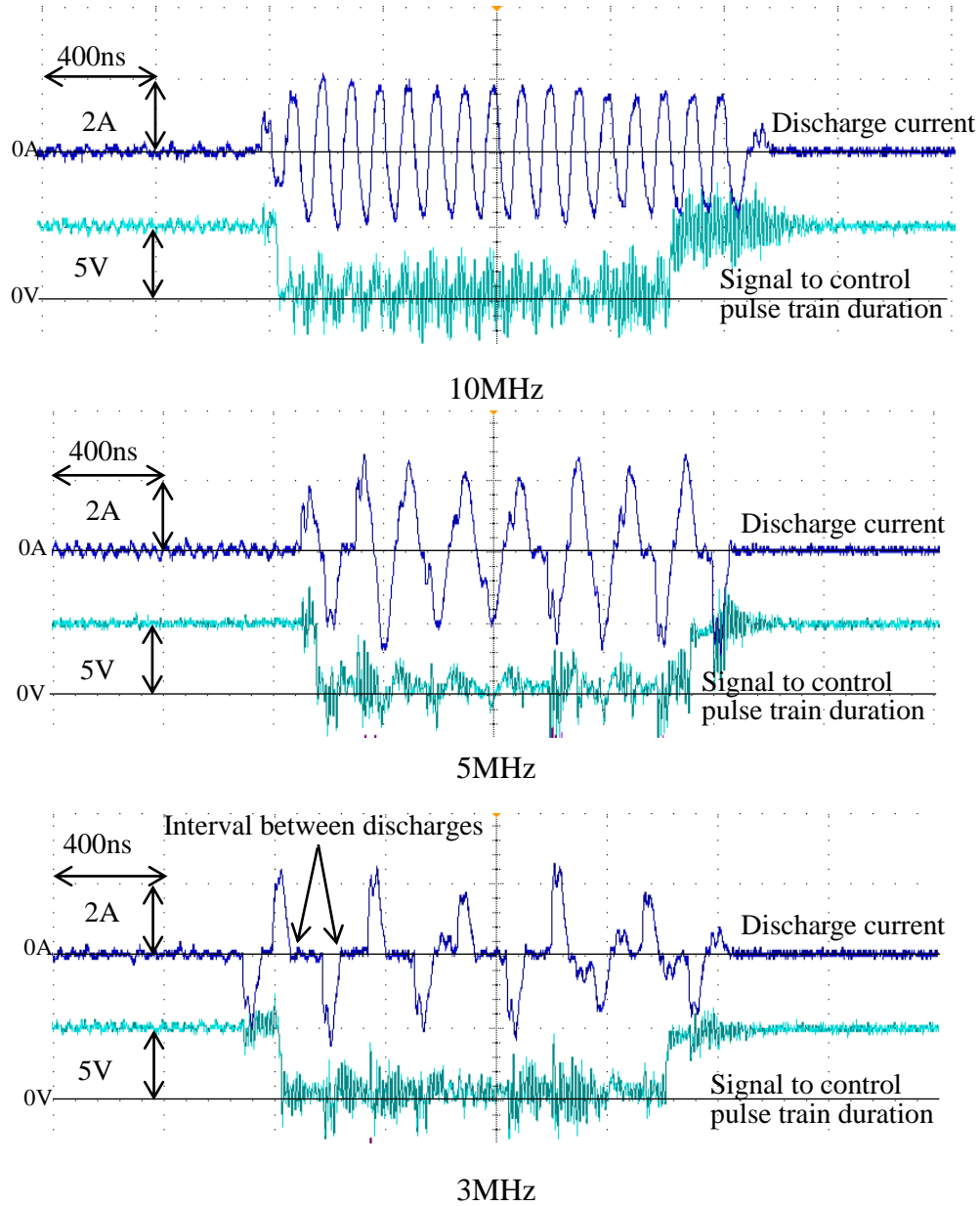
Fig. 3.4: Discharge waveforms at pulse train duration of 1400ns.

With frequency of 10 and 5MHz, diameter of craters was enlarged as the pulse train duration increased. This is because during the period of the pulse train, discharges occurred continuously at the same location, and the number of discharges per pulse train increased with increasing of the pulse train duration. However, for machining with 3MHz as the pulse train duration increased, there was only a slight increase in the diameter of discharge craters. This is because, there is a longer interval between the discharges at 3MHz than that in 10 and 5MHz. Hence, it is considered that discontinuity of discharges during the pulse train duration occurred more often with 3MHz. A discharge current waveform in the case of discontinuity is shown in Fig. 3.5. With C_1=470pF the duration of individual discharge was about 100ns, much shorter than 166.7ns; the duration of the

half cycle of the 3MHz pulse. Therefore, at lower frequency, the long interval between individual pulse discharge leads to the deionization of the plasma which causes the interruption of discharges within the pulse train duration.
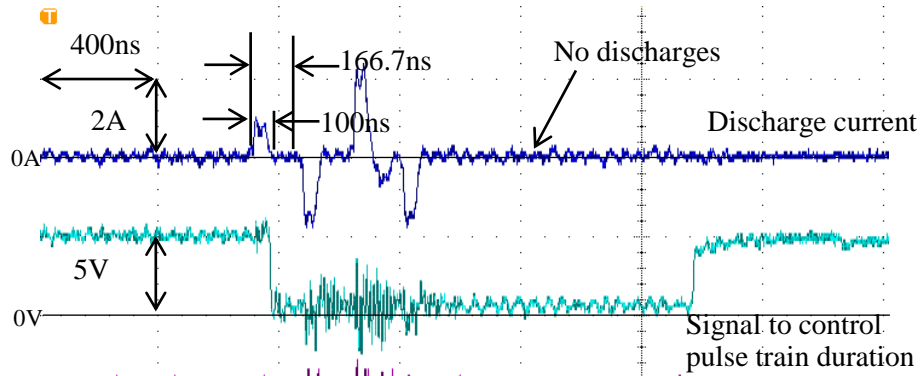
Fig. 3.5: Incomplete discharge waveforms at 3MHz and 1400ns pulse train duration

3.1.2   Effect of Pulse Train Duration on Material Removal Rate (MRR)

When CPTM is employed, the crater size can be enlarged with the increase in pulse train duration. Thus, it is important to investigate the increment of MRR as the pulse train duration increases. In this investigation, the duty factor was varied with the cycle time kept constant. The machining was performed at the pulse frequency of 5MHz, and the cycle time was kept constant at 7400ns. Illustration of discharge current waveforms at different duty factors are shown in Fig. 3.6, and the machining conditions are given in Table 3.2. In the figure, the triangles represent the number of discharges which can be generated at every pulse train duration. The MRR was obtained by dividing the volume of removed material with machining time. By measuring the depth and diameter of machined hole using Olympus OLS3000 confocal laser microscope, the volume of removed material was calculated.

Machining was performed by increasing the feed speed under the same duty factor until the maximum MRR was reached. Then, another duty factor was selected, and the process was reiterated. With this method, MRR can be increased with increasing the feed speed. Under a low feed speed, discharge does not continue during the pulse train duration, while the probability of discharge continuity increases with increasing the feed speed, resulting in higher discharge frequency. However, tool will collide with the workpiece surface when the feed speed is set to be higher than the maximum MRR which can be achieved when the pulse discharge can always continue until the end of the pulse train duration. Thus, the maximum MRR of every duty factor can be achieved. Fig. 3.7 shows the maximum MRR with respect to the pulse train duration. The MRR increases with increasing of the pulse train duration.
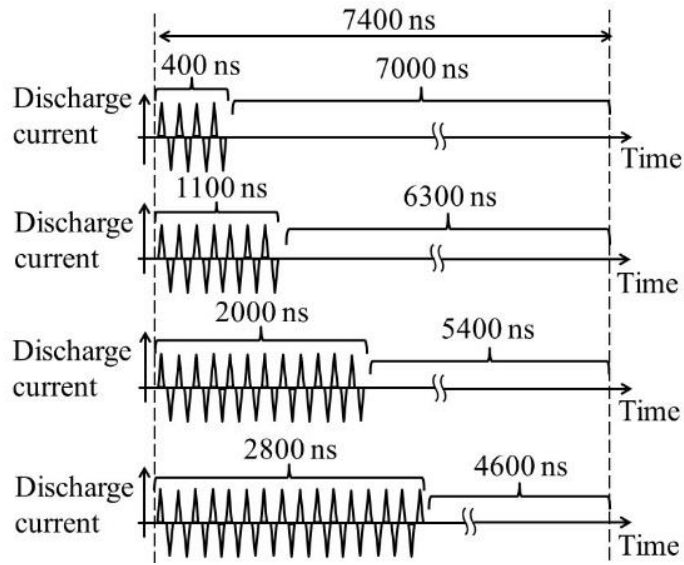
Fig. 3.6: Illustration of discharge current waveforms at different duty factors

Table 3.2: Experimental conditions to investigate the MRR by increasing the pulse train duration

Pulse power supply(V)	100
Feeding capacitance, C_l	470 pF
Electrode	Tungsten carbide (Ø = 250μm)
Workpiece	Stainless steel (SUS 304)
Machining time (s)	120
Pulse frequency (MHz)	5
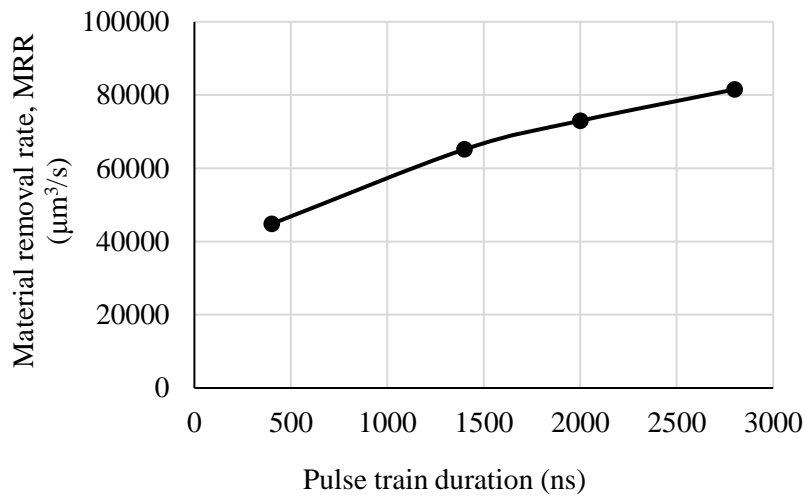
Fig. 3.7: Relationship between MRR and pulse train duration with CPTM

Highest MRR was achieved when machining was performed with the longest pulse train duration. In CPTM, both the duration of the high frequency discharge and the pulse train interval can be controlled. The pulse train interval allows sufficient time for the recovery of dielectric breakdown strength and removal of the gap contamination. Thus, using the same feeding capacitance C_1, the MRR can be increased as the pulse train duration increases.

3.2 Influence of Frequency on Discharge Continuity

In CPTM, the number of discharges generated within the pulse train duration influences on the total discharge energy used to remove the workpiece. Hence, if number of discharges is not constant, it will affect the diameter of discharge craters and surface roughness. Because of this, sustainability of discharges within the pulse train duration was investigated by observing the number of generated discharge current pulses.

In this experiment, 100 samples of pulse train were observed. Fig. 3.8 illustrates the discharge current waveforms with different frequencies with the number of pulse discharges kept constant. About 15 pulse discharges can be generated within the selected pulse train durations of 300ns, 900ns and 1400ns, at frequencies of 3, 5 and 10MHz respectively. At the selected pulse train duration, 15 discharges can be generated because the actual pulse train duration is longer than the selected pulse train duration due to the time lags in the developed circuit. Discharge can continue to occur during the delay of about 400ns in total to activate the one-shot multivibrator circuit and to stop the pulse power supply. Table 3.3 shows the machining conditions used in the experiment.

Fig. 3.9 shows the relationship between the number of occurrences and number of discharges within the pulse train duration. Larger number of discharge indicates higher continuability of the bipolar pulse discharges within the pulse train duration. It was found that number of discharges per pulse train is higher at higher frequency. This is because of shorter interval time between discharges. Thus, discharge can be maintained within the pulse train duration after the occurrence of discharge ignition until the pulse power supply is stopped. In the case of 3MHz, the interval between discharges led to discontinuation of discharges within the pulse train duration. This result verified the fact that the discharge crater did not increase with increasing the pulse train duration at 3MHz in Fig. 3.2.
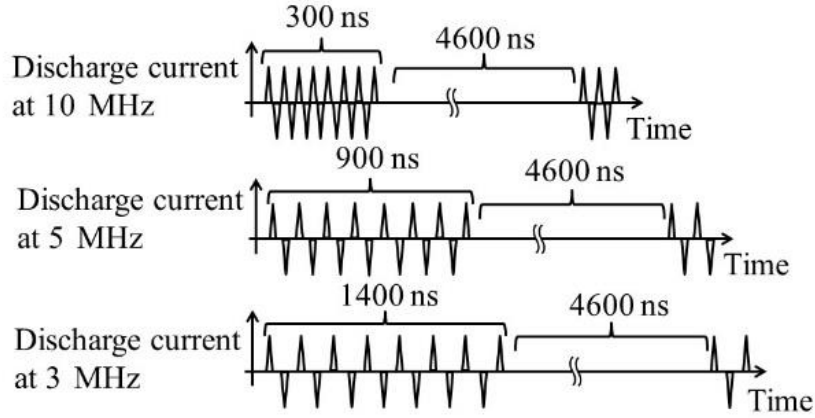
Fig. 3.8: Discharge current waveforms at various frequencies with same number of pulse discharges within pulse train duration

Table 3.3: Experimental conditions to investigate discharge continuability

Amplitude of pulse voltage (V)	100
Frequency (MHz)	3, 5, 10
Feeding capacitance, C_1 (pF)	470
Electrode (Rod)	Tungsten carbide (Ø = 300µm)
Workpiece	Stainless steel (SUS 304)
Dielectric	EDM oil
Pulse train duration (ns)	1400 (3MHz), 900 (5MHz), 300 (10MHz)
Pulse train interval (ns)	4600
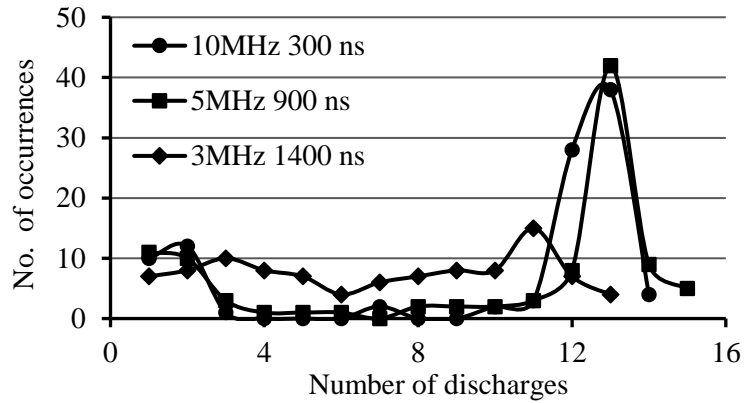
Fig. 3.9: Discharge continuability at different frequencies

3.3 Comparison of Energy Efficiency between CPTM and Conventional EIFM

Energy per individual discharge in conventional EIFM is determined by the feeding capacitance C_1, and the material removal volume corresponds to the total number of discharges. However, the individual discharges continue to occur at the same location with CPTM. Hence, the material removal volume per individual discharge may be different from the conventional EIFM. This is because the material removal volume does not increase linearly with the number of pulse discharges duration when the discharge continues to occur at the same location [1].

3.3.1 Experimental Method

To investigate the material removal per individual discharge, the machining was done at the same total number of discharges for both methods. With CPTM, at frequency of 5MHz, 7 discharges can be generated within 300ns pulse train duration followed by 4600ns pulse train interval. In order to obtain the same number of discharges within the same period of time with the conventional EIFM, a frequency of 700kHz was used during machining. The illustration of discharge current waveforms is shown in Fig. 3.10, and the machining conditions are given in Table 3.4. The machining was performed at constant machining time of 120 seconds by increasing the feed speed.
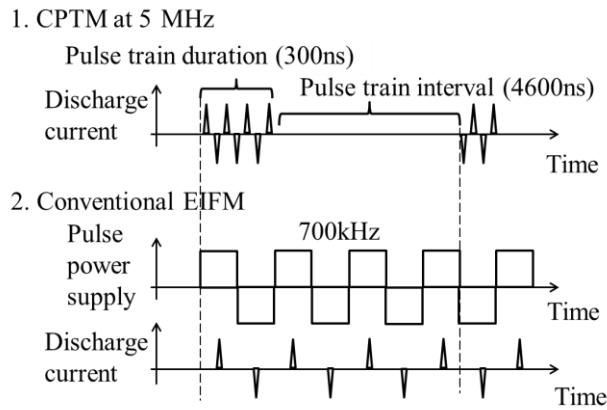
Fig. 3.10: Illustration of discharge current waveforms used to compare energy efficiency between CPTM and conventional EIFM

Table 3.4: Experimental conditions to compare energy efficiency between CPTM and Conventional EIFM

Pulse power supply(V)	100
Feeding capacitance, C_1	470 pF
Electrode	Tungsten carbide (Ø = 250µm)
Workpiece	Stainless steel (SUS 304)
Machining time (s)	120
Conventional EIFM	
Frequency (kHz)	700
CPTM	
Frequency (MHz)	5
Pulse train duration (ns)	300
Pulse train interval (ns)	4600

3.3.2 Comparison of Machined Surface and Diameter of Discharge Craters

Comparison of machined surfaces between both methods is shown in Fig. 3.11. Machining with CPTM results in larger diameter of craters compared to the conventional EIFM even if the same number of discharges was generated within the same period of time. The average diameter of craters for CPTM and conventional EIFM is 11.52µm and 7.57µm, respectively. This is because, in the case of CPTM discharge occurs continuously at the same spot during the pulse train duration. With conventional EIFM however, since there was enough time for dielectric strength to recover after every pulse discharge, discharge spot of every discharge was scattered on the machined surface resulting in smaller discharge craters. Laser microscope (OLYMPUS OLS3000) was used to measure the arithmetic mean roughness, Ra of the machined surface. The measurement results are shown in Table 3.5. The surface roughness is better with conventional EIFM because for each pulse, the discharge duration is very short resulting in small discharge craters. However, the change in the surface roughness is insignificant compared to the crater diameter. This is because of the well-known fact that the plasma diameter increases with the passage of time after the dielectric breakdown, leading to decrease in the heat flux [1-3].

Table 3.5: Comparison of surface roughness between CPTM and Conventional EIFM

	CPTM	Conventional EIFM
Ra (µm)	0.152	0.145
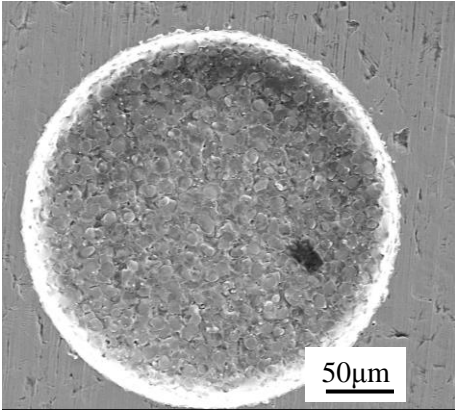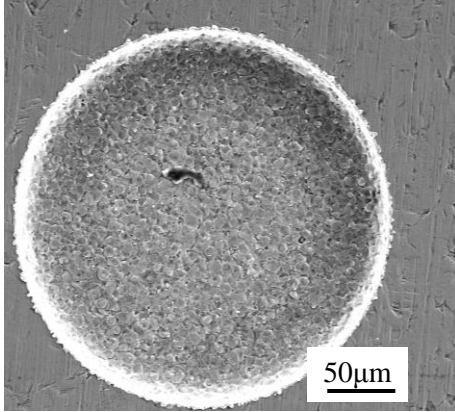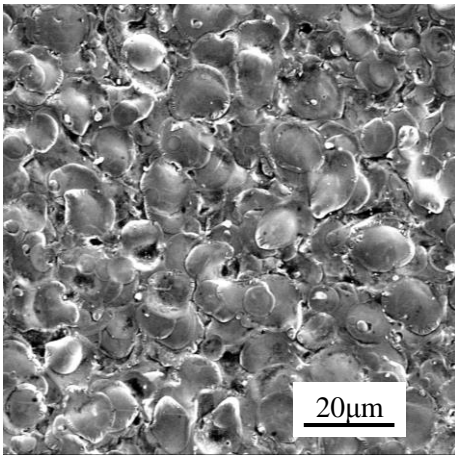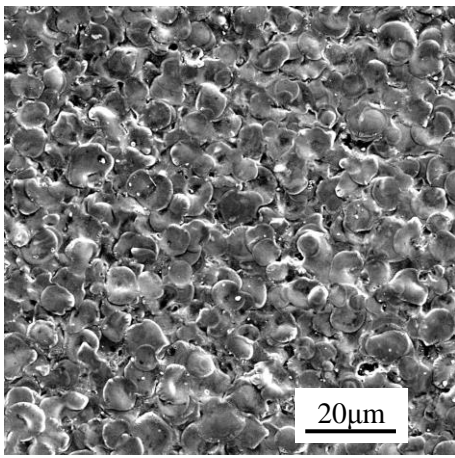
CPTM	Conventional EIFM
a) Average diameter of discharge craters: 11.52μm	b) Average diameter of discharge craters: 7.57μm

Fig. 3.11: Comparison of machined surface and diameter of discharge craters between CPTM and conventional EIFM using same feeding capacitance C_1

3.3.3 Material Removal Rate (MRR)

Fig. 3.12 shows the results of MRR. For conventional EIFM, the maximum feed speed was 0.9μm/s while the maximum feed speed for CPTM was 1.4μm/s. Above the feed speed limit, the machining was not possible due to short circuit. Three trials were performed to confirm the condition. The MRR should be the same at the same feed speed. However, with the conventional EIFM, the tool wear also increased when the feed speed increased as described in the next section. This was the reason why the MRR was higher with CPTM under the same feed speed.

The maximum feed speed with CPTM was higher than that of the conventional EIFM. Discharge frequency increases as the feed speed increases. However, for conventional EIFM, this leads to unstable machining and limits the feed speed. This was because,

discharge occurred continuously at every half cycle of the pulse during the high feed speed. This led to insufficient time for plasma to extinguish during the interval time between the individual discharges. Furthermore, since the half cycle time of 700kHz pulse is only 0.7μs, it is difficult for discharge ignition to occur within 0.7μs as described in Section 1.1.2. On the other hand, with controlled CPTM, sufficiently long pulse train interval was fixed after every accumulation of discharges, and the pulse train is controlled. Thus, the machining was stable leading to higher MRR.
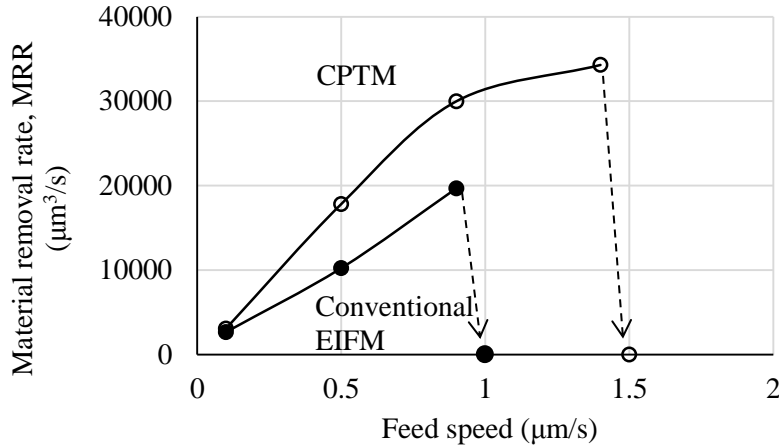
Fig. 3.12: Relationship between MRR and feed speed

3.3.4 Tool Wear Ratio (TWR)

Fig. 3.13 shows the results on TWR. TWR was obtained by dividing the volume of tool wear with the removal volume of workpiece. Under the same feed speed, TWR was lower with the controlled pulse train method. In conventional EIFM, the discharge with a high peak current within short duration in alternating polarity caused high tool wear [4]. With the pulse train method however, bipolar high frequency discharge over a long period of time in oil dielectric leads to carbon deposition on the tool surface, preventing excessive wear. It is well known that longer discharge duration results in lower TWR because of the carbon deposition [5-7]. When machining is performed with constant feed speed, the MRR for both conventional EIFM and CPTM under the same feed speed should be the same. However, the tool wear was higher with conventional EIFM. This is the reason why MRR was higher with CPTM under the same feed speed.
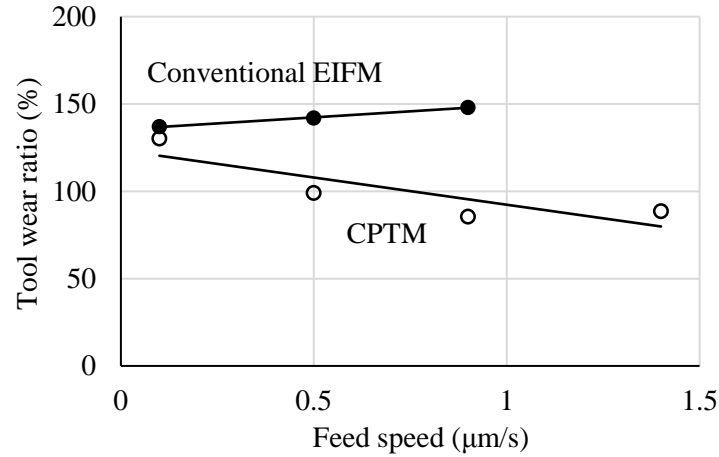
Fig. 3.13: Relationship between TWR and feed speed

3.4 Investigation on Optimum Pulse Train Interval

In the previous sections, characteristics of CPTM have been investigated by changing the discharge current conditions within the pulse train duration. However, the influence of pulse train interval is also important. This is because, MRR can be increased by decreasing the interval. Hence, if the pulse train interval is too short, there is not enough time for the temperature to decrease during the interval [1,8,9]. Machining will be unstable and will results in low MRR.

To optimize the pulse train interval, machining was performed at a constant pulse train duration of 400ns. Five different pulse train intervals were selected. The discharge current waveforms used in the experiment are illustrated in Fig. 3.14. Table 3.6 shows the machining parameters for the experiment. The pulse train duration was kept constant at 400ns. Every hole was drilled for 120 seconds at a constant feed speed. For every pulse train interval, the feed speed was increased in order to increase the discharge frequency, thereby the maximum MRR was obtained for every pulse train interval.
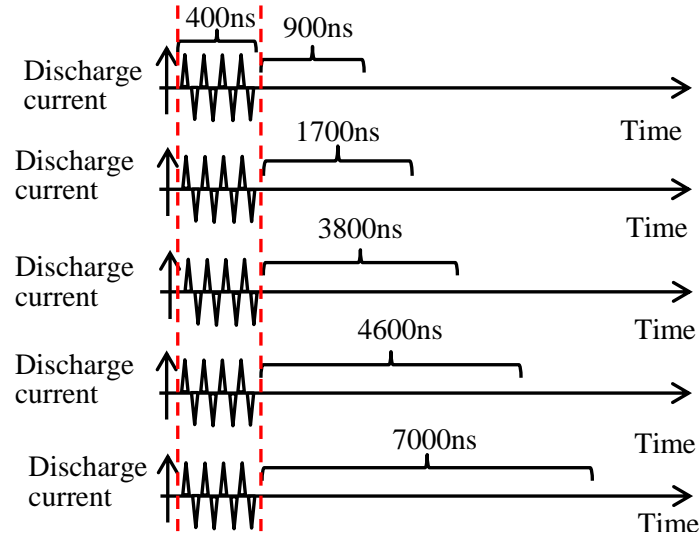
Fig. 3.14: Discharge current waveforms with different pulse train interval

Table 3.6: Experimental conditions to investigate the optimum pulse train interval

Pulse power supply(V)	100
Feeding capacitance, C_1	470 pF
Frequency (MHz)	5
Electrode	Tungsten carbide (Ø = 250µm)
Workpiece	Stainless steel (SUS 304)
Machining time (s)	120
Pulse train duration (ns)	400
Pulse train interval (ns)	900, 1700, 3800, 4600, 7000

The relationship between the maximum MRR and pulse train interval is shown in Fig. 3.15. As the pulse train interval increased, MRR also increased because machining stability was improved. After the optimum pulse train interval was reached at 3800ns, the MRR decreased. This is because, when the interval time is too long, the total number of discharges which can be generated within the same machining time is reduced. In the conventional EIFM, the maximum MRR was 40000µm^3/s as shown in Fig. 2.10, with the feeding capacitance of 470pF. There was no other way to increase the MRR in conventional EIFM. In CPTM, however, the maximum MRR in Fig. 3.15 is about 50000µm^3/s; higher than that in conventional EIFM. Since the pulse train duration used in the experiment was only 400ns, the MRR can be increased furthermore. Fig. 3.16 shows the relationship between TWR and pulse train interval. The tool wear keeps increasing even after the interval time of 3800ns.
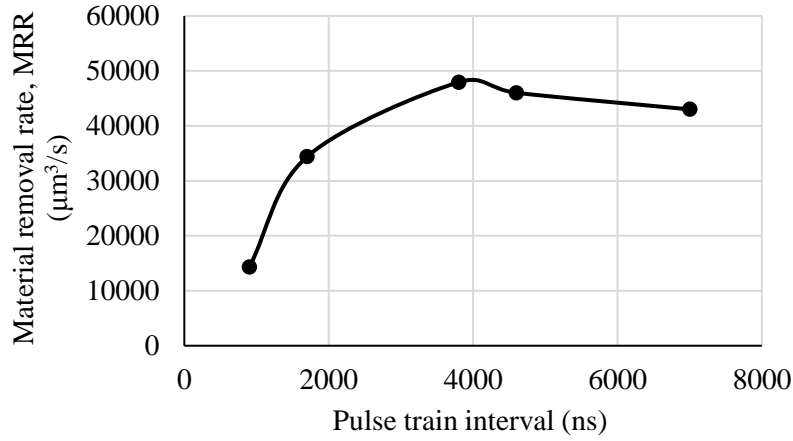
Fig. 3.15: Relationship between MRR and pulse train interval
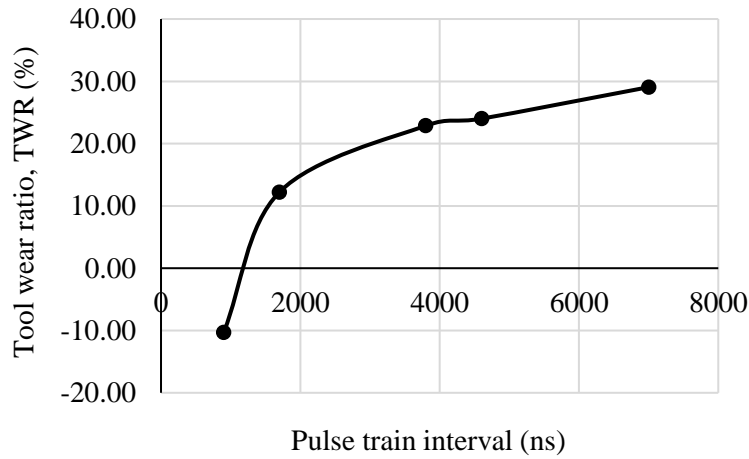
Fig 3.16: Relationship between TWR and pulse train interval

3.5 Comparison Between CPTM and RC Circuit

Relaxation pulse generator, or simply called RC circuit is commonly used in many micro EDM machine because low discharge energy and short pulse duration can be generated. Machining with a very high rotation speed of the tool helps in decreasing the electrode surface temperature and increasing machining speed [10,11]. However, it is not possible to rotate the tool electrode at very high speed with RC circuit because the pulse power supply must be connected to the tool using a brush. Rotating the tool at a very high speed can cause vibration which may influence the accuracy of machined holes. On the other hand, the development of CPTM is expected to improve the MRR of conventional EIFM and to allow the tool to be rotated at very high speed. Here, machining characteristics between CPTM and RC circuit are compared. Results on diameter of discharge craters, TWR, MRR and removal volume per crater are discussed.

3.5.1 Experimental Method

In the experiment, the discharge energy per pulse train for CPTM was calculated using Eq. 3.1 [12] where n is number of bipolar pulse discharges within the pulse train duration, u_e is the discharge voltage, i_e is the discharge current and t_e is discharge duration.

$$W_{\text{CPTM}} = n \int_o^{t_e} u_e.i_e dt \qquad (3.1)$$

Within the 300ns pulse train duration with frequency of 5MHz, 6 to 7 discharges can be generated, and total discharge energy per pulse train is about 11.78μJ. Then, this discharge energy is substituted into Eq. 3.2 [13] which shows the discharge energy of the RC circuit.

$$W_{\text{RC}} = 2C\,u_e\,(u_o - u_e) \qquad (3.2)$$

Assuming that the total discharge energy for both CPTM and RC circuit methods are the same, the equivalent capacitance, C to be used in the experiment for RC circuit can be calculated. In this calculation, u_e is the discharge voltage of 20V, and u_o is 100V which is the value of the open voltage. From the calculation, C was obtained as 3700pF.

Table 3.7 presents the machining conditions employed in the experiment. For CPTM, the pulse train duration and pulse train interval were selected based on the results obtained in Section 3.4. The machining was performed by drilling hole for 120 seconds at constant feed speeds. For the respective method, the feed speed was increased to obtain the maximum MRR.

Table 3.7: Experimental conditions to compare CPTM with RC circuit

Pulse power supply(V)	100
Electrode	Tungsten carbide (Ø = 250μm)
Workpiece	Stainless steel (SUS 304)
Machining time (s)	120
Dielectric	EDM oil
Relaxation pulse generator	
Capacitor (pF)	3700
Resistance (kΩ)	1
Controlled pulse train method (CPTM)	
Frequency (MHz)	5
Feeding capacitance, C_1	470 pF
Pulse train duration (ns)	300
Pulse train interval (ns)	3800

3.5.2 Discharge Waveforms, Machined Surface and Diameter of Discharge Craters

Fig. 3.17a and 3.17b shows the discharge waveforms generated with CPTM and RC circuit, respectively. The machined surface using CPTM and RC circuit at a feed speed of 0.5μm/s is shown in Fig. 3.18. With CPTM, since crater size depends on the continuity of discharges within a predetermined pulse train duration, some small craters due to the less number of discharges per pulse train can be seen among large craters on the machined surface. On the other hand, with the RC circuit, the crater size looks uniform, and it is similar to the large craters in CPTM since C was determined by $W_{CPTM}=W_{RC}$.

The relationship between the diameter of discharge crater and feed speed is presented in Fig. 3.19. During machining, as the feed speed increases the gap becomes small. Therefore, more discharges can be sustained within the pulse train duration with CPTM. As a result, there is a slight increase in diameter of discharge crater with the increase in the feed speed. On the other hand, there is a slight decrease in the size of discharge crater as the feed speed increases with the RC circuit. This is because as the feed speed increases, discharge occurs earlier before the capacitance is fully charged, resulting in smaller discharge crater [14].

Under the same feed speed of 0.5μm/s, the arithmetic mean roughness, Ra of the machined surfaces were measured. The measurement results are shown in Table 3.8. The surface roughness was almost the same for both methods. This is because Ra is determined by the large craters in CPTM.

Table 3.8: Comparison of surface roughness between CPTM and RC circuit

	CPTM	RC circuit
Ra (μm)	0.131	0.133
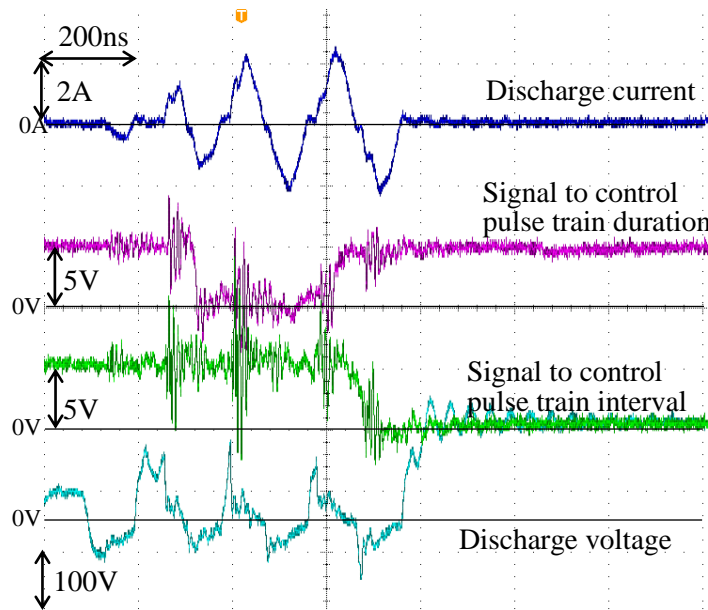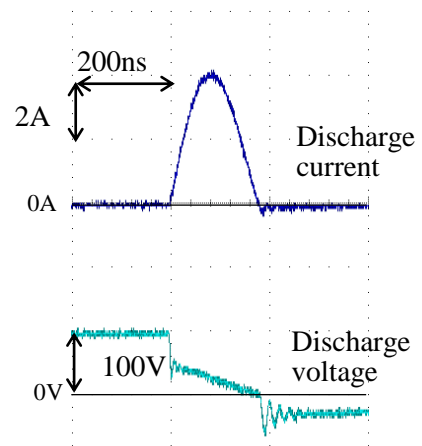
a) CPTM   b) RC circuit

Fig. 3.17: Comparison of discharge waveforms
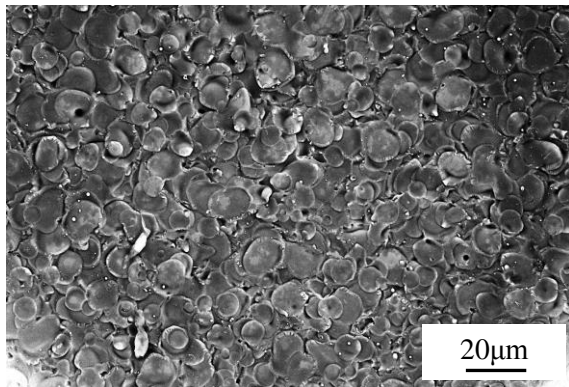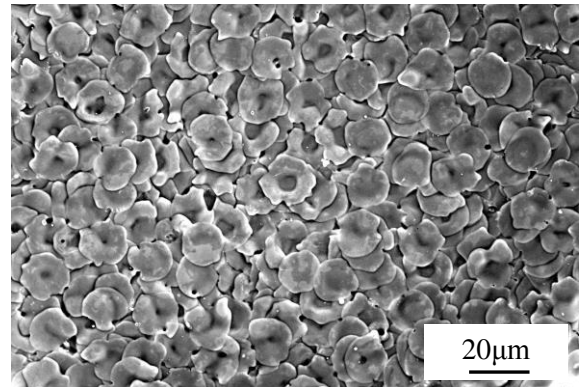
a) CPTM   b) RC circuit

Fig. 3.18: Comparison of machined surface
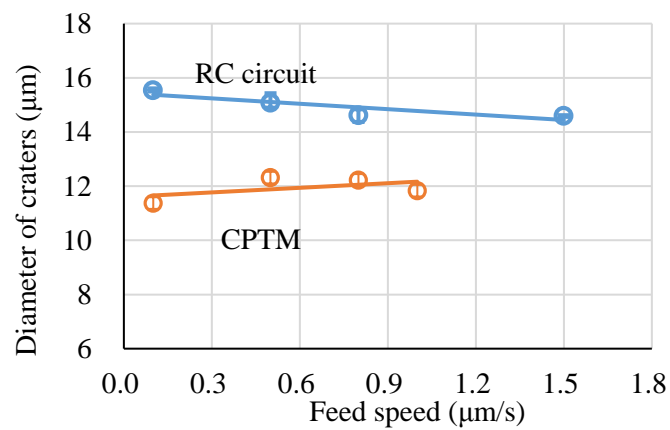
Fig. 3.19: Relationship between diameter of craters and feed speed

3.5.3 Tool Wear Ratio (TWR)

The relationship between TWR and feed speed is shown in Fig. 3.20. The TWR was obtained by dividing the volume of tool wear with the removal volume of workpiece. In the experiment, the maximum feed speed for the RC circuit was 1.5µm/s while for CPTM was 1.1µm/s. Beyond the maximum feed speed, machining cannot be completed within the pre-set machining time because the tool collided with the workpiece. This result was confirmed with three trials. CPTM results in higher TWR compared to the RC circuit because of the bipolar discharge. However, TWR decreases gradually with the increase in the feed speed because carbon deposition on the tool surface prevents excessive wear [5-7].
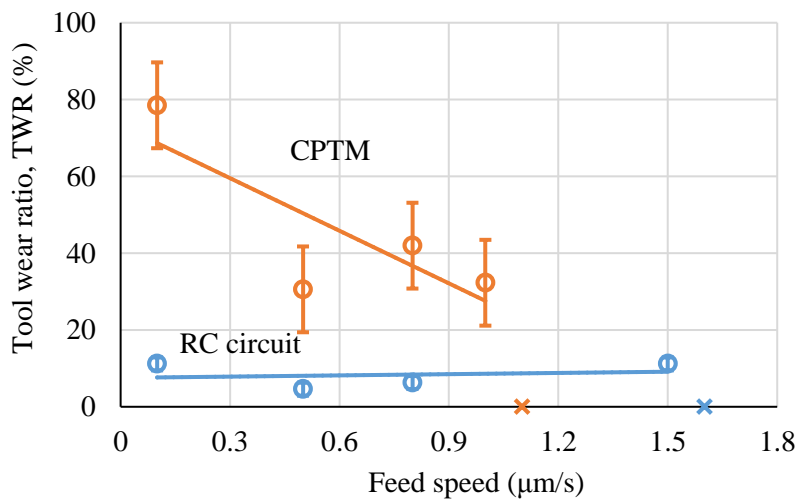
Fig. 3.20: Relationship between TWR and feed speed

3.5.4 Material Removal Rate (MRR)

Fig. 3.21 shows the relationship between the MRR and feed speed. As the feed speed increased, MRR for both methods increased. Under the same feed speed, the rate for material removal should be the same. However, the tool wear was higher with the CPTM as shown in Fig. 3.20. This is the reason why under the same feed speed, the MRR was higher for machining with the RC circuit.

With CPTM, the maximum MRR is only two thirds of that with the RC circuit. Long discharge duration and lower peak current with CPTM caused small melted and evaporated region in workpiece, thereby more energy is lost due to the heat conduction into the workpiece [15]. This results in lower energy efficiency compared to the high peak current and short discharge duration of the RC circuit even though the discharge energy is the same. In addition, the discontinuity of discharges during the pulse train duration also decreased the MRR in CPTM.

83
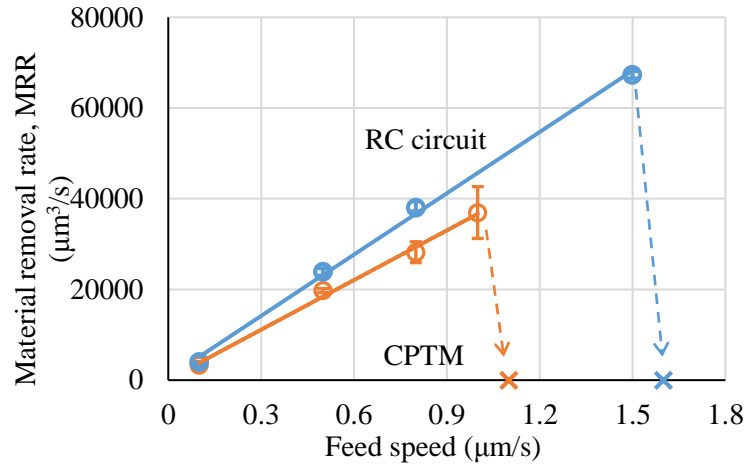
Fig. 3.21: Relationship between MRR and feed speed

3.5.5　Removal Volume per Crater

Removal volume per crater was obtained by dividing the volume of material removal with the number of discharges generated during machining. Discharges in the gap were detected by current sensor and were counted using a universal counter (Hewlett Packard 5313A). The relationship between the removal volume per crater and feed speed is shown in Fig. 3.22. The removal volume is lower with CPTM because the discharge is bipolar, and there is a difference in energy distribution between cathode and anode [15-17]. The influence of the discharge duration on the energy efficiency is another reason as described in the previous section.

Removal volume per crater decreased as the feed speed increased in the case of RC circuit. This is because discharge occurred earlier before the capacitance was fully charged. However, with CPTM, the removal volume per crater increased with the increase of the feed speed because more discharges were sustained within the pulse train duration. The results coincide with the changes of the discharge craters shown in Fig. 3.19.
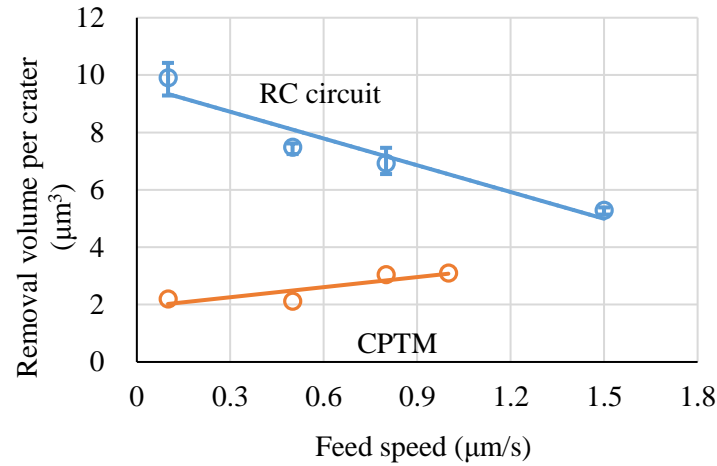
Fig. 3.22: Relationship between removal volume per crater and feed speed

3.6 Concluding Remarks

With CPTM, since discharges can occur at a single location, larger diameter of craters can be obtained at higher frequency and longer pulse train duration. The MRR increased steadily with the increase in pulse train duration. It was also verified that, machining is faster with CPTM compared to the conventional EIFM under the same discharge energy per unit time. In the conventional EIFM, there is a limit in the MRR under a feeding capacitance determined by the configuration of the feeding electrode. In contrast, there is no limit in CPTM, because the discharge energy can be increased by increasing the pulse train duration. Even though CPTM is developed in order to increase the machining speed, the surface roughness is not so bad compared to the conventional EIFM because the increase of plasma diameter with respect to time decreases the heat flux. Lower TWR with CPTM is an advantageous so that the tool can retain the shape to achieve better machining accuracy. On the other hand, the energy efficiency of CPTM was lower than RC circuit because of low peak current occurs within long discharge duration. By increasing the feed speed, diameter of discharge craters and removal volume per crater increased with CPTM, whereas those decreased with the RC circuit.

3.7 References

1. Kojima A, Natsu W, Kunieda M, 2008, Spectroscopic measurement of arc plasma diameter in EDM, CIRP Annals-Manufacturing Technology, vol. 57, no. 1, pp. 203–207.
2. Hiroaki Hashimoto, Masanori Kunieda, 1997, Spectroscopic analysis of temperature variation of EDM arc plasma, Journal of Japan Society of Electrical Machining Engineers, vol. 31, no. 68, pp. 32-40 (in Japanese).

3. Heng Xia, Hiroaki Hashimoto, Masanori Kunieda, Nobuhiko Nishiwaki, 1996, Measurement of energy distribution in continuous EDM process, Journal of Japan Society of Precision Engineering, vol. 62, no. 8, pp. 1141-1145 (in Japanese).

4. Yuna Yahagi, Wataru Natsu, Tomohiro Koyano, Masanori Kunieda, 2011, Reduction of tool wear in non-contact electrostatic induction feeding EDM, Proceeding The 6th International Conference on Leading Edge Manufacturing in the 21st Century (LEM21).

5. Naotake Mohri, Masayuki Suzuki, Masanori Furuya, Nagao Saito, 1995, Electrode wear process in electrical discharge machining, CIRP Annals-Manufacturing Technology, vol. 44, no. 1, pp.165-168.

6. Wataru Natsu, Masanori Kunieda, Nobuhiko Nishiwaki, 2004, Study on influence of inter-electrode atmosphere on carbon adhesion and removal amount, International Journal of Electrical Machining, no. 9, pp. 43-50.

7. Masanori Kunieda, Teruki Kobayashi, 2004, Clarifying mechanism of determining tool electrode wear ratio in EDM using spectroscopic measurement of vapor density, Journal of Materials Processing Technology, no. 149, pp. 284-288.

8. Shinya Hayakawa, Heng Xia, Masanori Kunieda, Nobuhiko Nishiwaki, 1996, Analysis of time required to deionize an EDM gap during pulse interval, Symposium on Molecular and Micro Scale Heat Transfer in Materials Processing and Other Applications, pp. 368-377.

9. Wataru Natsu, Satoyuki Ojima, Teruki Kobayashi, Masanori Kunieda, 2004, Temperature distribution measurement in EDM arc plasma using spectroscopy, JSME International Journal, Series C, vol. 47, no. 1, pp. 384-390.

10. Yuna Yahagi, Tomohiro Koyano, Masanori Kunieda, Xiaodong Yang, 2012, Micro drilling EDM with high rotation speed of tool electrode using the electrostatic induction feeding method, 5th CIRP Conference of High Performance Cutting 2012, Procedia CIRP 1, pp.162-165.

11. Y. Zhang, H. Zhao, G. Zhang, Z. Wang, W. Zhao, 2008, Research on a micro-EDM system and its techniques, Journal of China Mechanical Engineering, vol. 5, no. 19, pp. 526-530, (in Chinese).

12. M. Kimori, M. Kunieda, S. Sano, 2007, Mechanism of determining discharge energy in electrostatic induction feeding EDM, Proceeding of Asian Electrical Machining Symposium '07, pp. 242-245.

13. T. Masuzawa, 2001, Micro-EDM, Proceedings of the 13th International Symposium for Electromachining, ISEM XIII 1 pp.3-19.

14. T. Koyano, M. Kunieda, 2010, Achieving high accuracy and high removal rate in micro-EDM by electrostatic induction feeding method, CIRP Annals-Manufacturing Technology, vol. 59, pp.219-222.

15. Xia H., Kunieda M., Nishiwaki N., 1996, Removal amount difference between anode and cathode in EDM process, International Journal of Electrical Machining, no. 1, pp. 45-52.

16. Hayakawa, S., Yuzawa, M., Kunieda, M., Nishiwaki, N., 2001, Time variation and mechanism of determining power distribution in electrodes during EDM process, International Journal of Electrical Machining, no. 6, 19-26.

17. Mohd Zahiruddin and Masanori Kunieda, 2010, Energy distribution ratio into micro EDM electrodes, Journal of Advanced Mechanical Design, Systems, and Manufacturing, vol.4, no.6, pp. 1095-1106.

(This page is intentionally left blank)

Chapter 4

Increasing Discharge Energy using Resonance in Circuit

By having capacitance C and inductance L in a circuit, resonance occurs at a specific value of frequency called resonant frequency, f_r. At this condition, impedance in the circuit is minimum allowing the AC voltage to be amplified at higher amplitude in the discharge gap. The high open voltage, u_o is one of the factors which influence the discharge energy as shown in Section 1.3.2. Okada et al. [1] examined the effects of resonant frequency when working with radio-frequency plasma EDM. Their circuit however, is equivalent to the conventional RC pulse generator except that a radio-frequency power supply is used instead of the conventional constant voltage power supply. Hence, non-contact feeding cannot be achieved with their method. In addition, since a pause period is not inserted, machining becomes unstable when the resonant frequency is high. In contrast, EIFM with the controlled pulse train method introduces intervals between groups of discharges, thereby resolving the problem of instability.This chapter discussed the utilization of resonance in the circuit to increase the discharge energy for micro electrical discharge machining (EDM) with controlled pulse train method (CPTM). The influences of capacitance and inductance on the resonant frequency were investigated. The probability of discharge continuity within the pulse train duration when machining is performed at f_r was observed. Finally, the dependence of MRR on the frequency was obtained.

4.1 Resonance Circuit in Series

Fig. 4.1 shows the experimental setup used to investigate the influence of resonance in order to increase the discharge energy. Here, W_L is the length of the coaxial cable connecting the pulse power supply to the tool and C_1 is a silver mica capacitor served as

the feeding capacitance. The equivalent circuit having inductance L, feeding capacitance C_1, working gap capacitance C_2 and resistance R is shown Fig. 4.2, where R is the resistance of the arc discharge. The inductor stores energy in the magnetic field while capacitor stores energy in the electric field; creating AC voltage and current cycles. The oscillation amplitude depends on the size of inductor and capacitor due to the exchange of energy back and forth between them thereby the amplitude of the working gap voltage can exceed the amplitude of AC power supply. Assuming that R is negligible, resonant frequency, f_r in the circuit can be calculated using Eq. (4.1)
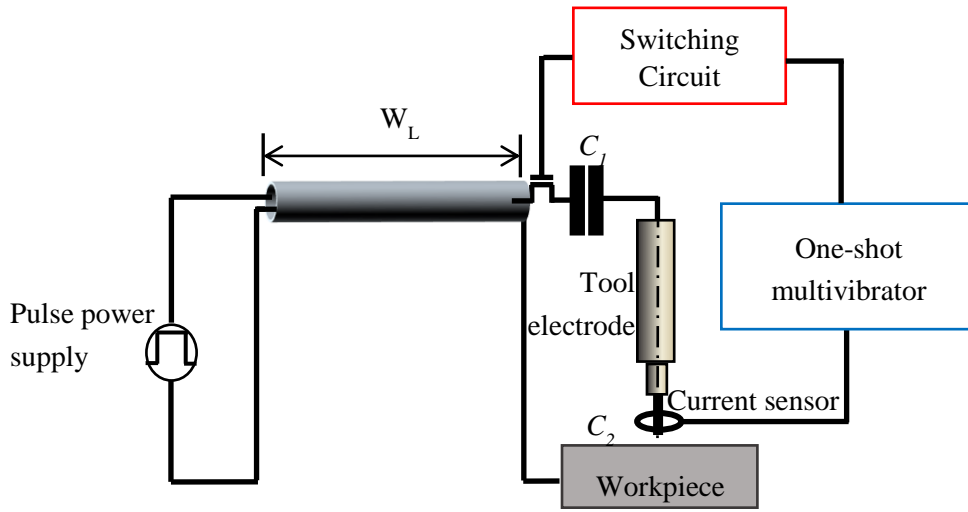
Fig. 4.1: Experimental setup
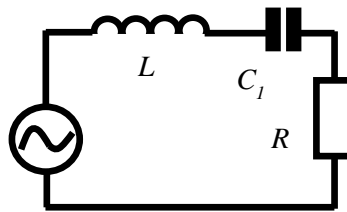
Fig. 4.2: Equivalent circuit of the system

$$f_r = \frac{1}{2\pi\sqrt{LC_1}}$$
(4.1)

Using the Agilent 4294A Precision Impedance Analyser, inductance in the circuit was measured. Instead of the pulse power supply, the impedance analyser was connected to the setup shown in Fig. 4.1, and the working gap was short circuited. Three coaxial cables with different lengths were tested. Since the resonance frequency depends on L, measurement was conducted around the f_r. With wire length of 1200mm, 2100mm, and 3700mm , the total inductance in the circuit at $f_r = 7$MHz were 1µH, 2µH, and 3.8µH, respectively.

4.2 Waveforms Observation

4.2.1 Gap Voltage Waveforms

In this study, a square waveform was supplied by the pulse power supply to the discharge gap. Fig. 4.3 shows the influence of different supplied waveforms on the discharge current. In the case of square waveform as shown in Fig. 4.3(a), the same discharge energy and discharge duration can be achieved at any time independent of discharge delay time, t_d; if the rise time is quick enough for the supply voltage to reach the maximum amplitude. On the other hand, discharge energy and discharge duration are different depending on t_d with the sine waveform. Fig. 4.3(b) shows the discharge current at different t_d. This is undesirable because it will influence the size of discharge crater and surface roughness.

(a) Square waveform   (b) Sine waveform
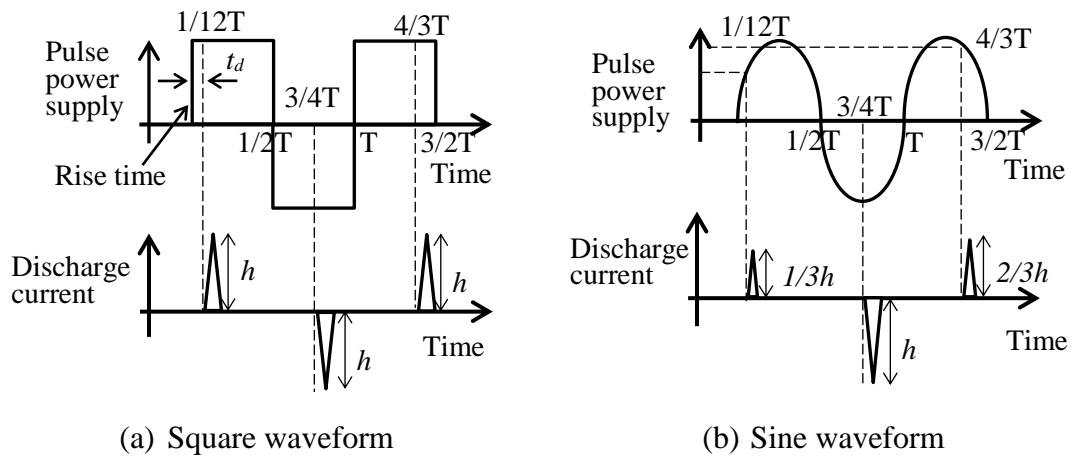
Fig. 4.3: Influence of different waveform on discharge current

In conventional EIFM, low frequency pulse was employed so that every pulse discharge can be dispersed at different location. In this case, square waveform should be used in order to obtain the same discharge energy which results in the same discharge crater. Since EIFM is used for finish machining, this is important in order to obtain good surface finish. In CPTM however, high frequency pulses is used to obtain several continuous discharges occurring at the same location. The total discharge energy depends on the number of generated discharges.

Based on the preliminary investigation, continuous discharge can be generated at the same location within the pulse train duration at a minimum frequency of 3MHz. Even in this case, it is necessary to use square waveform because there exists interval between successive discharges to keep the discharge current of individual pulse discharges the same. With increasing the frequency however, even if square waveform is being supplied by the pulse power supply, the output voltage waveform is deformed to like a sine wave

because of frequency limit of the power supply.

Fig. 4.4 shows the deformation of the square wave supplied by the pulse power supply (NF high speed bipolar amplifier with frequency limit of 10MHz, HSA 4104) as the frequency increases from 1MHz to 10MHz. Thus, for simplicity it is assumed that a sine wave is being applied to the gap and the influence of resonance can be investigated. During the investigation, amplitude of pulse power supply was 100V, $L=1\mu H$ and $C_1=470pF$.

a) 1MHz

b) 3MHz

c) 5MHz

d) 7MHz

e) 10MHz
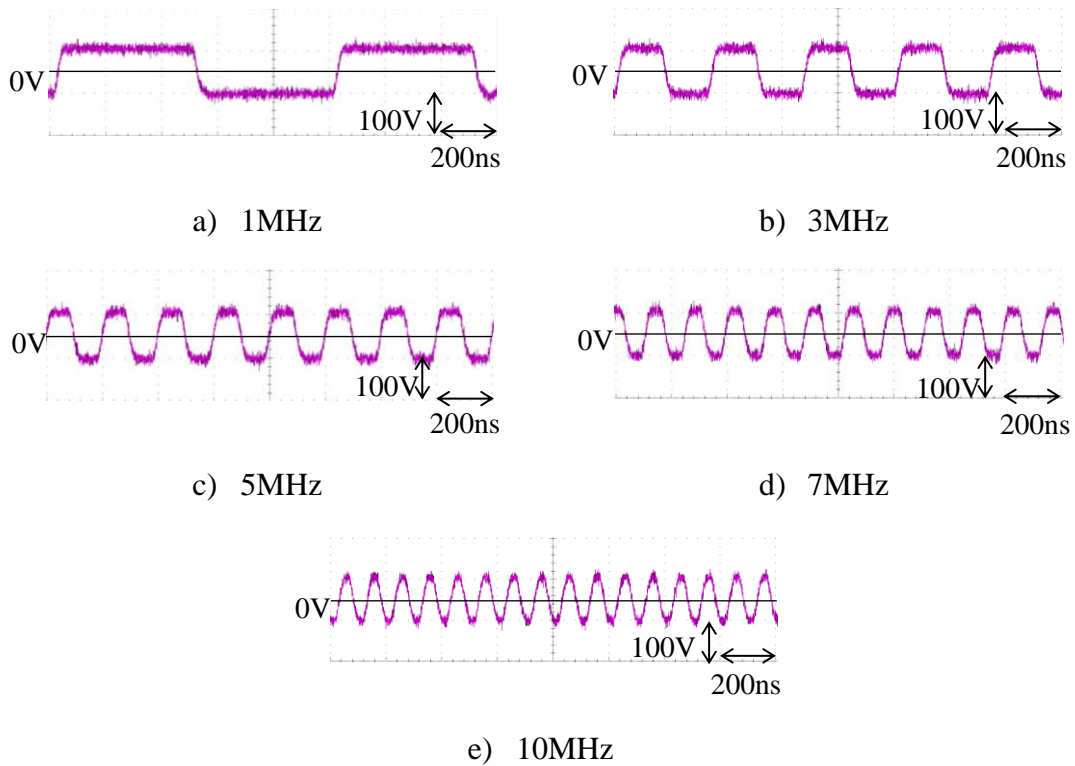
Fig. 4.4: Output of voltage waveform at different frequency using bipolar pulse power supply HSA 4104 by NF.

4.2.2 Voltage Waveforms Across Feeding Capacitance, C_1

Using the same machining conditions as in Section 4.2.1, the change in voltage amplitude across C_1 was investigated. During the measurement, discharge gap was short circuited in order to eliminate the influence of C_2. Frequency was increased from 1MHz to the calculated f_r of 7MHz. It was found that voltage amplitude increases as frequency is increased as shown in Fig. 4.5. Due to the exchange of energy back and forth between capacitor and inductor in the circuit, the voltage amplitude can exceed 100V. Voltage amplitude is highest at 7MHz within the frequency used in the experiment. This shows that there exists the influence of resonant frequency in the circuit.
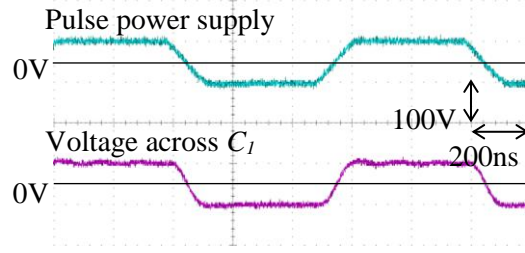
a) 1MHz
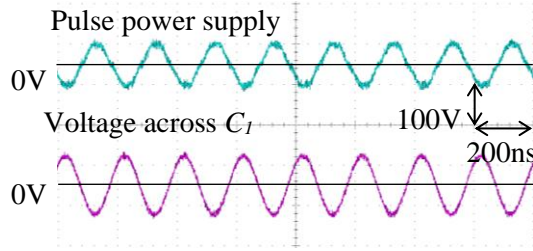
b) 5MHz
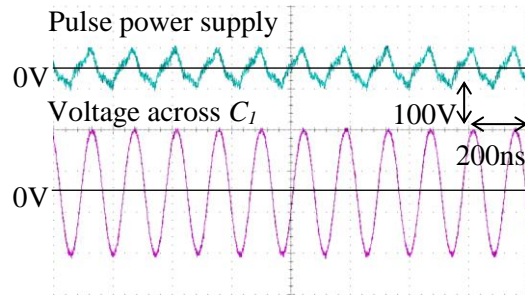
c) 7MHz

Fig. 4.5: Voltage waveform at different frequency across C_1

4.2.3   Discharge Current Waveforms

A preliminary observation on the discharge waveform was carried out at five different frequencies. Machining was performed using the CPTM with 600ns pulse train duration using machining conditions shown in Table 4.1. At C_1=470pF and L=1μH, the calculated f_r was 7MHz. Fig. 4.6 shows the discharge current waveforms at the calculated resonant frequency of 7MHz, and also at frequencies lower and higher than that.

Table 4.1: Experimental conditions to investigate the average discharge energy per pulse, q at $1\mu H$

Amplitude of pulse voltage (V)	100
Frequency (MHz)	3, 5, 6, 7, 8
Capacitance, C_1 (pF)	470
Inductance, L (µH)	1
Tool electrode (Rod)	Tungsten carbide (Ø 250µm)
Workpiece	Stainless steel (SUS 304)
Dielectric fluid	EDM oil
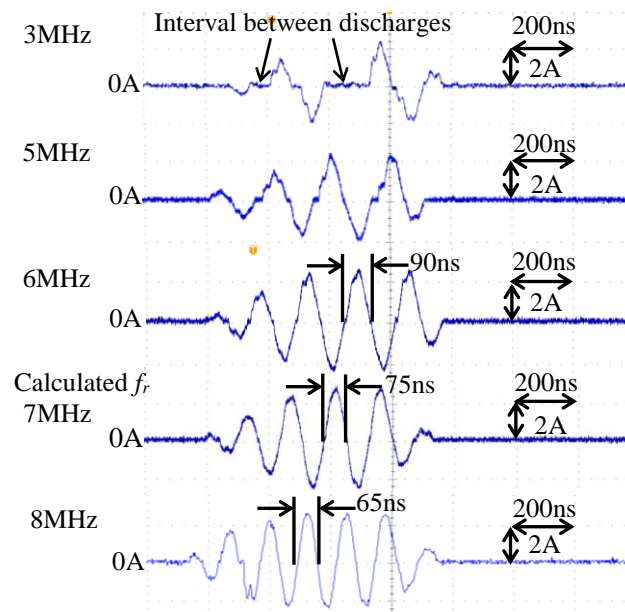
Fig. 4.6: Discharge current waveforms at different frequencies with CPTM

The amplitude of discharge current was lower when there was no resonance at 3MHz compared to 6MHz or 7MHz. The low pulse frequency resulted in interval existing between the discharges. Fig. 4.7 shows the discharge waveforms obtained at the frequency of 1MHz with the same machining parameters using the conventional EIFM. The waveform of each discharge was similar to 3MHz. The discharge current was small in the case of 1MHz with conventional EIFM, and discharge location dispersed at different locations on the machined surface. Without resonance, discharge energy was small and discharge was difficult to continue at the same place.
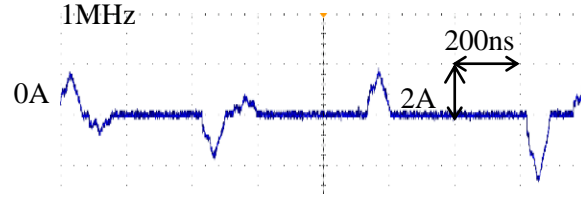
Fig. 4.7: Discharge waveform with conventional method at 1MHz

At 8MHz, when the frequency was higher than the calculated f_r, the amplitude of discharge current was slightly smaller than that with 7MHz. Furthermore, the pulse width was shorter with 8MHz as shown in Fig. 4.6. This shows that, both the amplitude and pulse width can be increased when machining is performed at the f_r. The increase in both the amplitude and pulse width can help to increase discharge continuity within the pulse train duration. In order to confirm that 7MHz is the actual f_r for selected C_1 and L, an experiment was carried out using the machining conditions shown in Table 4.1 with 1400ns pulse train duration. A longer pulse train duration of 1400ns as shown in Fig. 4.8 was used in order to obtain more samples of pulse discharge within the pulse train duration.
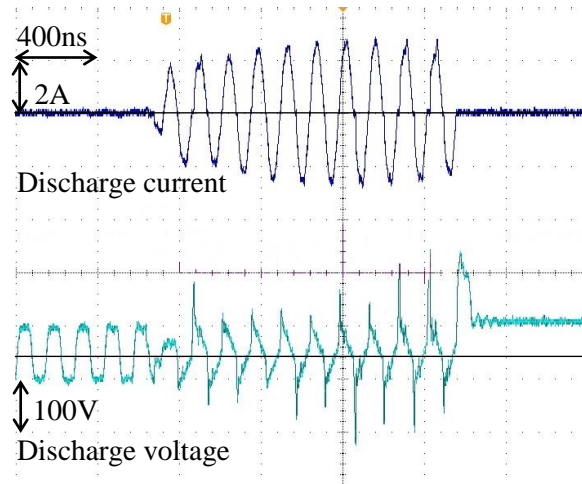
Fig. 4.8: Discharge waveform at 7MHz, 470pF and 1μH

The average discharge energy per pulse, q was obtained from all the pulses generated within the pulse train duration using the following equation,

$$q = \frac{1}{n} \Sigma \int_o^{t_e} u_e . i_e dt \qquad (4.2)$$

In this equation, n is the number of occurrences of discharge during the pulse train duration, u_e is the discharge voltage, i_e is the discharge current, and t_e is the discharge duration of every pulse. The discharge energy was calculated by integrating each pulse of discharge current with the respective discharge duration, summed and multiply with

discharge voltage of 20V. Then, q was obtained by dividing the value of integral with the number of discharge pulses within the pulse train duration.

Fig. 4.9 shows the relationship between q and frequency. It was found that highest q was obtained at 6MHz, which was slightly different from the calculated value. During the process of measuring the inductance in the circuit, the pulse power supply was replaced with the impedance analyzer. The voltage used during measurement was different from the pulse voltage during the machining and the gap was short circuited. In this study, these are the possible reasons why there is a slight difference between the calculated and experimental results.
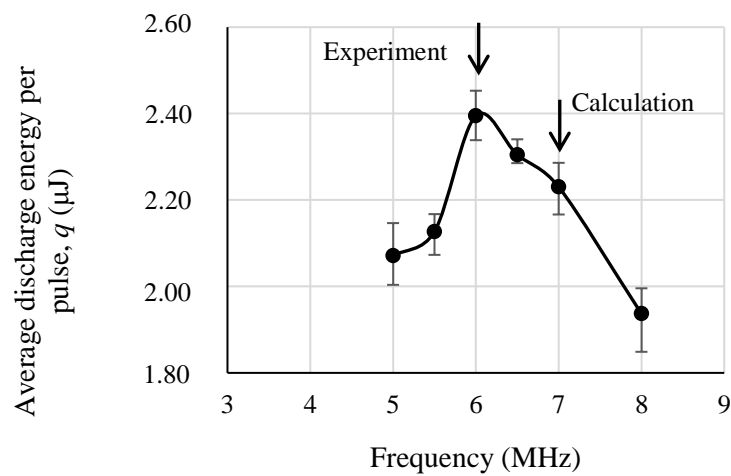
Fig. 4.9: Relationship between q and frequency at 1μH

Fig. 4.10 shows the discharge current waveform at 6MHz and 1400ns pulse train durations. There is an amplification of discharge current immediately after the dielectric breakdown due to resonance. This shows that resonance has a tendency to increase the amplitude of discharge current and stimulate discharge continuity within the pulse train duration.
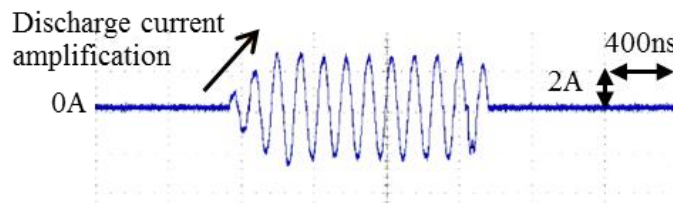
Fig. 4.10: Discharge current waveform at 6MHz and 1400ns pulse train duration

4.3 Influence of Capacitance, C_1 on Resonant Frequency, f_r and Average Discharge Energy per Pulse, q

Any change in C_1 or L, will influence the f_r. Understanding the influence of C_1 on f_r is desirable especially when this method is to be applied to non-contact feeding electrode. Therefore, q was investigated at three different capacitances using the same experimental setup shown in Fig. 4.1, under the machining conditions shown in Table 4.2. Machining was conducted near the f_r which was calculated using Eq. (4.1). In addition, machining was also carried out at frequencies higher and lower than the calculated f_r to identify any difference between the calculation and experimental results. After that, q was calculated using Eq. (4.2).

Table 4.2: Experimental conditions to investigate relationship between resonant frequency, f_r and capacitance, C_1

Amplitude of pulse voltage (V)	100	
Capacitance, C_1 (pF)	150, 220	470
Frequency (MHz)	1, 7,7.5, 8, 8.5, 9	1, 5, 5.5, 6, 6.5, 7,8,
Inductance, L (μH)	2	
Tool electrode (Rod)	Tungsten carbide (Ø 250μm)	
Workpiece	Stainless steel (SUS 304)	
Dielectric fluid	EDM oil	
Pulse train duration (ns)	1400	

Figs. 4.11a to 4.11c show the relationship between q and frequency at three different capacitances. In each graph, q peaks near the f_r which was calculated by Eq. (4.1). These findings confirm that even if low capacitance is used, higher discharge energy can be achieved when machining is carried out at f_r of the circuit. To show the relationship between f_r and C_1, the peak value from each graph is selected and tabulated in Fig. 4.12. This figure compares the calculation and experimental results of f_r. Both show that f_r becomes higher when C_1 is smaller even if there is slight difference between the calculation and experimental results.

When machining is performed at 1MHz using the conventional EIFM, discharge is dispersed at different locations. Fig. 4.13 shows the comparison of q between the conventional EIFM at 1MHz and the CPTM at f_r with different capacitances. It is found that q can be significantly increased when machining is carried out at f_r.
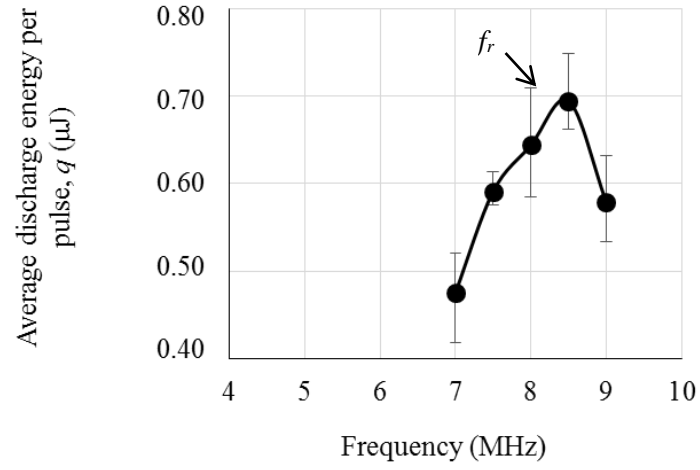
a) *q* at 150pF
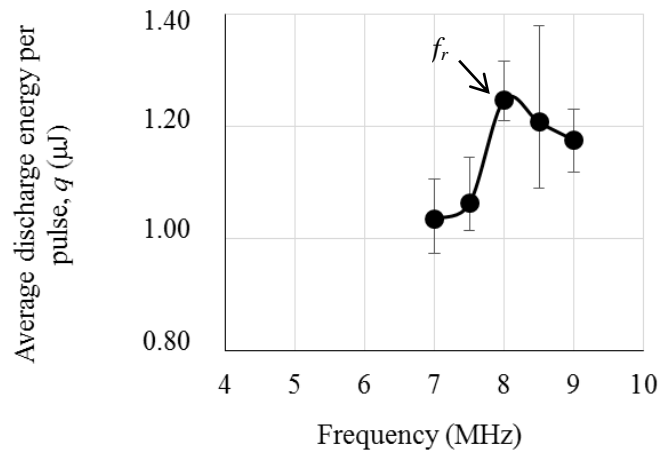
b) *q* at 220pF
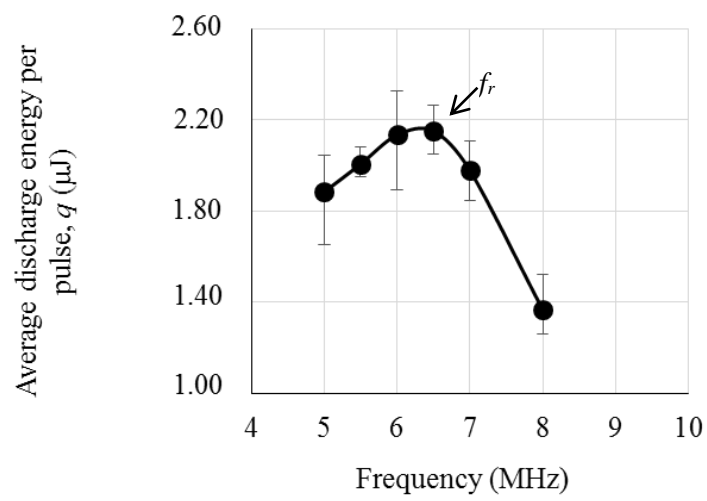
c) *q* at 470pF

Fig. 4.11: Investigation on relationship between *q* and C_1
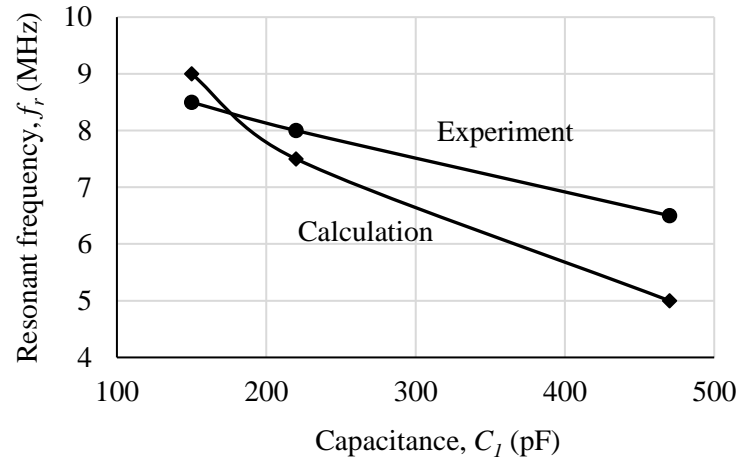
Fig. 4.12: Relationship between resonant frequency, f_r and capacitance, C_1
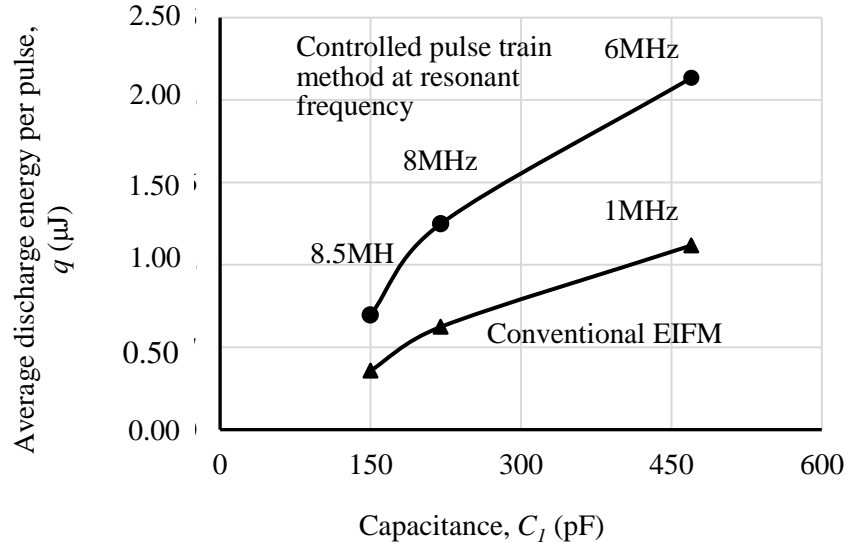
Fig. 4.13: Comparison of q between controlled pulse train method at f_r and conventional
EIFM at 1MHz

4.4 Influence of Inductance, L on Resonant Frequency, f_r

In the application to non-contact feeding electrode, the capacitance formed in the gap, C_1 was only about 16.3pF [2]. Thus, when L=1µH, f_r of approximately 40MHz needs to be supplied. However, the available pulse power supply (NF: HSA 4104) can only generate a maximum frequency of 10MHz. To solve this problem, f_r can be reduced by increasing L. The L can be increased by reducing the cable diameter, increasing the length of the cable, or by adding an inductor in the circuit. To investigate the relationship between f_r and L, the machining conditions shown in Table 4.3 were used. With C_1=220pF, three different inductances were used, and the change in q was investigated.

Figs. 4.14a, b and c show the relationship between q and frequency at L=1µH, 2µH, and 3.8µH, respectively. The peak in those figures shows the resonance at the respective L. The values of q and f_r obtained from every peak in Figs. 4.14a – 4.14c were then plotted in Fig. 4.15 to compare between the experiment and the calculation results. This graph shows that with increasing L, the f_r decreases. Hence, by increasing L, machining with the CPTM becomes possible at lower f_r even if C_1 is significantly small.

Table 4.3: Experimental conditions to investigate relationship between resonant frequency, f_r and inductance, L

Amplitude of pulse voltage (V)	100		
Frequency (MHz)	8, 9, 10	7, 8, 9	6, 7, 8
Inductance, L (µH)	1	2	3.8
Capacitance, C_1 (pF)	220		
Tool electrode (Rod)	Tungsten carbide (Ø 250µm)		
Workpiece	Stainless steel (SUS 304)		
Dielectric fluid	EDM oil		
Pulse train duration (ns)	900		

a) q at 1μH

b) q at 2μH

c) q at 3.8μH

Fig. 4.14: Investigation on relationship between q and L
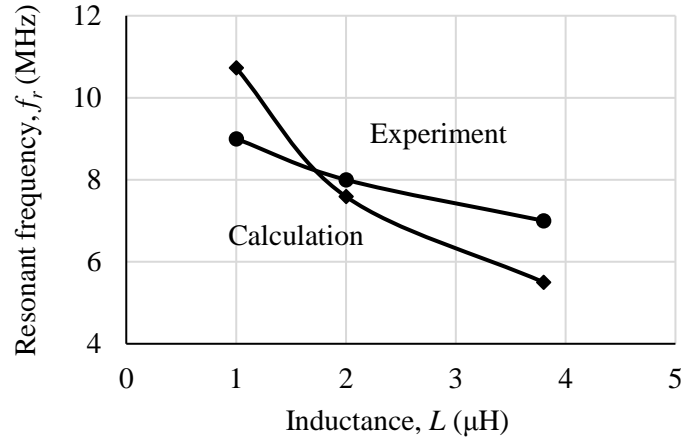
Fig. 4.15: Relationship between f_r and L

4.5 Probability of Discharge Continuity within Pulse Train Duration

In Figs. 4.11 and 4.14, q peaks at f_r. However, there is no significant change in q with respect to the frequency. Nevertheless, if we consider that the machining is carried out with CPTM, this small difference in discharge energy may stimulate discharge continuity within the pre-determined pulse train duration. With this, more discharges can be sustained within the pulse train duration. Uniform crater size can be achieved, and higher MRR can be obtained. To confirm this, the probability of discharge continuity within the pulse train duration was examined and discussed.

Discharge sustainability was examined using the experimental results presented in Fig. 4.12. The influence of resonant frequency on the continuity of discharges within pulse train duration was investigated by identifying the number of discharges n, which occur continuously within the pulse train duration. Three hundred pulse trains with the number were sampled at and around the f_r. Except for the pulse train duration, the machining conditions shown in Table 4.3 were used in the experiment. Because of the difference in frequency, the pulse train duration was changed in order to achieve 20 pulse cycles per pulse train duration for respective frequency. During the machining, the discharge waveforms were observed, and the number of pulse discharges which occurred continuously within the pulse train duration was counted.

The probability of discharge occurring at different frequencies is shown in Fig. 4.16. The machining was carried out at $L=1\mu H$ and $C_l=220pF$. From the figure, the probability of discharges continuing throughout the pulse train duration is highest, over 50%, when machining was carried out at $f_r=9MHz$. Also, at $L=2\mu H$ and $L=3.8\mu H$, the highest probability of discharge endurance can be obtained at the f_r of the circuit as shown in Figs. 4.17 and 4.18, respectively. This is because at f_r, the discharge energy per pulse is higher,

and the discharge pulse width is longer compared to other frequencies. Thus, when discharge occurs, it is able to continue until the pulse power supply is stopped. When machining is performed at the frequencies higher or lower than the f_r, the probability to complete 20 discharges within the pulse train duration is low.

According to the probability theory, the expected value is the average repetition of random variable over its range of values. In this case, the expected number of discharges per pulse train duration, n_e should be highest when machining is carried out at f_r. The expected numbers for C_1=220pF is shown in Fig. 4.19. It is found that the highest repetition of discharges per pulse train duration always occurs at f_r. On average, 17, 12 and 14 discharges can be sustained within the pulse train duration when L=1, 2, and 3.8μH respectively. However, it is still difficult to sustain the pulse discharges always until the end of the pulse train duration, even at the f_r. This is because, the discharge current becomes zero after every pulse discharge, which may result in extinction of the arc plasma.
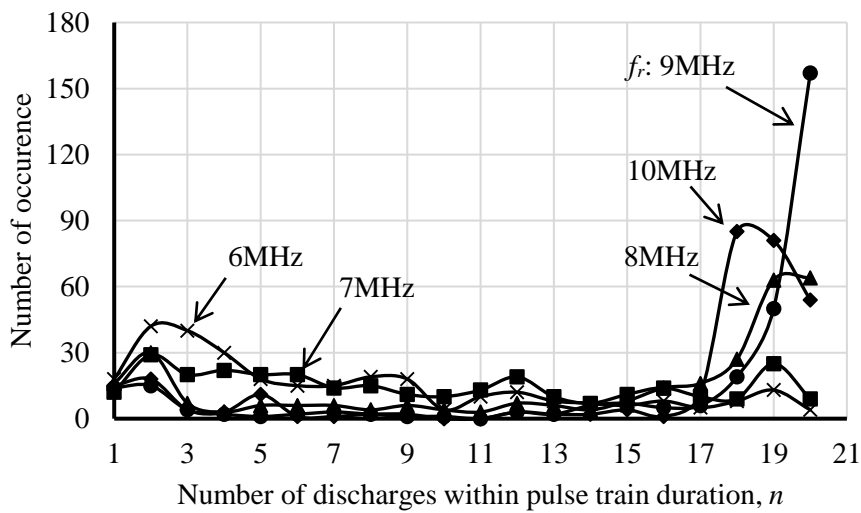
Fig. 4.16: Discharge occurrence at L =1μH and C_1 = 220pF
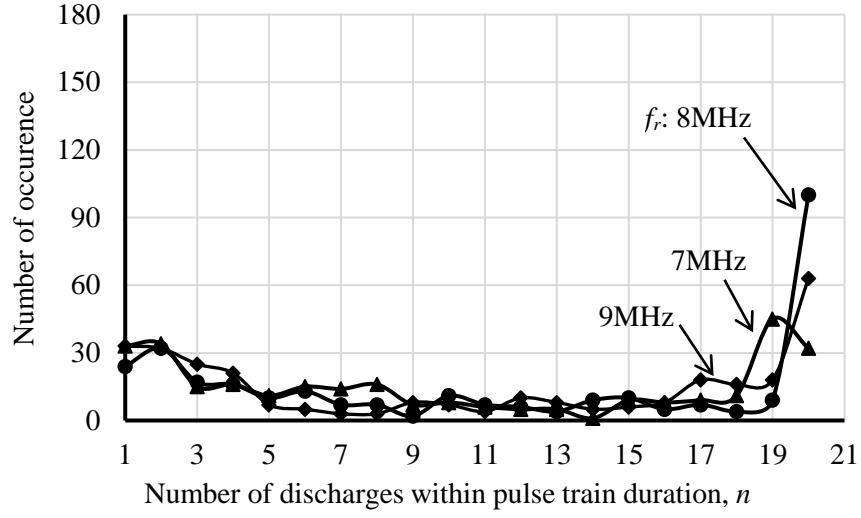
Fig. 4.17: Discharge occurrence at $L = 2\mu H$ and $C_1 = 220pF$
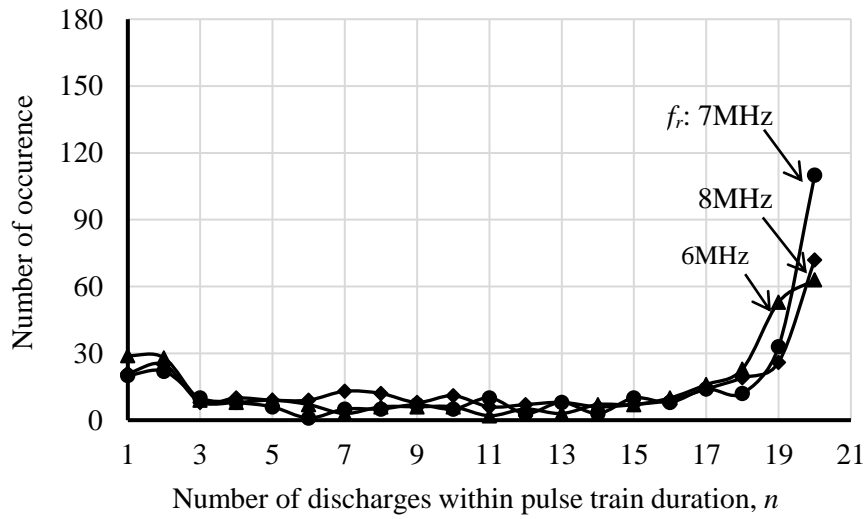
Fig. 4.18: Discharge occurrence at $L = 3.8\mu H$ and $C_1 = 220pF$
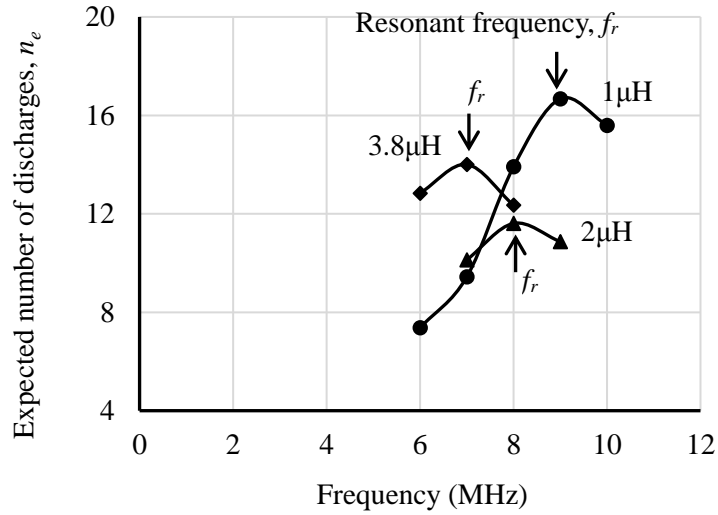
Fig. 4.19: Expected number of discharges within pulse train duration at $C_1 = 220pF$

4.6 Comparison of Machining Characteristics at Different Frequencies

As highest discharge energy and better discharge continuity can be achieved when machining is performed at f_r, machining characteristics at different frequencies were investigated. Fig. 4.20 shows the illustration of the pulse train duration and pulse train interval at respective frequencies. The triangles represent the number of discharges which can be generated at every pulse train duration. The pulse train duration was determined so that the same number of discharges, $n=20$, can occur consecutively and the cycle time of the repetition of the pulse train discharge was 4700ns. Using the machining conditions shown in Table 4.4, machining was performed by increasing the feed speed. As the feed speed increases, number of discharges can be increased because the gap width is decreased. However, the tool will collide with the workpiece surface when the feed speed is higher than the maximum material removal, and machining is stalled. With this method, maximum material removal rate (MRR) for each frequency can be obtained by dividing the maximum volume of material removal with the machining time.

Table 4.4: Experimental conditions to investigate the machining characteristics with resonance in circuit

Amplitude of pulse voltage (V)	100
Frequency (MHz)	7, 8, 9, 10
Inductance, L (µH)	1
Capacitance, C_I (pF)	220
Tool electrode (Rod)	Tungsten carbide (Ø 250µm)
Workpiece	Stainless steel (SUS 304)
Dielectric fluid	EDM oil
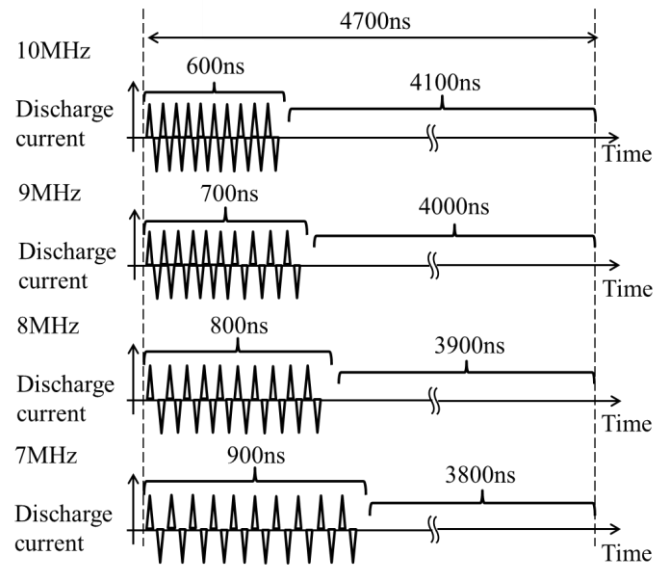
Fig. 4.20: Illustration on number of discharges n, pulse train duration and pulse train interval

4.6.1 Crater Size and Machined Surface at Same Number of Discharges

Surfaces machined at feed speed of 0.1µm/s at different frequencies are shown in Fig. 4.21. When machining is performed at 8-10MHz, uniform crater sizes can be seen. At 7MHz however, smaller craters are obvious among the large craters due to low discharge continuity within the pulse train duration. To clarify the difference at respective frequencies, the diameters of craters were measured and averaged. The results are given in Fig. 4.22. It shows that the crater size peaks when machining is performed at f_r=9MHz. This is because highest discharge continuity within the pulse train duration can be achieved when machining is performed at f_r.

a) 7MHz   b) 8MHz

c) f_r: 9MHz   d) 10MHz
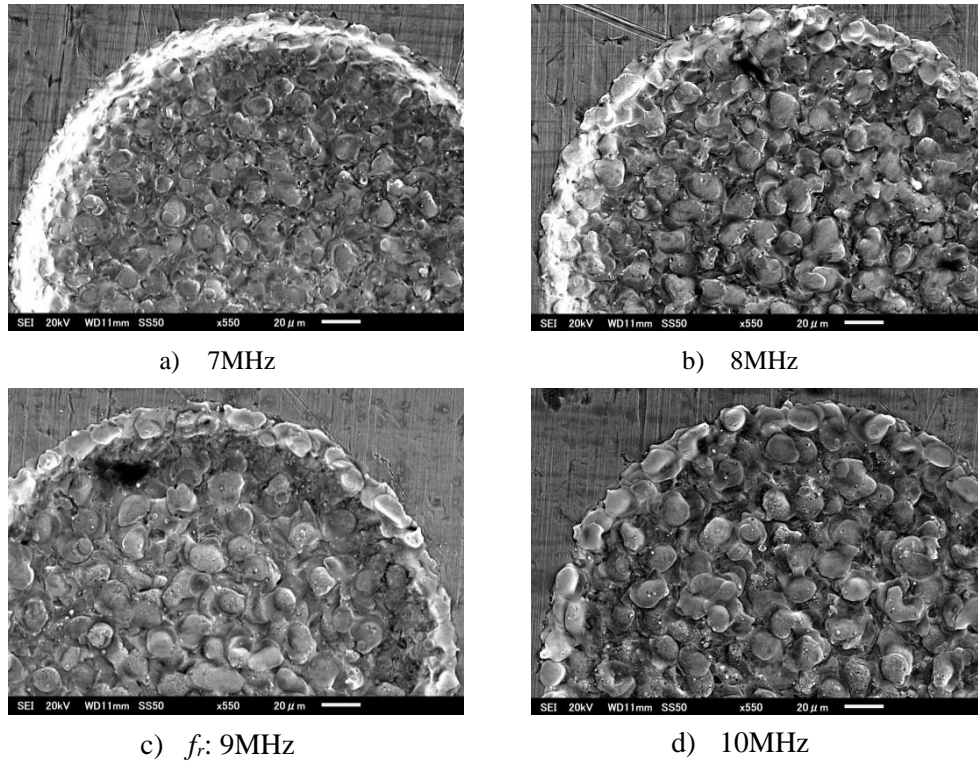
Fig. 4.21: Machined surfaces at different frequencies
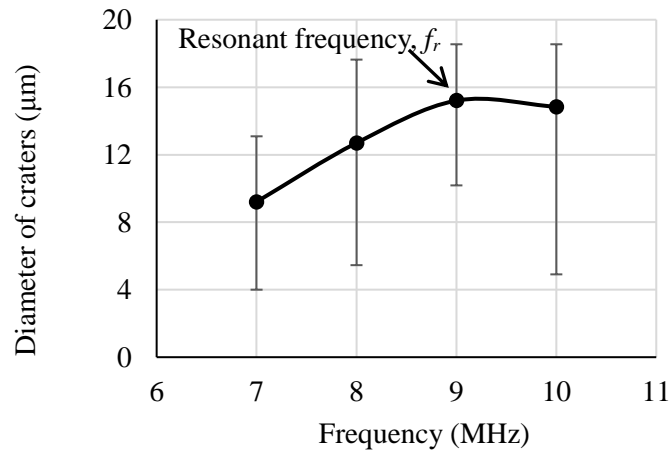
Fig. 4.22: Diameter of craters

4.6.2   Material Removal Rate (MRR)

The relationship between MRR and feed speed is shown in Fig. 4.23. The results show that maximum MRR can be achieved with f_r=9MHz at feed speed of 0.6μm/s. At f_r, largest discharge energy and highest probability of discharge continuity allowed more material to be heated and evaporated during the pulse train duration resulting in highest MRR. This result agrees with the change in the expected number of discharges, n as presented in Fig. 4.19, and it proves that MRR can be increased using resonance in the circuit.
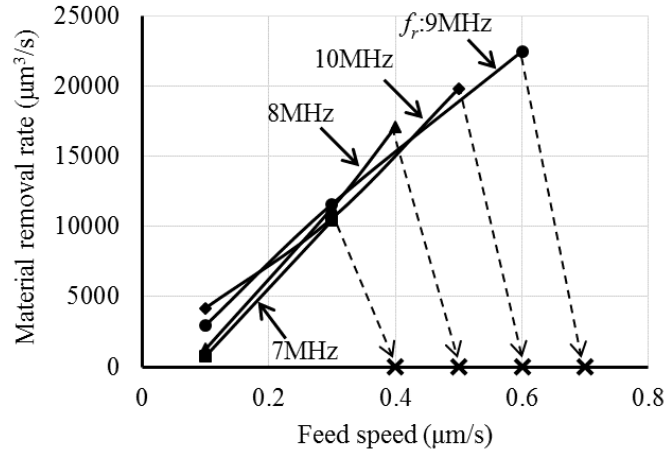
Fig. 4.23: Relationship between MRR and feed speed with C_l=220pF and L=1µH

During the investigation on the comparison of CPTM with conventional EIFM and RC circuit; which has been presented in Chapter 3, capacitance of 470pF was used. On the other hand, smaller capacitance of 220pF was used in investigating the CPTM with resonance in the circuit presented in this chapter. Hence, it is difficult to compare the results obtained in Chapter 3 with the one obtained in this chapter. However, it is believed that if machining is performed using capacitance of 470pF with the influence of resonance in circuit, higher MRR than the CPTM without resonance can be achieved.

For example, if comparison is done between CPTM with resonance and conventional EIFM, it is expected that the diameter of discharge craters will be larger than 11.52µm and the MRR will be higher than 34285µm³/s (shown in Fig. 3.12) since the average of discharge energy per pulse can be increased with the influence of resonance in the circuit and discharge continuity within the pulse train duration can be maintained.

4.6 Concluding Remarks

This chapter discussed the method to increase discharge energy of CPTM by utilizing the resonance in the circuit. Initial investigation shows that average discharge energy per pulse is highest at f_r. In addition, discharge continuity within the pulse train duration of CPTM can be improved when machining is performed at f_r. If small capacitance C_l is used, f_r can be achieved within the frequency limit of the pulse power supply by increasing the inductance. As a result, largest diameter of discharge craters and maximum MRR can be achieved at f_r. In the next chapter, the feasibility to employ this method in non-contact electrical feeding is investigated.

4.7 References

20. A. Okada, J.A. McGeough, D. MacMillan and B. Flynn, 2006, Machining characteristics of EDM by radio-frequency plasma, Ann CIRP - Manufacturing Technology, vol.55, no. 1, pp. 167–70.

21. Tomohiro Koyano, Yuna Yahagi, Masanori Kunieda and Xiaodong Yang, 2010, High spindle speed micro EDM using electrostatic induction feeding method, Proceedings of the 16th International Symposium on Electromachining, pp.599-602.

(This page is intentionally left blank)

Chapter 5

Machining with Non-Contact Electrical Feeding

In the foregoing chapters, a capacitor was used to connect the pulse voltage and the discharge gap to carry out fundamental experiment. Thus, this chapter discusses the utilization of controlled pulse train method (CPTM) using non-contact electrical feeding. In this method, by fixing a cylindrical feeding electrode coaxially to the mandrel, capacitance C_1 can be formed in the gap between these two. However, by fixing the small feeding electrode to the mandrel, only small capacitance was able to be formed. As a result, small pulse of discharge current was generated in a very short duration causing a long interval between the discharges leading to difficulty for the discharges to be maintained within the pulse train duration. Referring to Eq. (1.14) in Section 1.3.2, discharge energy can be increased by increasing the feeding capacitance, C_1. Therefore, methods to increase C_1 were proposed and discussed. Then, influences of tool rotation speed on material removal rate (MRR) and machining accuracy were investigated using the newly developed feeding electrode.

5.1 Controlled Pulse Train Method (CPTM) with Non-contact Electrical Feeding

In machining with non-contact electrical feeding, shown in Fig. 5.1, the feeding capacitance C_1 can be calculated using the following equation [1]:

$$C_1 = 2\pi\varepsilon \, \frac{L}{\ln\left(\frac{b}{a}\right)} \tag{5.1}$$

In this equation, ε is permittivity of the gap (air: 8.8542×10^{-12} F/m), a is the outer diameter of tool electrode holder, b is the inner diameter of feeding electrode and L is the length of the feeding electrode.

5.1.1 Experimental Setup

Figure 5.1a shows the mandrel used to hold the tool electrode. Fig. 5.1b shows the feeding electrode made from copper pipe with inner diameter of b and length of L. The assembly of the mandrel and feeding electrode when attached to the Z-axis of the micro EDM machine is shown in Fig. 5.2. The equipment named mandrel holder was designed and modified by M. Kunieda et al. [2] based on the development done by Kawata K. et al. [3]. The V-groove was attached to the system to secure the position of the feeding electrode. V-guide is made of electrical insulator and is used as the support for the mandrel. Rubber belt is used to seize and to rotate the mandrel around the Z-axis of the machine. A copper plate is used to connect the pulse power supply to the feeding electrode. The inner diameter of the feeding electrode b is made slightly larger than the outer diameter of the mandrel. The pulse train generator is coupled to the tool electrode by capacitance C_1 which is formed in the gap between feeding electrode and the mandrel. Since there is no contact between the surfaces, capacitance C_1 can be formed between them.

(a) Mandrel   (b) Feeding electrode
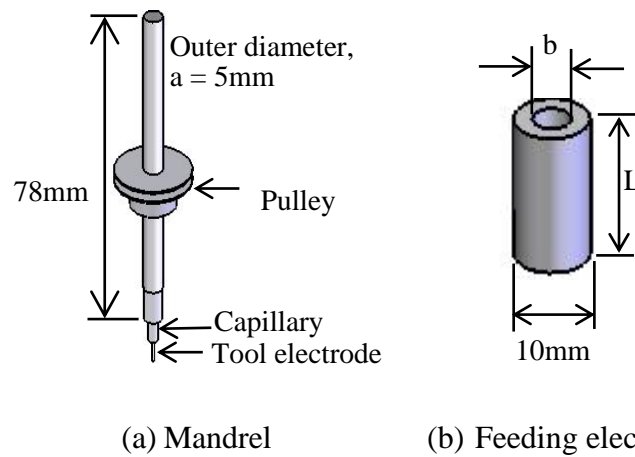
Fig. 5.1: Equipment for non-contact electrical feeding
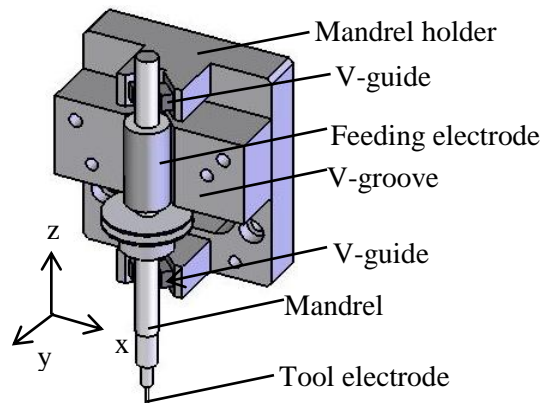
Fig. 5.2: Setup for micro EDM with non-contact electrical feeding [1]

112

5.1.2 Influence of Capacitance C_1 on Diameter of Discharge Craters

In order to investigate the feasibility of machining with non-contact electrical feeding, a preliminary experiment on the influence of capacitance C_1 on the diameter of discharge craters was performed. Machining system as shown in Fig. 5.3 was used. In this experiment, three different sizes of the cylindrical feeding electrode: a, b and L were selected as shown in Table 5.1. The value of C_1 was calculated using Eq. (5.1). Under the machining conditions shown in Table 5.2, discharge craters were generated using the conventional electrostatic induction feeding method (EIFM).

The craters generated on machined surface was observed using scanning electron microscope (SEM). The diameter of discharge craters were measured, and average crater size was calculated. Fig. 5.4 shows the relationship between the diameter of discharge craters and the feeding capacitance C_1. From the experiment, it was found that the smaller C_1 results in smaller discharge crater. Since low frequency was utilized with conventional EIFM, individual discharge was independent for every half cycle of each pulse period resulting in small and scattered discharge craters on the machined surface.
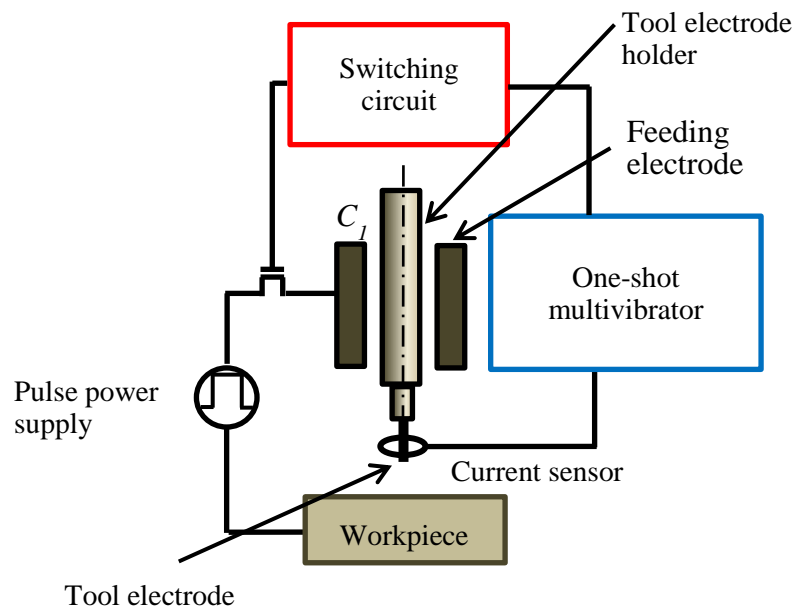
Fig. 5.3: Machining system

Table 5.1: Capacitance C_1

Diameter of mandrel a (mm)	Feeding electrode		Capacitance C_1 (pF)
	Inner diameter, b (mm)	Length, L (mm)	
	5.1	23	64.6
5.0	5.2	20	28.4
	5.2	10	14.2

113

Table 5.2: Machining conditions

Amplitude of pulse voltage (V)	100
Frequency (MHz)	1
Duty factor (%)	50
Electrode (Rod)	Tungsten carbide (Ø = 220μm)
Workpiece	Stainless steel (SUS 304)
Dielectric	EDM oil
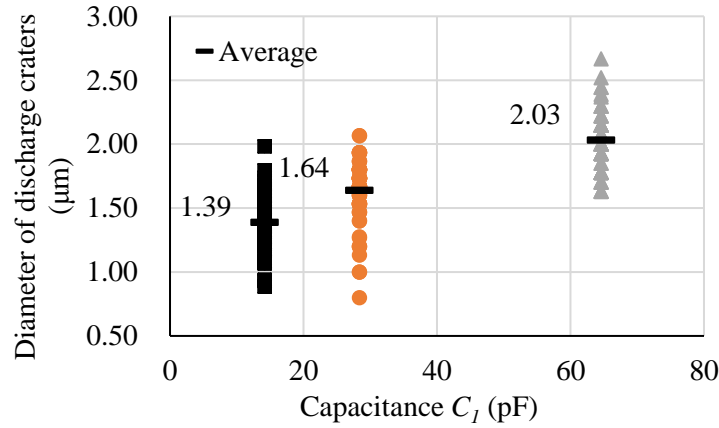
Fig. 5.4: Relationship between diameter of discharge crater and feeding capacitance C_1

In CPTM, the discharge energy per individual pulse discharge is roughly the same as the conventional EIFM when the same C_1 is used. However, in CPTM the diameter of discharge craters is influenced by the number of discharges which can be generated within a pre-determined pulse train duration. Furthermore, the resonance of the circuit increases the discharge energy per pulse. Investigation on the diameter of discharge craters with non-contact electrical feeding CPTM was performed by increasing the frequency with 300ns in pulse train duration. Influences of two different feeding capacitances on the crater diameter were investigated under the machining conditions shown in Table 5.3. Since capacitance of 14.2pF is too small, it is not used in the following investigation. From now on, feeding electrode which can generate 28.4pF and 64.6pF, is named as feeding electrode 1 and 2, respectively.

Fig. 5.5a and 5.5b show the example of discharge waveforms at 5MHz using feeding electrode 1 and 2 respectively. The duration of individual discharge per half cycle of the high frequency discharge was about 8ns for feeding electrode 1 and about 33ns for feeding electrode 2. Since the pulse width of the pulse frequency of 5MHz is was100ns, the short duration of individual pulse discharge using the small capacitance resulted in long intervals between the discharges.

Table 5.3: Machining conditions

Amplitude of pulse voltage (V)	100
Frequency (MHz)	5, 7, 9
Capacitance, C_1 (pF)	28.4, 64.6
Inductance, L (μH)	1
Electrode (Rod)	Tungsten carbide (Ø = 220μm)
Workpiece	Stainless steel (SUS 304)
Dielectric	EDM oil
Pulse train duration (ns)	300
Pulse train interval (ns)	600
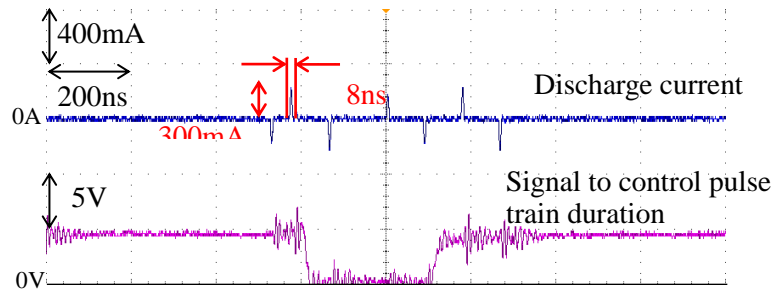
a) Feeding electrode 1 (28.4pF)
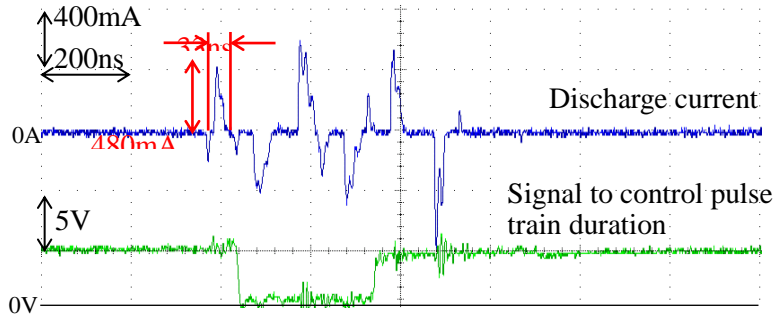
b) Feeding electrode 2 (64.6pF)

Fig. 5.5: Discharge waveforms at 5MHz

The relationship between diameter of discharge craters and frequency for non-contact electrical feeding with CPTM is shown in Fig. 5.6. From the comparison between Figs. 5.4 and 5.6, it was found that larger craters can be obtained when the CPTM is employed compared to the conventional EIFM. This is because, multiple discharges continuously occur at the same location when the CPTM is employed. In addition, larger craters can be obtained with larger C_1 due to higher discharge energy.

It is expected that as the frequency increases, crater diameter is also increased for the respective capacitance. This is because, with the increase of frequency, number of pulses

115

per pulse train increases as long as the high frequency discharge can persist within the pulse train duration. However, the result showed no significance increase in the diameter of discharge crater with increase in the frequency for both capacitances. Therefore, investigation on discharge continuity within the pulse train duration was performed.
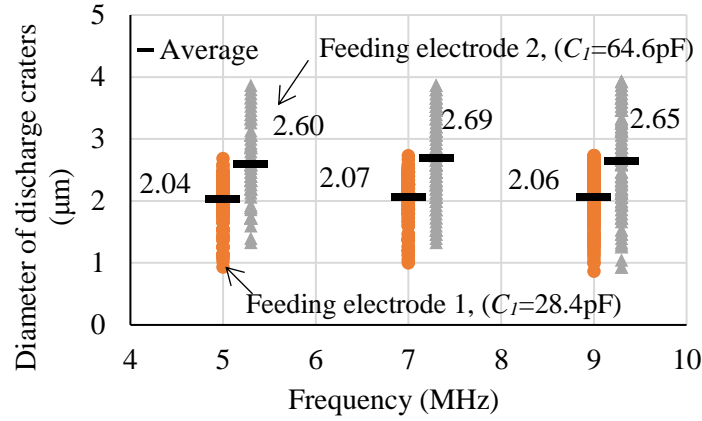
Fig. 5.6: Relationship between diameter of discharge craters and frequency with CPTM

5.1.3   Investigation on Continuity of Discharges within Pulse Train Duration

Since the duration of individual discharge is very short, it was considered that discharges cannot be sustained within the controlled pulse train duration. Sustainability of discharges within the pre-determined time is important because it will influence the size of discharge crater. Using the machining conditions shown in Table 5.4, 300 samples of pulse trains at 500ns pulse train duration were observed. 15 discharges were generated at a maximum within the designated pulse train duration. Theoretically, with 8.5MHz in pulse frequency, bipolar pulse discharges can occur only 8.5 times at a maximum within the pulse train duration of 500ns. This is because there are time lags of about 400ns in total to activate the one-shot multivibrator circuit and to stop the pulse power supply. Due to the delay in response, discharge can continue to occur for a duration longer of 700ns at longest. Fig. 5.7 shows the discharge waveforms at 8.5MHz. In this example, eight bipolar discharges occurred continuously. Since every discharge occurred when the gap voltage peaked, the discharge current was almost constant. However, the pulse duration was 8ns and significantly short compared to the half cycle of the pulse voltage.

Fig. 5.8 shows the relationship between the number of occurrence and number of discharges within pulse train duration. It was found that more than 50% discharges occurred with the number of continuous discharges of only between 1 to 3.

The difficulties to maintain the continuity of the discharges within the pulse train duration are due to the short duration of individual discharge and the existence of interval between the discharges. On average, only 4 discharges can be sustained within the pulse train duration (n_e=4). This is significantly low compared to the available number of discharges which can be generated within the given time.

Table 5.4: Machining conditions

Amplitude of pulse voltage (V)	100
Frequency (MHz)	8.5
Capacitance, C_1 (pF)	28.4
Inductance, L (μH)	1
Electrode (Rod)	Tungsten carbide (Ø = 250μm)
Workpiece	Stainless steel (SUS 304)
Dielectric	EDM oil
Pulse train duration (ns)	300

Fig. 5.7: Discharge waveforms at frequency of 8.5MHz and L=1μH
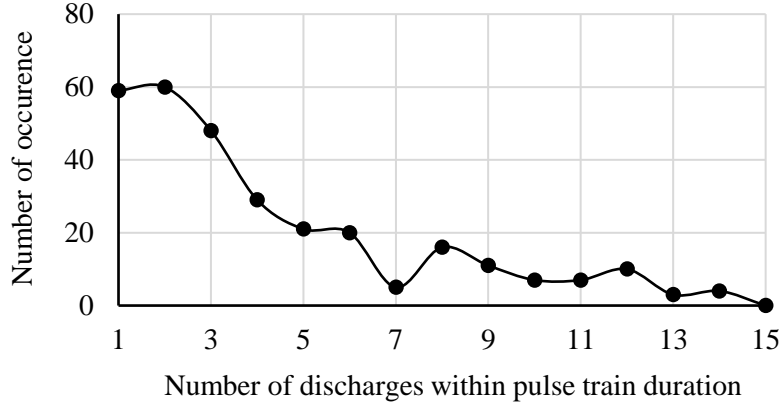
Fig. 5.8: Continuity of discharges at 8.5MHz and $L=1\mu H$

Higher discharge amplitude and longer discharge duration can be achieved when machining is done at f_r of the circuit. Therefore, observation on discharge waveform and continuity of discharges within the pulse train duration at f_r of the circuit using the same feeding electrode was conducted.

Resonant frequency, f_r of a circuit can be calculated using Eq. (4.1). On the other hand, f_r in the experiment can be obtained by measuring the change in the discharge energy per pulse q with pulse frequency. During machining, discharge waveforms were sampled, and the average discharge energy per pulse, q was calculated using Eq. (4.2) from all the pulses generated within the pulse train duration at the selected frequency. Several frequencies near the calculated f_r should be tested in order to get the actual f_r. Since impedance in the circuit is minimum at f_r, the actual f_r can be obtained when q is highest.

From Eq. (4.1), when $L=1\mu H$ and $C_1=28.4pF$, the calculated f_r is 29.8MHz. However, the frequency limit of the available pulse power supply is only 10MHz. Using the same feeding electrode, machining at f_r of the circuit can be performed within the limit of the available pulse power supply by adding an inductor to increase the inductance. If L is increased to 7.8μH, the calculated f_r is 10.7MHz. From experience in the previous works, there will be slight difference between the calculated and actual f_r. To find the actual f_r for selected L and C_1, an experiment was done using machining conditions in Table 5.4 at $L=7.8\mu H$ and frequencies around 9MHz.

Fig. 5.9 shows the average discharge energy per pulse between 8 to 9MHz. The q peaked at 8.5MHz. Therefore, this is the actual f_r of the circuit. Fig. 5.10 shows the discharge waveform at $f_r=8.5MHz$. The width and the amplitude of the pulse discharge current are about 10ns and 600mA, respectively. It is obvious that the discharge current amplitude is higher compared to the discharge waveform shown in Fig. 5.7. Since the gap voltage was amplified due to resonance, large u_o resulted in higher current based on the theory described in Introduction.

118
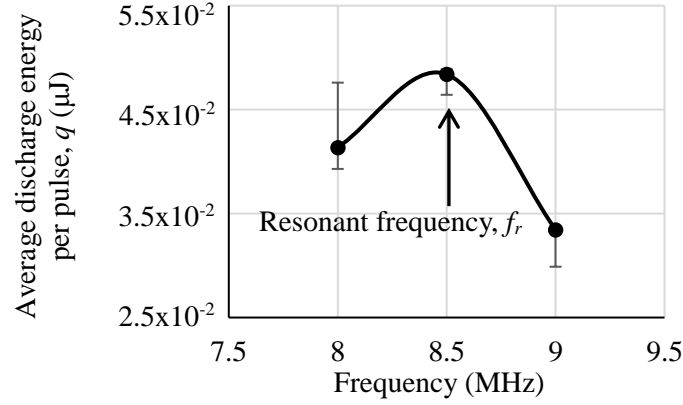
Fig. 5.9: Relationship between average discharge energy per pulse and frequency at $L=7.8\mu H$
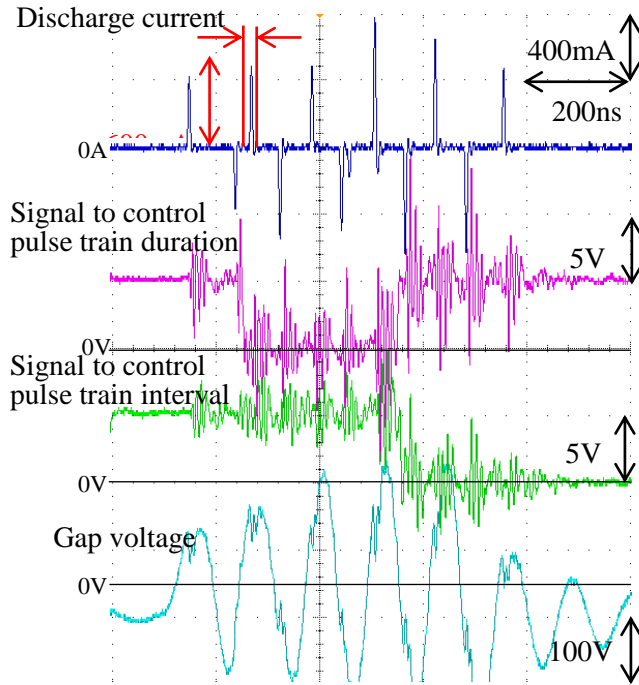
Fig. 5.10: Discharge waveforms at $f_r=8.5$MHz and $L=7.8\mu H$

The influence of f_r on the continuity of discharges within the controlled pulse train duration was investigated using the same machining conditions shown in Table 5.4 with $L=7.8\mu H$. The results in Fig. 5.11 show that in many cases discharge was interrupted after one or two consecutive pulse discharges. However, the number of pulse discharges between 9 to15 occurred more often compared to the results presented in Fig. 5.8. On average, 7 discharges can be sustained within the pulse train duration ($n_e=7$), while without considering f_r, n_e was only 4.
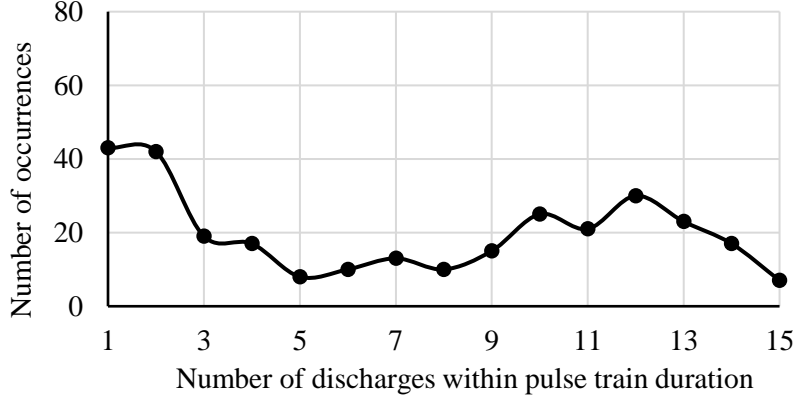
Fig. 5.11: Continuity of discharges at f_r=8.5MHz and L=7.8μH

5.2 Problem Related to Non-contact Electrical Feeding

When C_1 is small, discharge energy per pulse is small. As shown in Fig. 5.7, the discharge current at 28.4pF is about 300mA, and width of pulse discharge is short at about 8ns. There is a long interval between the discharges because of the individual discharge duration is small compared to the half cycle of the pulse frequency of 8.5MHz (58.8ns). The long interval between the discharges causes difficulty to obtain continuous discharge within the pulse train duration when C_1 is small. This leads to incomplete discharges within the pulse train duration. By utilizing f_r in the circuit, discharge energy can be increased and discharge continuity within the pulse train duration can be improved. In addition, if the capacitance C_1 can be increased, discharge energy can be increased furthermore, as indicated by Eq. (1.14) in Section 1.3.2.

As discussed in Section 5.1.1, capacitance can be increased from 28.4pF to 64.6pF by reducing the gap between the feeding electrode and the mandrel from 100μm to 50μm, and also by increasing the length of feeding electrode from 20mm to 23mm. However, the discharge energy cannot be increased significantly with this method. This is because, the minimum gap is required for the tool to rotate without any contact with the feeding electrode or electrical discharge in the inter electrode gap. In addition, the length of the feeding electrode is limited depending on the height between the v-guide and the pulley of the mandrel shown in Fig. 5.2. Therefore, other method to increase the capacitance was proposed.

5.3 Solution 1: Increasing Capacitance by Changing the Dielectric

Referring to the Eq. (5.1), capacitance C_1 can be increased by changing the dielectric. With feeding electrode 1, 28.4pF can be formed when gap between the feeding electrode and the tool was filled with air. However, if the same feeding electrode was used and the gap was filled with ethanol, the calculated capacitance was 689.7pF. This is because, the relative permittivity, ε_r for ethanol is 24.3 times higher than air. Fig. 5.12a shows the feeding electrode used in the experiment. Using the same experimental setup as shown in Fig. 5.2 and machining conditions as shown in Table 5.5, the change in the discharge waveforms was observed.

Fig. 5.12b shows the discharge waveforms when machining is conducted at 8.5MHz. Here, the amplitude of discharge current is about 700mA, and the width of the pulse discharge is about 72ns. This method shows that the discharge current and discharge energy per pulse can be improved tremendously compared to Fig. 5.7. However, ethanol is easy to evaporate and must be constantly fed to the gap of rotated mandrel using a pipette during machining. Since this method caused difficulty to maintain the existence of ethanol in the gap, another method was proposed.

Table 5.5: Machining conditions

Amplitude of pulse voltage (V)	100
Frequency (MHz)	8.5
Capacitance, C_1 (pF)	689.7
Inductance, L (μH)	1
Electrode (Rod)	Tungsten carbide (Ø = 250μm)
Workpiece	Stainless steel (SUS 304)
Dielectric	EDM oil
Pulse train duration (ns)	300
Pulse train interval (ns)	900

a) Feeding electrode   b) Discharge waveforms

Fig. 5.12: Increasing discharge energy with ethanol

5.4 Solution 2: Increasing Capacitance by Increasing The Diameter of Feeding Electrode

From Eq. (5.1), if L is maintained at the same length, the change in diameter of a and b will influence the value of C_1. Thus, by increasing the diameter of the existing feeding electrode, C_1 can be increased because the surface area is enlarged. To realize this, the feeding electrode was designed to have two separate parts: inner and outer. The inner part should be rotated together with the mandrel. A stop screw was used to fix the inner part to the mandrel. This was to ensure that the inner part rotates together with the mandrel. On the other hand, the outer part was stationary. The dimension of the feeding electrode is shown in Fig. 5.13a. Holes with 13mm diameter and 6mm depth on top and bottom part of the inner feeding electrode were made to reduce the weight. With this design, the calculated C_1 is 111.8pF. This is about 4 times larger than feeding electrode 1.

The experimental setup is shown in Fig. 5.13b. The same setup as the previous experiment was employed. However, since the diameter of the outer feeding electrode was larger than the feeding electrode 1, v-groove was replaced with the base support. Fig. 5.14 shows the difference between v-groove and base support. The surface of the outer feeding electrode was ground, leaving a flat surface of 6mm width and 20mm length (in vertical direction). During assembly, this flat surface was placed on the base support. An insulator is placed in between the outer feeding electrode and the base support to prevent electrical contact between the two surfaces.

To ensure that the gap between the two feeding electrodes is the same at any point, a naflon sheet with 100µm thickness was placed on the surface in between the feeding electrodes. During assembly, the position of the inner feeding electrode on the mandrel must be adjusted so that the centres of the two feeding electrodes coincide. A copper plate was used to place the outer feeding electrode in its position and connect the pulse power supply to the feeding electrode. After the assembly, the naflon sheet was removed before the machining started. From now on, this feeding electrode is named as feeding electrode 3.
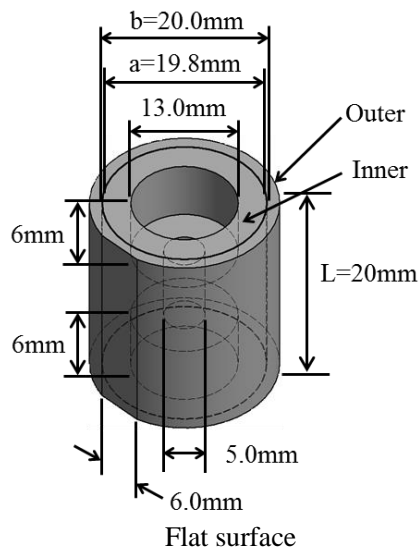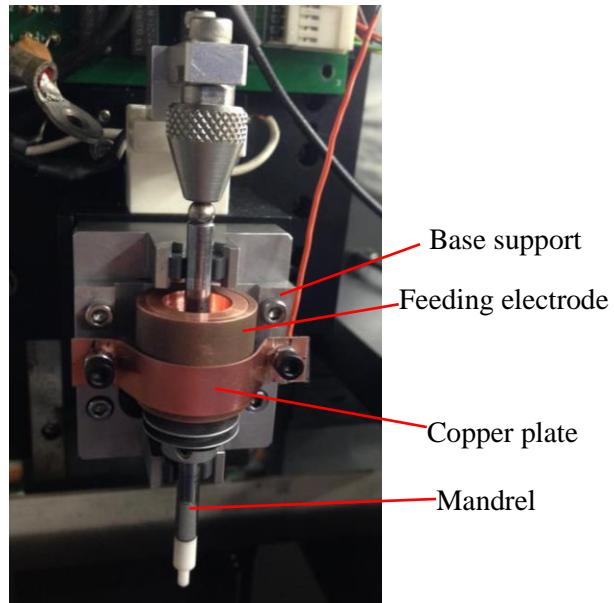
a) Feeding electrode 3   b) Experimental setup

Fig. 5.13: Increasing discharge energy by increasing the diameter of feeding electrode
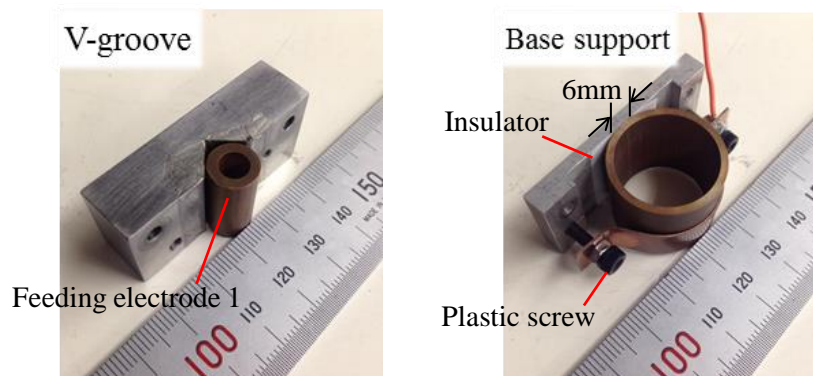
Fig. 5.14: Comparison between v-groove and base support

Using the machining conditions shown in Table 5.5, the discharge waveforms were observed using feeding electrode 3. The results are shown in Fig. 5.15. It is found that the amplitude of discharge current was increased from 300mA to 800mA, and the discharge duration was increased from 8ns to 14ns compared to the feeding electrode 1 of 28.4pF as presented in Fig. 5.7. To investigate the influence of f_r, L=2.8μH was used in order to supply the pulse frequency within the limit of the existing pulse power supply. Using Eq. (4.1) the calculated f_r is 9MHz. Thus, the machining was performed around that frequency using the machining conditions shown in Table 5.6. The results presented in Fig.5.16 show that the discharge energy is higher than that obtained with 28.4pF at f_r as shown in Fig. 5.9. This proves that larger capacitance can be formed with the new feeding electrode. The results also show q is highest at f_r=8MHz. The discharge waveform at 8MHz is shown in Fig. 5.17. At this condition, the discharge amplitude is about 1.2A, and the discharge duration is about 17ns.
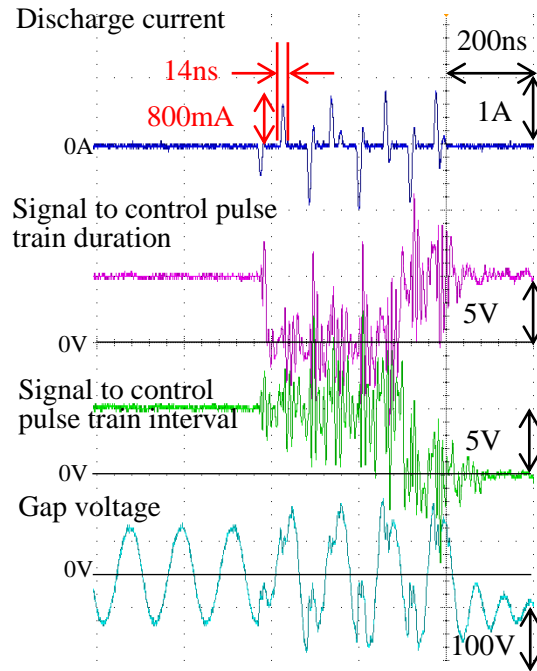
Fig. 5.15: Discharge waveforms at 8.5MHz, L=1μH
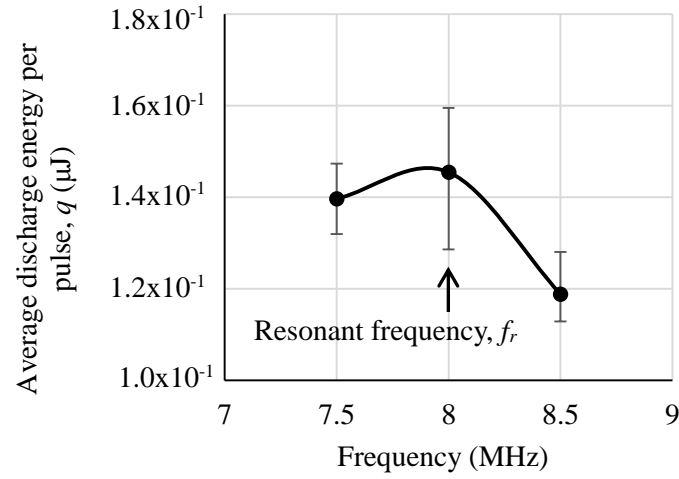
Fig. 5.16: Relationship between average discharge energy per pulse and frequency at C_1=111.8pF
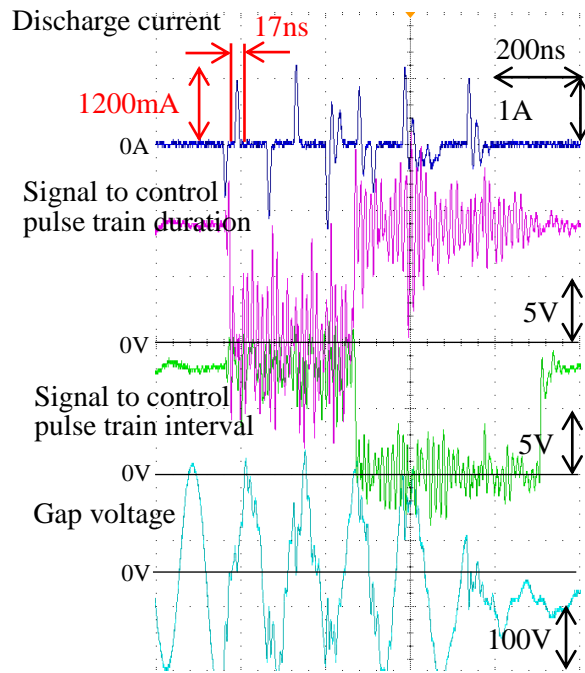
Fig. 5.17: Discharge waveforms at f_r=8.0MHz, L=2.8μH

5.5 Solution 3: Increasing Capacitance by Changing the Configuration of the Feeding Electrode

Capacitance can be increased further if the surface area between the inner and outer feeding electrode can be increased. Considering the design and the manufacturing process, a new feeding electrode with a labyrinth structure was designed and produced.

5.5.1 The Feature of Labyrinth Feeding Electrode

The labyrinth feeding electrode consists of two parts; inner and outer feeding electrodes. The dimension of the parts are shown in Fig. 5.18a and Fig. 5.18b respectively. The inner electrode was designed to be smaller than the outer electrode. The centre hole shown in Fig. 5.18a has the same diameter as the mandrel. Thus, the inner feeding electrode rotates together with the mandrel during machining while the outer part remains static. The pair assembly is shown in Fig. 5.18c with 0.1mm gap between them. With this design, there is more area for the capacitance to form. To achieve larger capacitance, more pairs were assembled together. The two holes beside the centre hole (Fig. 5.18a) were used to join the inner part together using screw. In the same manner for the outer part, three screws were used to join all the parts together. In addition, two dowel pins were used and inserted in the holes marked as 1 and 2, to keep the accurate alignment.

Seven pairs of labyrinth feeding electrode were produced with a total length of 21.07mm (after assembly). With this, the calculated capacitance which can be formed is 195.6pF. Brass was used as the material and the parts were made by turning. The machined parts are shown in Fig. 5.19a. However, due to lack of experience in operating the machine tool, the desired accuracy of the produced parts was difficult to be achieved. In addition, due to residual stress during turning process, there was a slight bending at the edge of almost all of the inner electrodes as shown in Fig. 5.19b. To solve this, the deformed surfaces of the inner feeding electrodes were ground. The outer parts were also grounded due to the same problem related to the accuracy of the machined parts. Fig. 5.20 shows the new dimension for both feeding electrodes marked in red. Since both outer and inner parts were ground, the thickness of the labyrinth feeding electrode was reduced and the gap between the inner and the outer part in axial direction increased.

a) Inner   b) Outer   c) Pair assembly
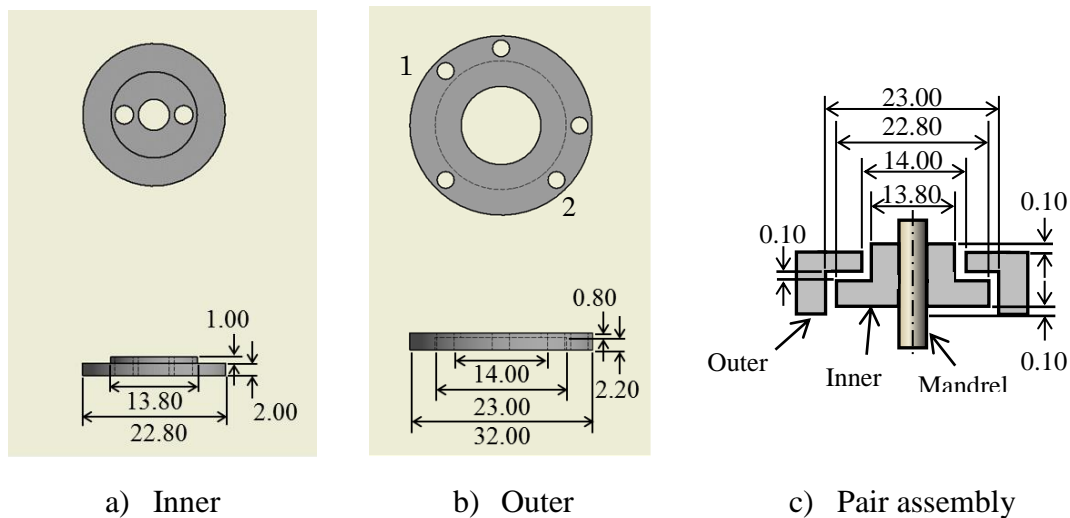
Fig. 5.18: Feature of labyrinth feeding electrode
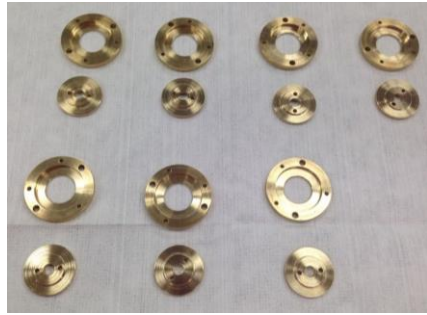
a) Machined parts   b) Defect on the inner part

Fig. 5.19: The production of labyrinth feeding electrode
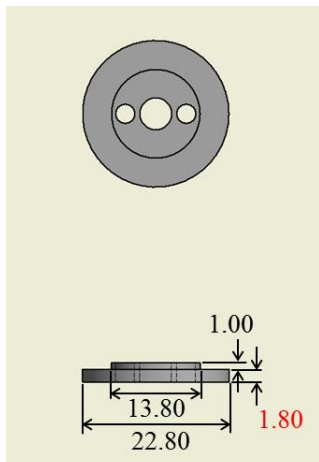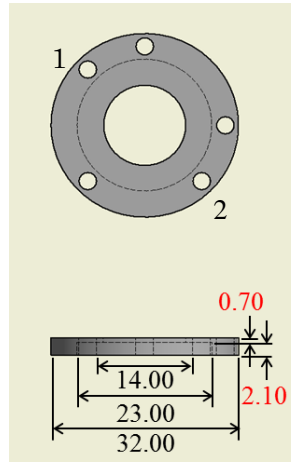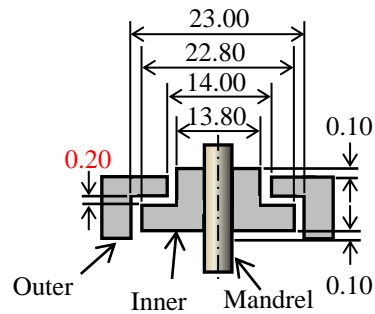
a) Inner   b) Outer   c) Pair assembly

Fig. 5.20: Feature of labyrinth feeding electrode after repair

5.5.2 Assembly and Positioning of Labyrinth Feeding Electrode

Fig. 5.21 shows the assembly and positioning of the labyrinth feeding electrode on the z-axis of the micro EDM machine. Several steps were taken before the assembly was successfully done. First, a flat surface on the outer part as shown in Fig. 5.22 was made. All of the outer feeding electrodes were screwed together. Two dowel pins were inserted to keep the accurate alignment. Then, the grinding process was performed on the flat surfaces at the same time for all the outer parts. After that, a base support was fabricated. The thickness of the base support (shown in Fig. 5.24) determines the position of the outer feeding electrode in y-direction. On the other hand, for the inner part, a small device called as the inner part holder was designed and was fabricated as shown in Fig. 5.23. This was used to hold all the inner parts together and to ensure that all the inner parts rotated together with the mandrel.

127
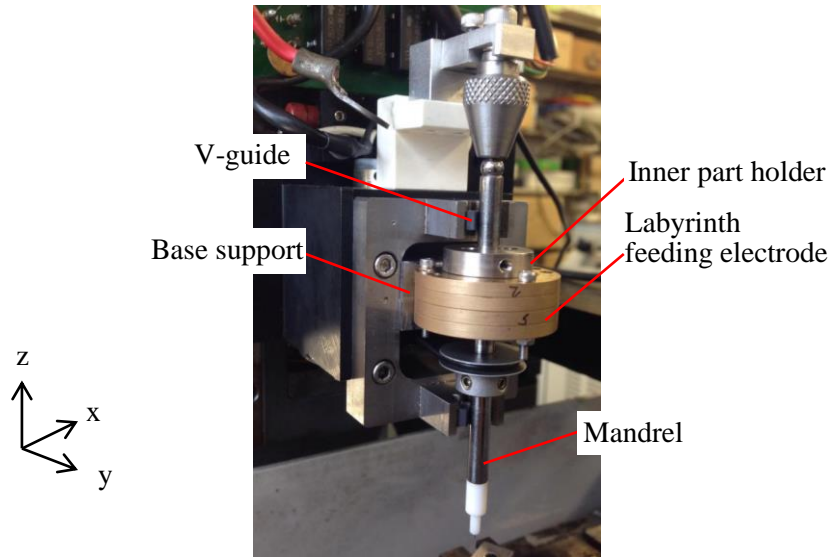
Fig. 5.21: Position of the labyrinth on EDM machine
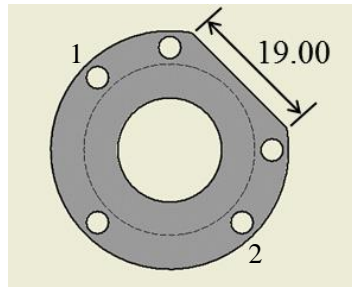
Fig. 5.22: Position of flat surface on the outer part
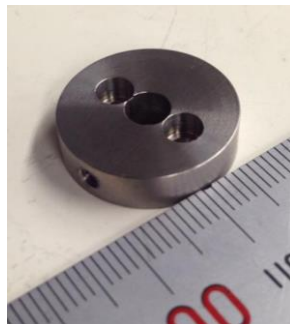
Fig. 5.23: Inner part holder

Then, the next step was to set the labyrinth feeding electrode to the base support. Fig. 5.24 shows the labyrinth feeding electrode and inner part holder which was placed on the base support (before proper fixing). The width of base support was made so that it can be placed in the centre of the mandrel holder. Then, the mandrel was inserted into the labyrinth feeding electrode and placed on v-guides as shown in Fig. 5.25. In this condition, position in y-direction is fixed. Then, the set of the devices shown in Fig. 5.25 were placed next to a precision x-y table on a magnetic table as in Fig. 5.26. The magnetic table was

used to set the position of the labyrinth feeding electrode on the base support because during the positioning process, only the labyrinth feeding electrode can be moved.
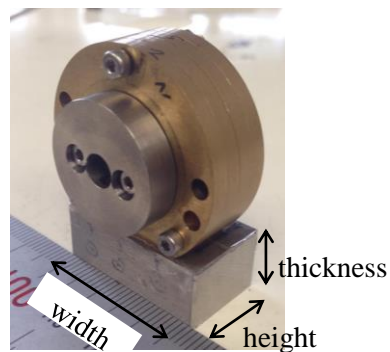
Fig. 5.24: Feeding electrode and inner part holder on the base support
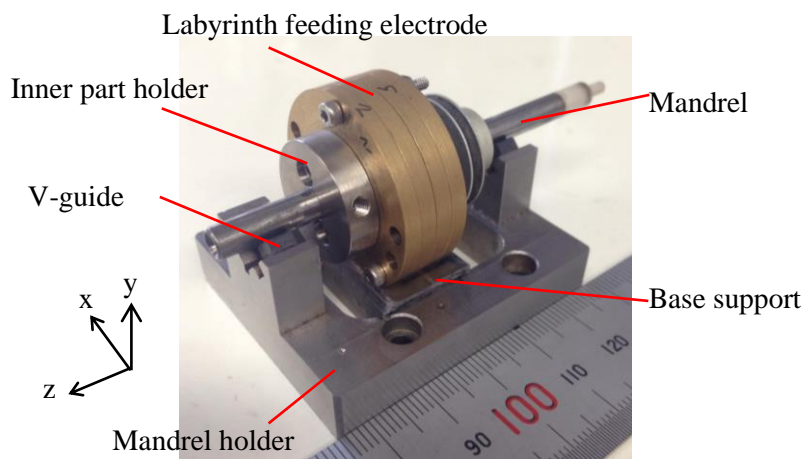
Fig. 5.25: Feeding electrode and inner part holder on the base support
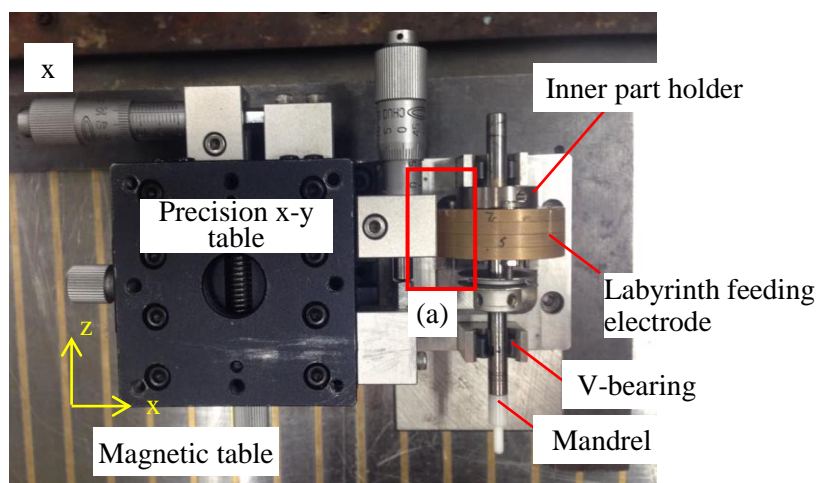
Fig. 5.26: Method to position feeding electrode on base support

At this condition, the gap on both sides in the radial direction (x- direction) were not known; the cross section is shown in Fig. 5.27a. Thus, the outer feeding electrode was pushed to the left (as in Fig. 5.27b) so that there was no gap between the inner and outer feeding electrode on the right side. The view from the outside is as shown in Fig. 5.26 at location (a) highlighted in the red box. The outer feeding electrode touches the side surface of the precision x-y table. Then, the table was moved by 0.1mm to the right using micrometer (label as x). As a result, the clearance became even at both sides. Then, adhesive was applied to join the labyrinth feeding electrode and the base support. Until here, the positioning in x and y-axis has been completed.

a) Initial condition

b) After the outer feeding electrode is pushed to the left
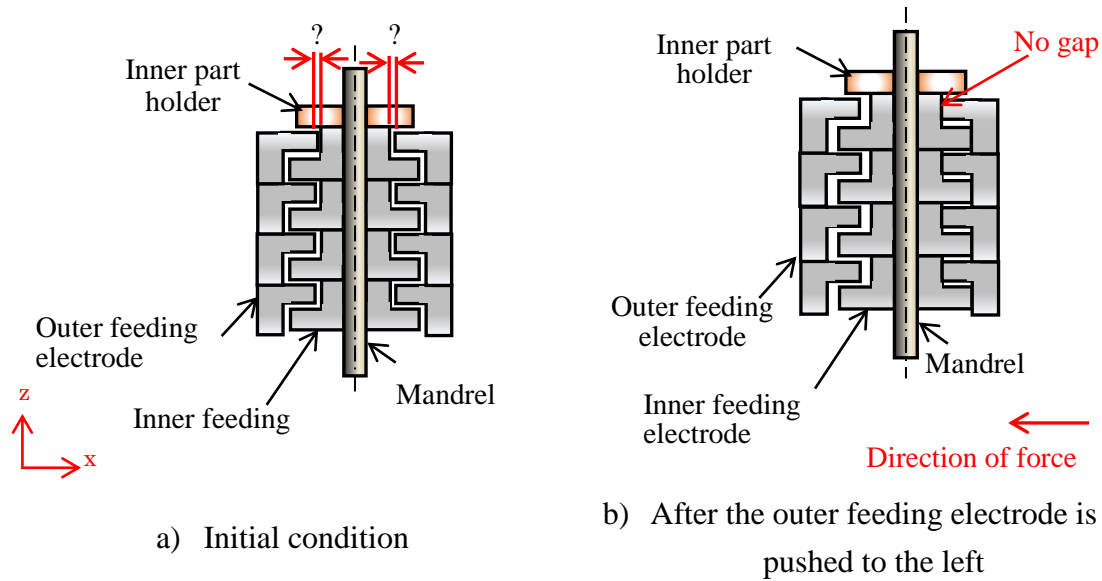
Fig. 5.27: Method to position feeding electrode on base support

The final step was to position the labyrinth feeding electrode on the micro EDM machine. First, the mandrel holder was positioned on the z-axis of the machine. Then, rubber belt was hooked to the mandrel and the set of mandrel together with the labyrinth feeding electrode, inner part holder and base support was placed on the mandrel holder. Stainless steel plate with 0.1mm thickness was temporarily placed in the gap between the inner part holder and the outer feeding electrode to keep the gap. After that, the position of the base support and the labyrinth feeding electrode were adjusted along the z-axis. Once confirmed, adhesive was used to set the base support to the mandrel holder. Then, the inner part holder was tightened to the mandrel and the 0.1mm stainless steel plate was removed.

In the final assembly, only 4 pairs of feeding electrode were used. This is because, during the pre-assembly, it was found that the other 3 inner parts of the feeding electrode were having contact with the outer part. As a result, the calculated capacitance of the labyrinth feeding electrode formed by 4 pairs was 95.6pF.

5.5.3 Investigation on Discharge Waveforms and Average Discharge Energy per Pulse

The discharge waveforms of the labyrinth feeding electrode were observed using the machining conditions shown in Table 5.5. The observed discharge waveforms are shown in Fig. 5.28. It was found that the amplitude of discharge current is 700mA, and the discharge duration is 13ns. To investigate the influence of f_r, L=2.8µH was used. Through calculation using Eq. (4.1), f_r is 9MHz. Then, machining was performed around that frequency using the same machining conditions shown in Table 5.5. The results presented in Fig. 5.29 shows that the actual f_r was at 8MHz. The discharge waveform at 8MHz is shown in Fig. 5.30. At this condition, the discharge amplitude is about 1.0A, and the discharge duration is about 15ns. Even though the discharge current amplitude and discharge duration with 4 pairs of labyrinth feeding electrode is shorter than feeding electrode 3 in Section 5.4, it should be noted that the length of the feeding electrode is only 11.4 mm; which is about half of feeding electrode 3.
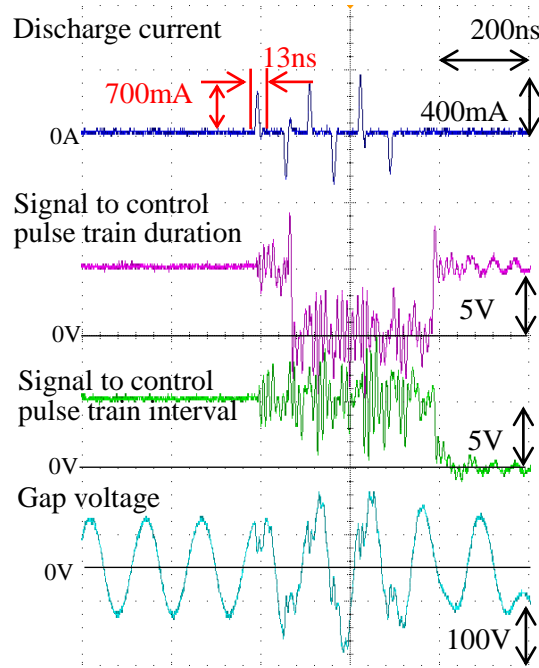
Fig. 5.28: Discharge waveforms with labyrinth feeding electrode at 8MHz, L=1µH
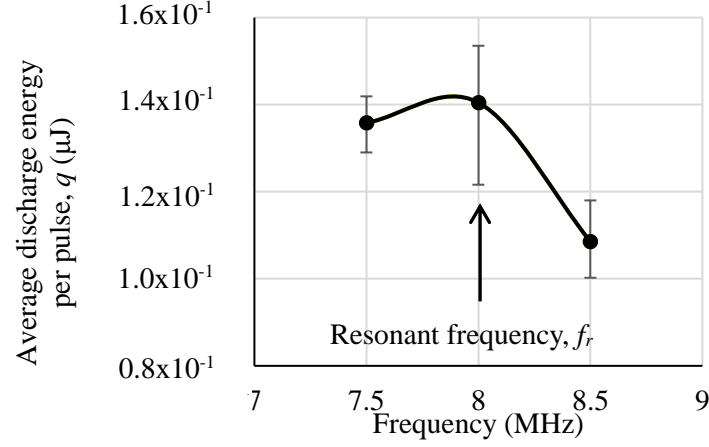
Fig. 5.29: Relationship between average discharge energy per pulse and frequency at C_1=95.6pF
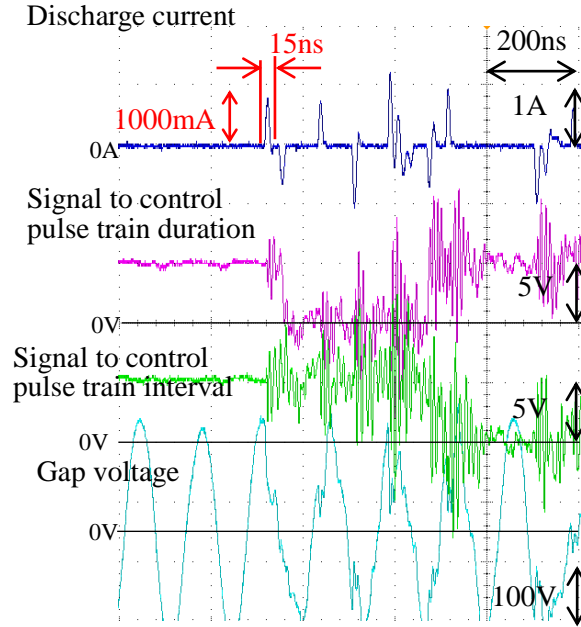
Fig. 5.30: Discharge waveforms with labyrinth feeding electrode at 8MHz, L=2.8μH

5.6 Comparison of Average Discharge Energy per Pulse for the Proposed Feeding Electrodes

Fig. 5.31 shows the comparison of the average discharge energy per pulse, q for the proposed feeding electrodes. Comparison was made based on the average q at f_r. The feeding electrode 1 with ethanol in the gap is not included in the graph. This is because, it is difficult to continuously supply the ethanol using a pipette during the experiment. Thus, a reliable data is difficult to be obtained.

The q for feeding electrode 1 is the lowest because only 28.4pF can be formed in the gap between the feeding electrode and the mandrel. Even though the graph shows that the highest q can be achieved with feeding electrode 3, it must be noted that the 4 pairs labyrinth feeding electrode used in this work is only about half the length of feeding electrode 1 and 3. Thus, if more pairs were added to the labyrinth feeding electrode, and the total length is the same with the other feeding electrodes, the q can be higher. If 7 pairs of labyrinth feeding electrode is used, the total length will be 19.8mm and the capacitance will be 172.3pF. It is estimated that q for 7 pairs feeding electrode can be somewhere in the dotted red box. From this work, it was found that higher discharge energy can be achieved by increasing the capacitance through changing the configuration of the feeding electrode.
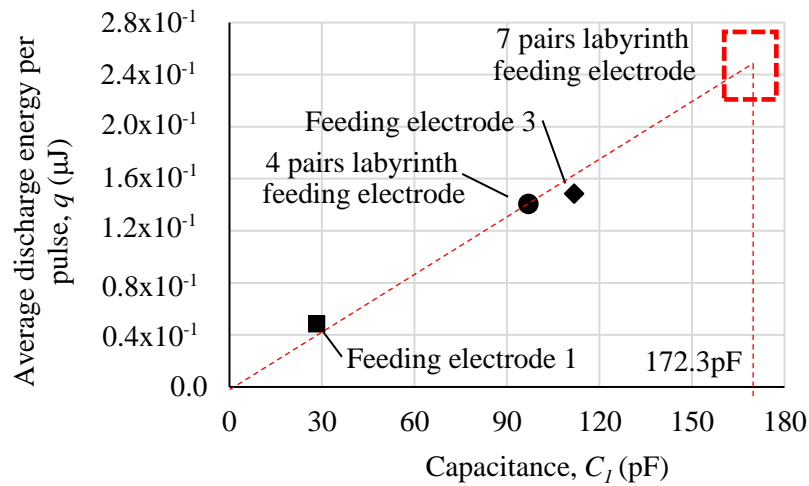
Fig. 5.32: Comparison on the average discharge energy per pulse for different capacitance at f_r

5.7 Investigation on the Influence of Spindle Speed on Machining Process

Using the developed feeding electrode, the influence of tool rotation speed on MRR was investigated. For simplicity, the feeding electrode 3 of 111.8pF was used in the experiment. Table 5.6 shows the machining conditions used in the experiment. At selected tool rotation speed of 900rpm and 3300rpm, the machining was carried out at constant feed speed with feeding depth of 150μm. Then, the feed speed was increased until machining cannot be completed at the selected machining depth. With this, the maximum MRR at selected rotation speed can be achieved.

5.7.1 Comparison on Material Removal Rate (MRR) at Different Spindle Speed Rotation

MRR was obtained by dividing the volume of removed material with machining time. At respective tool rotation speed, MRR can be increased with increasing the feed speed due to the increase in discharge frequency. However, tool will collide with the workpiece surface when the feed speed is higher than the maximum material removal. With this, the maximum MRR of respective tool electrode rotation can be obtained. Fig. 5.32 shows the experimental results. The maximum MRR for 900rpm was $7323\mu m^3$/s at 0.2μm/s in feed speed. The cross marks on the x-axis shown in the figure indicates that trials were made for higher feed speed but failed.

On the other hand, the maximum MRR for 3300rpm was $42077\mu m^3$/s at 1.0μm/s. This shows that rotation speed does influence on the maximum material removal. This is because, the surface of the tool electrode can be cooled more efficiently during machining at higher tool rotation speed. Therefore, localized discharge and abnormal arc are less likely to occur resulting in higher MRR. Referring to the results obtained by Koyano et al. [1] as shown in Fig. 1.26, it is expected that the MRR can be increased furthermore if the tool electrode rotation is increased to higher speed than 3300rpm. This is because the interval between discharge locations increases with increasing the tool electrode rotation. However, there will exist a maximum limit of the MRR with respect of the tool electrode rotation, because the material removal basically depends on the discharge energy.

Table 5.6: Machining conditions

Amplitude of pulse voltage (V)	100
Frequency (MHz)	8
Capacitance, C_1 (pF)	111.8
Inductance, L (μH)	2.8
Electrode (Rod)	Tungsten carbide (Ø = 250μm)
Workpiece	Stainless steel (SUS 304)
Dielectric	EDM oil
Machining depth (μm)	150
Pulse train duration (ns)	300
Pulse train interval (ns)	3800
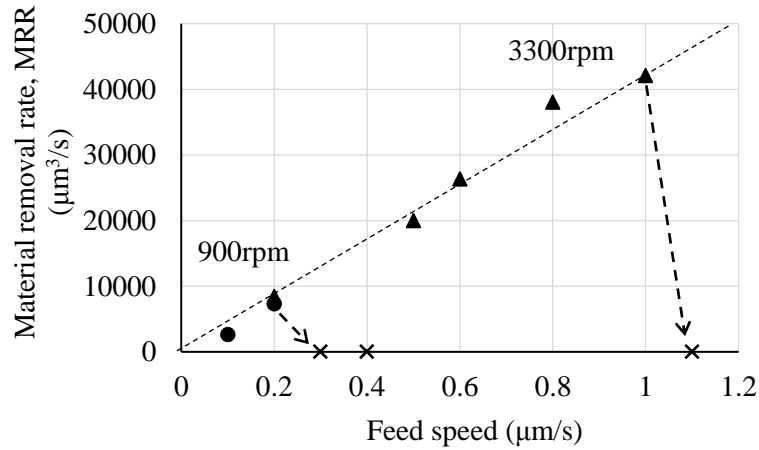
Fig. 5.32: MRR at different speed of tool electrode rotation

5.7.2 Tool Wear Ratio (TWR)

TWR was obtained by dividing the volume of tool wear with the removal volume of workpiece. For simplicity, the volume after machining was calculated without considering the wear due to the rounding of the tool edge. The results in Fig. 5.33 show that the tool wear is high at low feed speed. As the feed speed increases, the gap becomes smaller and discharges are easier to continue within the pulse train duration. The bipolar high frequency discharge over a long period of time in oil dielectric leads to carbon deposition on the tool surface, preventing excessive wear [4-6]. Under the same feed speed of 0.2μm/s, it was found that the tool wear is slightly lower when machining is performed at higher tool rotation speed.
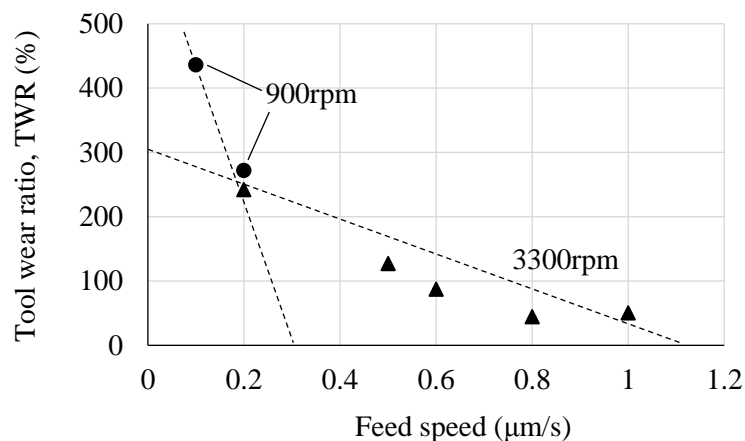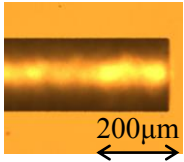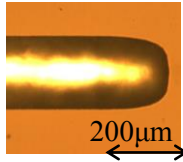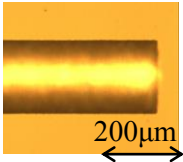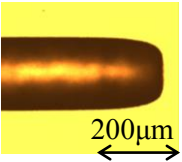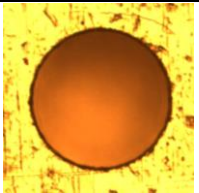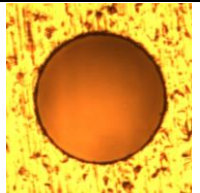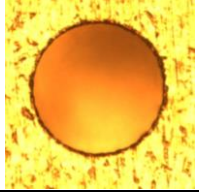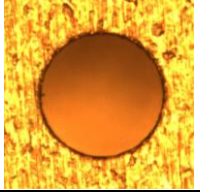
Fig. 5.33: TWR at different speed of tool electrode rotation

5.7.3 Through Hole Drilling

To investigate the accuracy of drilling at different tool rotation speed, through holes were drilled on SUS304 of 200μm thickness using tool electrode with 143μm diameter. Machining was performed using machining conditions given in Table 5.6 under the same feed speed of 0.2μm/s. Tool was fed with feeding depth of 400μm. Then, diameter of the machined holes were measured at the inlet and the outlet. Table 5.7 shows the tool electrode before and after machining and also the diameter of the inlet and outlet of the machined holes. It was found that, lateral gap is smaller with 3300rpm compared to 900rpm. This shows that when tool rotation speed is higher, better machining accuracy can be achieved because debris can be removed efficiently from the gap. The gap difference between the inlet and outlet diameters were 3.7μm and 5.2μm for 3300rpm and 900rpm, respectively. This indicates that better hole straightness can be achieved by rotating tool at higher rotation speed.

Table 5.7: Through hole drilling with different tool rotation speed

900rpm		3300rpm	
before	after	before	after
a) Tool electrode		b) Tool electrode	
c) Inlet: Ø 165.0μm Gap: 11.0μm		d) Inlet: Ø 155.2μm Gap: 6.1μm	
e) Outlet: Ø 154.6μm Gap: 5.8μm		f) Outlet: Ø 147.8μm Gap: 2.4μm	

5.8 Concluding Remarks

Non-contact electrical feeding is one of the advantage of EIFM and CPTM. By fixing a cylindrical electrode known as feeding electrode coaxially to the mandrel, capacitance can be formed in the gap between them. With this, tool can be rotated at high speed without concern on vibration. This chapter has discussed about methods to increase the capacitance in non-contact electrical feeding of CPTM based on the theory of discharge energy in CPTM. By changing the configuration of the feeding electrode, more area can be created leading to formation of higher capacitance. It was found that labyrinth feeding electrode can form the largest capacitance. With the newly fabricated feeding electrode, investigation on the influence of tool electrode rotation was made. It was found that with higher tool electrode rotation, better machining stability can be achieved because the surface of tool electrode can be cooled and localized discharge and abnormal arc can be eliminated resulting in higher MRR and lower. In addition, better machining accuracy can be obtained because debris can be easily flushed away from the gap when tool is rotated at higher speed.

5.9 References

1. Tomohiro Koyano, Yuna Yahagi, Masanori Kunieda, Xiaodong Yang, 2010, High spindle speed micro EDM using electrostatic induction feeding method, Proceedings of the 16th International Symposium on Electromachining, pp. 599-602.

2. M. Kunieda, A. Hayasaka, X. D. Yang, S. Sano and I. Araie, 2007, Study on nano EDM using capacity coupled pulse generator, Annals of The CIRP, vol. 56, issue 1, pp. 231-216.

3. Koichi Kawata, Takeo Sato, Takeshi Masaki and Takahisa Masuzawa, 1994, Study on micro EDM (1st Report) – Feasibility study, Journal of Japan Society of Electrical Machining Engineers, vol. 28, no. 57, (in Japanese).

4. Naotake Mohri, Masayuki Suzuki, Masanori Furuya, Nagao Saito, 1995, Electrode wear process in electrical discharge machining, CIRP Annals-Manufacturing Technology, vol. 44, no. 1, pp.165-168.

5. Wataru Natsu, Masanori Kunieda, Nobuhiko Nishiwaki, 2004, Study on influence of inter-electrode atmosphere on carbon adhesion and removal amount, International Journal of Electrical Machining, no. 9, pp. 43-50.

6. Masanori Kunieda, Teruki Kobayashi, 2004, Clarifying mechanism of determining tool electrode wear ratio in EDM using spectroscopic measurement of vapor density, Journal of Materials Processing Technology, no. 149, pp. 284-288.

(This page is intentionally left blank)

Chapter 6

Conclusions

In electrical discharge machining (EDM) unit removal per discharge should be reduced in order to achieve products in micro scale. Relaxation pulse generator or RC circuit is commonly used as the pulse generator for micro EDM because short discharge duration and high peak current can be achieved. With RC circuit however, discharge can occur even before the capacitance is fully charged; causing concentration of discharges leading to unstable machining. In addition, micro EDM cannot be performed in a machine having long electric feeders and large area size of machine structure. This is because, minimum limit of miniaturization is influenced by the stray capacitance existing between the electric feeders and the machine structure itself.

The advantages of electrostatic induction feeding method (EIFM) as the pulse generator for micro EDM gives a great possibility to improve the machining process over the RC circuit. Previous studies show that stray capacitance can be eliminated and machining stability can be achieved with EIFM because only one pulse discharge can occur at every half cycle of the pulse power supply. The basic circuit of EIFM consists of pulse power supply and capacitor which is connected to the tool electrode in series. With this, a contactless power supply to the tool electrode can be realized, allowing tool electrode to be rotated at high speed in order to achieve higher material removal rate (MRR) and higher accuracy. This is because, the interval of discharge locations at the periphery of the tool electrode surface increases with increasing the speed of the tool electrode rotation. Thus, the tool electrode surface can be cooled and abnormal arc can be eliminated. The non-contact electrical feeding can be realized by fixing a cylindrical feeding electrode to the tool electrode holder. However, the small feeding electrode resulted in small discharge energy causing a slow machining speed. Based on the

researches by the pioneers of EIFM, the discharge energy was expressed as a function of the feeding capacitance, C_1 and open circuit voltage, u_o. With the aim to accomplish machining process from roughing to finishing using the same pulse generator, this study proposed methods to increase machining speed and to control the discharge energy arbitrarily in non-contact EIFM.

Chapter 2 discussed about the principle of controlled pulse train method (CPTM). This method was introduced to increase discharge energy and enlarge removal volume per crater. When the high frequency pulse is applied, several discharges are allowed to occur within a pre-determined time called pulse train duration. Dielectric strength can be recovered during the pulse train interval allowing the next group of discharges to occur at a different spot. The diameter of discharge craters increases with the increase in pulse train duration. The accumulation of discharges at the same discharge spot was confirmed by observing the discharge phenomena using a high speed video camera through transparent electrode made of glass coated with indium tin oxide (ITO) film. From the observation, it was also found that threshold of deionization in micro EDM is about 5 times shorter than in macro EDM.

The fundamental characteristics of CPTM and comparison with conventional EIFM and RC circuit was clarified in Chapter 3. With CPTM, larger diameter of craters can be obtained at higher frequency and longer pulse train duration. Comparing to the conventional EIFM under the same total discharge energy, material removal rate (MRR) was about 1.7 times higher with CPTM under the conditions used in the experiment. This is because, there is enough time for the dielectric strength to recover after every accumulation of discharges. In the case of conventional EIFM, discharge occurred continuously at every half cycle of the pulse during the high feed speed. This led to insufficient time for plasma to extinguish during the interval time between the individual discharges which results in unstable machining. Hence, there was a limit of MRR in conventional EIFM under the same feeding capacitance which is determined by the configuration and size of the feeding electrode. With CPTM in contrast, the discharge energy can be controlled arbitrarily and increased by increasing the pulse train duration. With the RC circuit, as the feed speed increases, discharge occurs before the capacitor is fully charged, decreasing the removal volume per crater to nearly half of the initial volume. On the other hand, removal volume per crater increases with CPTM since more discharges can be sustained within the pulse train duration as the feed speed increases.

To affirm the continuation of pulse discharges at the same location, two methods were proposed based on the equation which shows the dependence of discharge energy on u_o and C_1. In Chapter 4, the influence of resonance was used to increase u_o. Impedance in the circuit during the pulse train duration is minimum at a specific frequency known as

resonant frequency, f_r. At f_r, the amplitude of the gap voltage peaks, resulting in higher discharge current and longer discharge duration. Hence, by performing machining at the influence frequency, the average discharge energy per pulse was increased leading to better discharge continuity within the pulse train duration. Significantly small capacitance may result in f_r higher than the frequency limit of the pulse power supply. This problem was solved by increasing the inductance of the circuit to lower the f_r. Using the same capacitance and inductance, largest diameter of craters and highest MRR could be achieved when machining was performed at f_r.

When applying CPTM in non-contact electrical feeding, the small feeding capacitance, C_1 caused longer interval between the pulse discharges. Thus, it is difficult to maintain the continuity of the discharges within the pulse train duration. In Chapter 5, C_1 was increased to affirm the continuation of pulse discharges. With the same feeding electrode length of 20mm, C_1 could be increased from 28.4pF to 172.3pF by changing the configuration. Using the developed feeding electrode of 111.8pF and inductance, L=2.8μH, the highest average discharge energy per pulse, q was obtained at f_r=8MHz with 0.15μJ. At this condition, the discharge amplitude and discharge duration was about 1.2A and 17ns, respectively. This was larger than the discharge amplitude of 300mA and discharge duration of 8ns with the feeding capacitance of 28.4pF. After that, investigation on the influence of the tool electrode rotation speed was performed using the feeding capacitance of 111.8pF. It was found that, the MRR can be 5.7 times higher when the rotation speed of the tool was increased from 900rpm to 3300rpm. This is because, the surface of the tool electrode can be cooled during higher tool rotation speed; eliminating localized discharge and abnormal arc. In addition, better machining accuracy could be obtained with higher tool rotation speed because debris can be flushed efficiently from the gap.

From this study, several recommendations for future works are suggested as follows;

i) The surface of the tool electrode can be cooled with a higher tool rotation speed. Thus, investigation on the machining characteristics can be performed at tool rotation speed higher than 50,000rpm. By observing the gap phenomena, the reasons for the machining characteristics obtained can be discussed.

ii) Investigation on the maximum MRR obtained by CPTM with a given feeding capacitance determined by the configuration and size of the feeding electrode.

iii) Effect of higher tool rotation on the limit of aspect ratio of micro holes drilled by CPTM.

iv) Application of CPTM to micro-rod machining.

v) In order to eliminate the wear of the feeding brush, the non-contact electrical feeding CPTM can also be applied to wire EDM.

vi) This study is applicable to increase discharge energy not only in micro but also macro EDM.

Appendix 1

Calculation of Gap Voltage and Discharge Current of Electrostatic Induction Feeding Method (EIFM)

Fig. 1 shows the equivalent circuit of EIFM method during (a) charge and (b) discharge. E_0 is the amplitude of the rectangle pulse with constant pulse duration, a, T is the rectangle pulse period, C_1 is the feeding capacitance, C_2 is the capacitance formed between the tool electrode and workpiece, $V(t)$ is the working gap voltage with respect to time and R_0 is the internal electric resistance. During discharge, voltage drop between the electrodes can be expressed by a resistance, R and discharge voltage, u_e. Current, $I_3(t)$ flows through the machining gap during the discharge. From these equivalent circuits, the Kirchoff's Current Law (KCL) and Kirchoff's Voltage Law (KVL) were applied. The resulting differential equations are given in Eqs. A.1-A.7.

c) Charge　　　　　　　　　　　　　　　　d) Discharge
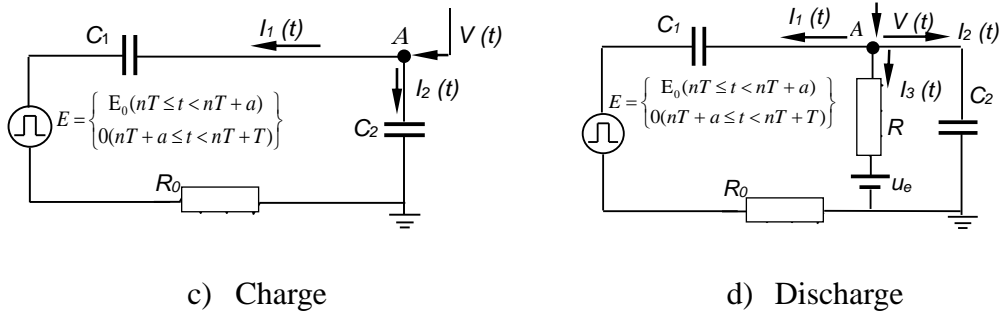
Fig. 1: Equivalent circuit for EIFM

c) Charge

$$V(t) = \frac{1}{C_1} \int I_1(t)dt + \begin{Bmatrix} E_0(nT \le t < nT + a) \\ 0(nT + a \le t < nT + T) \end{Bmatrix} + R_0 I_1(t) \tag{A.1}$$

$$V(t) = \frac{1}{C_2} \int I_2(t)dt \tag{A.2}$$

$$I_1(t) + I_2(t) = 0 \tag{A.3}$$

d) Discharge

$$V(t) = \frac{1}{C_1} \int I_1(t)dt + \begin{Bmatrix} E_0(nT \le t < nT + a) \\ 0(nT + a \le t < nT + T) \end{Bmatrix} + R_0 I_1(t) \tag{A.4}$$

$$V(t) = \frac{1}{C_2} \int I_2(t)dt \tag{A.5}$$

$$V(t) = R I_3(t) \pm u_e \quad (E_0 \ne 0: +, \ E_0 = 0: -) \tag{A.6}$$

$$I_1(t) + I_2(t) + I_3(t) = 0 \tag{A.7}$$

The Laplace equivalent circuit is shown in Fig. 2 and by applying the KCL and KVL, the equations during (a) charge and (b) discharge are as in Eqs. A.8-A.14.

a) Charge   b) Discharge
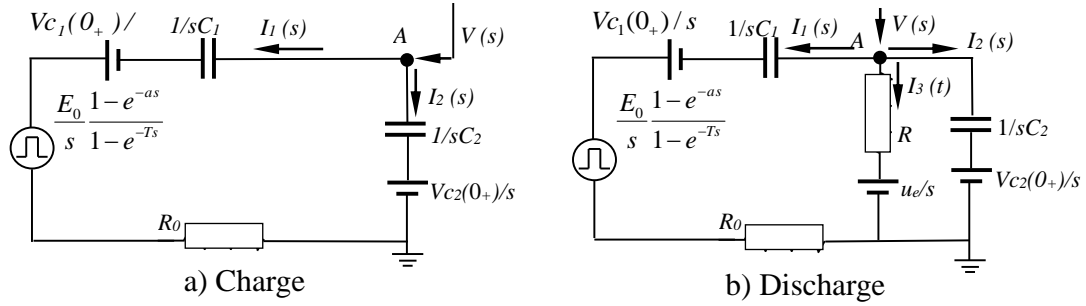
Fig. 2: Laplace conversion

a) Charge

$$V(s) = \frac{1}{sC_1} I_1(s) + \frac{Vc_1(0_+)}{s} + \frac{E_0}{s} \frac{1-e^{-as}}{1-e^{-Ts}} + R_0 I_1(s)$$ (A.8)

$$V(s) = \frac{1}{sC_2} I_2(s) + \frac{Vc_2(0_+)}{s}$$ (A.9)

$$I_1(s) + I_2(s) = 0$$ (A.10)

b) Discharge

$$V(s) = \frac{1}{sC_1} I_1(s) + \frac{Vc_1(0_+)}{s} + \frac{E_0}{s} \frac{1-e^{-as}}{1-e^{-Ts}} + R_0 I_1(s)$$ (A.11)

$$V(s) = \frac{1}{sC_2} I_2(s) + \frac{Vc_2(0_+)}{s}$$ (A.12)

$$V(s) = R I_3(s) \pm \frac{u_e}{s} \quad (E_0 \neq 0: +, \ E_0 = 0: -)$$ (A.13)

$$I_1(s) + I_2(s) + I_3(s) = 0$$ (A.14)

Here, V_{C1} and V_{C2} are voltage across C_1 and C_2, respectively. Using these equations, analysis of discharge circuit was done and the gap voltage and discharge current can be calculated.

a) During charge:

$$V(t) = Vc_1(0_+) \frac{C_1}{C_1+C_2} + Vc_2(0_+) \frac{C_2}{C_1+C_2} - (Vc_1(0_+) \frac{C_1}{C_1+C_2} - Vc_2(0_+) \frac{C_2}{C_1+C_2}) e^{-\frac{C_1+C_2}{R_0 C_1 C_2} t}$$

$$+ \frac{E_0 C_1}{C_1+C_2} \left[\sum_{n=0}^{\infty} (u(t-nT) - u(t-(nT+a))) + \sum_{n=0}^{\infty} (e^{-\frac{C_1+C_2}{R_0 C_1 C_2}(t-(nT+a))} u(t-(nT+a)) - e^{-\frac{C_1+C_2}{R_0 C_1 C_2}(t-nT)} u(t-nT)) \right]$$

(A.15)

144

$$I_2(t) = -\frac{Vc_2(0_+) - Vc_1(0_+)}{R_0} e^{-\frac{C_1 + C_2}{R_0 C_1 C_2} t} - \frac{E_0}{R_0} \left[\sum_{n=0}^{\infty} (e^{-\frac{C_1 + C_2}{R_0 C_1 C_2}(t - (nT + a))} u(t - (nT + a)) - e^{-\frac{C_1 + C_2}{R_0 C_1 C_2}(t - nT)} u(t - nT)) \right] \quad \text{(A.16)}$$

Here, $u(t - nT)$ and $u(t - (nT + a)$ is part of the unit step function and $I_2(t)$ is the gap current during charge.

b) During discharge:

$$V(t) = \frac{Vc_1(0_+)}{R_0 C_2} \cdot \frac{e^{gt} - e^{ht}}{g - h} + Vc_2(0_+) \frac{(\frac{1}{R_0 C_1} + g)e^{gt} + (-h - \frac{1}{R_0 C_1})e^{ht}}{g - h}$$

$$\pm \frac{u_e}{C_2 R_0}(\frac{1}{R_0 C_1 g h} + \frac{(-g - \frac{1}{R_0 C_1})e^{gt}}{-g(g - h)} + \frac{(-h - \frac{1}{R_0 C_1})e^{ht}}{h(g - h)})$$

$$+ \frac{E_0}{C_2 R_0} \left[\sum_{n=0}^{\infty} \frac{e^{g(t - nT)} - e^{h(t - nT)}}{g - h} u(t - nT) - \sum_{n=0}^{\infty} \frac{e^{g(t - nT - a)} - e^{h(t - nT - a)}}{g - h} u(t - (nT + a)) \right]$$

$$\text{(A.17)}$$

$$I_3(t) = (V(t) \mp u_e)/R \quad \text{(A.18)}$$

Where,

$$g, h = -\frac{1}{2}(\frac{(C_1 + C_2)R + C_1 R_0}{C_1 C_2 R_0 R_1} \pm \sqrt{(\frac{C_1 R + C_2 R + R_0 C_1}{C_1 C_2 R_0 R_1})^2 - \frac{4}{C_1 C_2 R_0 R_1}})$$

Therefore, gap voltage and current during discharge can be calculated using Eq. (A.17) and (A.18), respectively.

145

(This page is intentionally left blank)

Acknowledgements

List of Publications

Journal

1. Norliana Mohd Abbas and Masanori Kunieda, 2016, Increasing Discharge Energy of Micro-EDM with Electrostatic Induction Feeding Method through Resonance in Circuit, Precision Engineering, vol. 45, pp. 118-125.

2. Norliana Mohd Abbas and Masanori Kunieda, 2015, Improving Discharge Energy in Micro-EDM with Electrostatic Induction Feeding by Controlled Pulse Train Method, International Journal of Electrical Machining, ISSN 1341-7908, no. 20 pp. 45-51.

International Conference

1. Norliana Mohd Abbas and Masanori Kunieda, 2016, Micro EDM with Controlled Pulse Train Method using Small Feeding Capacitance, 18th CIRP Conference on Electro Physical and Chemical Machining,. Procedia CIRP, vol. 42, pp. 737-742.

2. Norliana Mohd Abbas and Masanori Kunieda, 2015, Increasing Discharge Energy in Micro EDM of Non-contact Electrical Feeding Through Resonance in Circuit, The 8th International Conference on Leading Edge Manufacturing in 21st Century: LEM 21, 18-22 Oct. 2015, Kyoto, Japan, pp. 343-346.

3. Norliana Mohd Abbas and Masanori Kunieda, 2014, High Spindle Speed EDM with Electrostatic Induction Feeding by Controlling the Duration of High Frequency Discharge, The 15th International Conference on Precision Engineering Kanazawa (ICPE), 23-25 Jul 2014, Ishikawa, Japan pp. 5-8.

4. Norliana Mohd Abbas, Masanori Kunieda and Tomohiro Koyano, 2013, Electrostatic Induction Feeding EDM by Controlling the Duration of High Frequency

Discharge,The 7th International Conference on Leading Edge Manufacturing in 21st Century: LEM 21, 7-8 Nov. 2013, Matsushima Miyagi, Japan, pp. 343-346.

National Conference

1. *Norliana Mohd Abbas and Masanori Kunieda, 2016, Micro Drilling EDM with Non-contact Controlled Pulse Train Method, will be presented in The Japan Society of Precision Engineering (JSPE) Autumn Meeting, 6-8 Sept 2016.*

2. Norliana Mohd Abbas and Masanori Kunieda, 2015, Observation on the Concentration of Discharges for Micro EDM with Controlled Pulse Train Method using Transparent Electrode, 2015 The Japan Society of Electrical Machining Engineers (JSEME) Winter Meeting, 3-4 Dec 2015, Tokushima, Japan.

3. Norliana Mohd Abbas and Masanori Kunieda, 2015, Increasing Discharge Energy in Micro EDM of Non-contact Electrical Feeding by Re-designing the Feeding Electrode, The Japan Society of Precision Engineering (JSPE) Autumn Meeting, 4-6 Sept 2014, Sendai, Japan.

4. Norliana Mohd Abbas and Masanori Kunieda, 2014, Investigation to Increase Discharge Energy using Resonance in Micro EDM of Electrostatic Induction Feeding, 2014 The Japan Society of Electrical Machining Engineers (JSEME) Winter Meeting, 4-5 Dec 2014, Niigata, Japan.

5. Norliana Mohd Abbas and Masanori Kunieda, 2014, Comparison between Electrostatic Induction Feeding with Controlled Pulse Train Method and Relaxation Pulse Generator for Micro EDM, Japan Society of Precision Engineering (JSPE) Autumn Meeting, 16-18 Sept 2014, Tottori, Japan.

6. Norliana Mohd Abbas and Masanori Kunieda, 2013, Comparison between Conventional Electrostatic Induction Feeding and Electrostatic Induction Feeding with High Frequency Discharge for Micro EDM, 2013 The Japan Society of Electrical Machining Engineers (JSEME) Winter Meeting, 5-6 Dec 2013, Nagoya, Japan.

7. Norliana Mohd Abbas and Masanori Kunieda, 2013, Micro Drilling EDM with Electrostatic Induction Feeding by Controlling the Duration of High Frequency Discharge, Japan Society of Precision Engineering (JSPE) Autumn Meeting, 12-14 Sept 2013, Osaka, Japan.